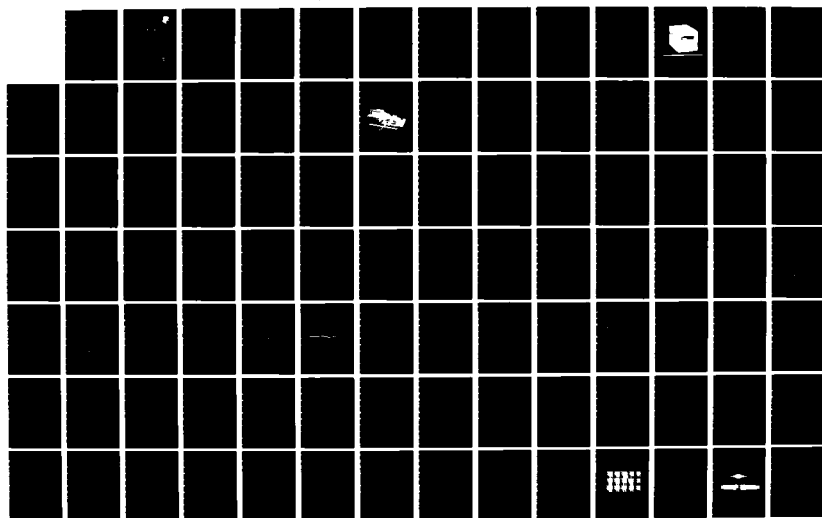AD-A134 713   RUBIDIUM FREQUENCY STANDARD STUDY(U) LITTON SYSTEMS INC   1/2
              WOODLAND HILLS CA GUIDANCE AND CONTROL SYSTEMS DIV
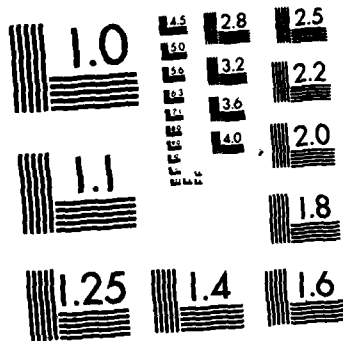   T M KWON ET AL. OCT 83 RADC-TR-83-230 F19628-83-C-0046

UNCLASSIFIED   F/G 9/5   NL

MICROCOPY RESOLUTION TEST CHART
NATIONAL BUREAU OF STANDARDS-1963-A

RADC-TR-83-230
Final Technical Report
October 1983

RUBIDIUM FREQUENCY STANDARD STUDY

Litton Guidance & Control Systems

T. M. Kwon
B. C. Grover
H. E. Williams

APPROVED FOR PUBLIC RELEASE; DISTRIBUTION UNLIMITED

ROME AIR DEVELOPMENT CENTER
Air Force Systems Command
Griffiss Air Force Base, NY 13441

83   12   15   054

This report has been reviewed by the RADC Public Affairs Office (PA) and is releasable to the National Technical Information Service (NTIS). At NTIS it will be releasable to the general public, including foreign nations.

RADC-TR-83-230 has been reviewed and is approved for publication.
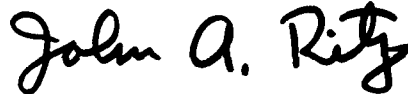
APPROVED: *[signature: Alfred Kahan]*

ALFRED KAHAN
Project Engineer

APPROVED: *[signature: Harold Roth]*

HAROLD ROTH
Solid State Sciences Division

FOR THE COMMANDER: *[signature: John A. Ritz]*

JOHN A. RITZ
Acting Chief, Plans Office

SECURITY CLASSIFICATION OF THIS PAGE (When Data Entered)

REPORT DOCUMENTATION PAGE	READ INSTRUCTIONS BEFORE COMPLETING FORM	
1. REPORT NUMBER RADC-TR-83-230	2. GOVT ACCESSION NO. A134713	3. RECIPIENT'S CATALOG NUMBER
4. TITLE (and Subtitle) RUBIDIUM FREQUENCY STANDARD STUDY		5. TYPE OF REPORT & PERIOD COVERED Final Technical Report February 1982 - March 1983
		6. PERFORMING ORG. REPORT NUMBER N/A
7. AUTHOR(s) T. M. Kwon B. C. Grover H. E. Williams		8. CONTRACT OR GRANT NUMBER(s) F19628-83-C-0046
9. PERFORMING ORGANIZATION NAME AND ADDRESS Litton Guidance & Control Systems 5500 Canoga Avenue Woodland Hills CA 91365		10. PROGRAM ELEMENT, PROJECT, TASK AREA & WORK UNIT NUMBERS PE 27423F 22770010
11. CONTROLLING OFFICE NAME AND ADDRESS Rome Air Development Center (ESE) Hanscom AFB MA 01731		12. REPORT DATE October 1983
		13. NUMBER OF PAGES 128
14. MONITORING AGENCY NAME & ADDRESS(If different from Controlling Office) Same		15. SECURITY CLASS. (of this report) UNCLASSIFIED
		15a. DECLASSIFICATION/ DOWNGRADING SCHEDULE N/A

16. DISTRIBUTION STATEMENT (of this Report)

Approved for public release; distribution unlimited.

17. DISTRIBUTION STATEMENT (of the abstract entered in Block 20, if different from Report)

Same

18. SUPPLEMENTARY NOTES

RADC Project Engineer: Alfred Kahan (ESE)

19. KEY WORDS (Continue on reverse side if necessary and identify by block number)
Rubidium Frequency Standard
Physics Package
Double Buffer Gas
Buffer Gas Adsorption
VCXO

20. ABSTRACT (Continue on reverse side if necessary and identify by block number)
The primary objectives of this contract were to design a physics package and to characterize the voltage controlled crystal oscillator (VCXO), which will satisfy the temperature and vibration requirements of a tactical rubidium frequency standard unit (FSU).

The double buffer gas resonance cell has demonstrated temperature performance that exceeds the requirement. Vibration sensitivities of a —⟩ cont

DD FORM 1 JAN 73 1473   EDITION OF 1 NOV 65 IS OBSOLETE

cont

FSU have been analyzed.

Improved FSU design under the tactical vibration inputs are discussed in detail with performance predictions. Experimental results are shown to demonstrate validity of the predictions. The SC-cut VCXO, the state-of-the-art, provides realistic potential for use in tactical FSU.

Accession For

NTIS GRA&I

DTIC TAB

Unannounced

Justification

By

Distribution/

Availability

Avail and/or

Dist   Special

A-1

DTIC

CONTENTS

ILLUSTRATIONS

ILLUSTRATIONS (cont)

SECTION I

PROGRAM DESCRIPTION

1.1 PROGRAM BACKGROUND

Litton Guidance and Control Systems Division's interest in rubidium frequency standards arose out of its familiarity with the rubidium atomic system which it has implemented, both as an optical pumping mechanism and as a sensitive magnetometer, in its nuclear magnetic resonance (NMR) gyro development program. In 1979 Litton first examined the marketplace for a Rb frequency standard unit (FSU) and postponed a decision to enter the marketplace until several market variables were better clarified. Again in early 1981 the marketplace was examined, and a positive outlook was foreseen on the basis of several military programs where potential existed for application of a Rb FSU. Litton considered its experience with rubidium and its superior reputation in delivering high quality, high-volume products to the military marketplace made it an ideal contender in the Rb FSU field.

As a result of its market surveys Litton undertook an initial IRAD program in company fiscal year (CFY) '81. This program has continued to have IRAD support in both CFY '82 and CFY '83. In addition, the USAF Rome Air Development Center has provided R&D funding (Contract No. F19628-83-C-0046) to investigate crystal oscillator performance under vibration, and physics sensitivity and aging characteristics associated with tactical, military Rb FSUs. This report is the summary of R&D investigations performed under this contract.

The Litton Rb FSU development program was made possible due to the availability of over ten years of laboratory experience in the successful application

of the special properties of the rubidium atom in connection with Litton's NMR
gyro development program. The NMR gyro program had seen the implementation of
the Rb atomic system as an angular momentum transducer, transferring angular
momenta from the nuclei. Simultaneously, nine years experience had been assim-
ilated on the use of rubidium as a sensitive magnetometer. The Litton Rb FSU
program is a natural exploitation of the NMR gyro's extensive scientific and
technological base and represents an appropriate addendum to GCS's family of
navigation instruments.

The Litton Rb FSU development program was planned as a 3-Phase program
from inception. The three phases, each including a hardware product goal were:
breadboard model (BBM) development, engineering model (EM) development, and pre-
production model (PPM) development. The BBM phase was completed in early 1982,
and the EM phase is well along with completion scheduled in early 1983. Shown
in Figure 1-1 is Litton's EM Rb FSU packaged in a size 3 1/4 × 3 1/4 × 4 1/2".
The R&D investigations described in this report were started in early EM design
phase in time to implement the results of investigation into the hardware.

1.2 FSU FOR TACTICAL APPLICATIONS

The need for precision time and frequency devices is growing rapidly in
both quantity and quality. Several technologies compete to satisfy these needs
including quartz oscillators, rubidium and cesium frequency standards, and hydro-
gen masers. Although the technologies overlap in some areas of performance,
each technology has some unique range of applicability.

Frequency standards for tactical applications demand small size, rapid
warmup, and low power consumption along with frequency stability, repeatability,
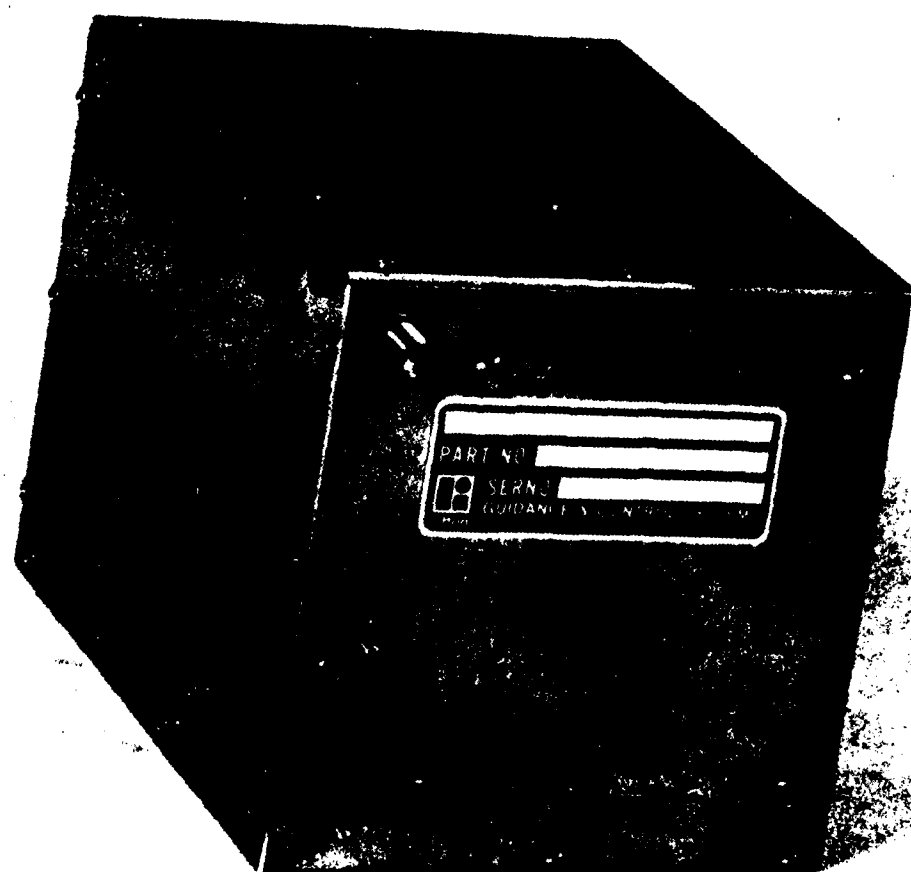
Figure 1-1.   Litton Engineering Model FSU

16708-1

and low frequency aging. Among the available technologies, the rubidium frequency standard appears to be the best fit for most current and near-term tactical precision frequency standard applications.

The rubidium frequency standard to be used in tactical applications must be capable of operating under severe environmental conditions, specifically extreme operating temperature and vibration environments. Such requirements are exemplified in the specification, Hazeltine Drawing No. 332819, Frequency Std Unit, designed for the U.S. Air Force Seek Talk program.

The specification calls for an operating temperature range of -55C to + and for vibration up to 10-g peak. No rubidium frequency standard available ' date satisfies either one of these requirements. Frequency standards, includ. ⌐ the rubidium device, have previously been employed in the laboratory, ground stations, or benign military vehicle environments. One current modular rubidium frequency standard, which is an off-the-shelf item, operates up to $\sim$ 55C ambient. Test results on this device report output frequency instabilities up to several parts in 10^8, and in some cases, loss of frequency control loop-lock, under 1-g peak vibration.

For a rubidium frequency standard to be used in a tactical environment, it is imperative that the unit be designed and constructed with the specific environment to be encountered in mind. Performance specifications for the unit must be reviewed as a whole at the unit level from the beginning of the design activities. It seems evident that more than dressup of the conventional rubidium frequency standard is required to meet the specification for a tactical environment.

In view of the growing demand for such a frequency standard, Litton's Guidance and Control Systems (GCS) Division has been developing a miniaturized

rub'dium frequency standard for tactical use. Emphasis has been placed on specifications of the U.S. Air Force Seek Talk program since inception.

1.3 SUMMARY AND ACKNOWLEDGEMENT

The R&D tasks described in this report are part of the continuing effort at Litton to design and build the state-of-the-art Rb FSU for military tactical applications. The tasks address specifically the physics package of a Rb FSU and the SC-cut voltage controlled crystal oscillator, each/or both of which demonstrate the potential for meeting the performance and environmental specifications of advanced tactical airborne platforms. Two most challenging specifications, operating temperature and vibration inputs, have been encountered during the course of this investigation.

The task of implementing a double buffer gas resonance cell in the physics parameter design (Task 0001A) and the investigation of buffer gas wall absorption processes (Task 0001B) are reported in Sections II and III of this report, respectively. Systems level study of vibration sensitivity of a Rb FSU is discussed in Section IV. Included in this section are the design aspects for and performance of the physics package undergoing vibration (Task 0001C). Section V describes characteristics of the voltage controlled crystal oscillator that Litton intends to incorporate into its tactical FSU.

The double buffer gas resonance cell, as it is implemented in the physics package of Litton design, demonstrates a significant improvement over a conventional single buffer gas cell in its frequency sensitivity to temperature vibrations. Buffer gas absorption on the glass cell wall is shown to be a potential source of long-term frequency aging of a tactical FSU.

Investigation of the Rb FSU has identified the sources of its vibration sensitivities. Litton believes this represents the most comprehensive study

to date on the subject. Expected performance of a tactical FSU under the current Litton design concept is given together with experimental results. The SC-cut voltage controlled crystal oscillator is indeed the state-of-the-art in its size and performance, in particular its vibration sensitivity.

1-6

SECTION II

DOUBLE BUFFER GAS PARAMETER OPTIMIZATION

2.1 DESIGN CONSIDERATIONS

At the beginning of Litton's program to develop a militarized version of a compact Rb frequency standard, a study was made to determine which of the two basic types of Rb frequency standards could best be developed into a unit capable of meeting the requirements of programs such as Seek Talk.

The first type of Rb standard is known as the integrated cell type. This approach uses a resonance cell that contains both ^{87}Rb, whose resonant frequency is the working standard, and ^{85}Rb, which acts as the optical filter necessary to obtain sufficiently large resonance signals. The second type Rb standard is the type being developed at Litton and the one felt most likely to offer the best frequency stability over the operating temperature environment while satisfying the other requirements of a militarized FSU. In this version, the resonance cell contains only the working standard ^{87}Rb, while the optical filtering is performed using the ^{85}Rb in a separate cell, the filter cell. The advantage to this approach is that the temperature, optical path length, and buffer gas content associated with the ^{87}Rb resonance process can be optimized independently from the ^{85}Rb optical filtering process. As will be shown, these additional degrees of freedom associated with the separate filter cell approach are desirable to meet the frequency stability requirements under the constraints imposed by the operating temperature environment. To date, Litton's choice of the separate filter cell Rb frequency standard has been experimentally justified.

For a unit designed to operate with a baseplate temperature as high as 80C, the elements of the physics package (resonance cell, filter cell, and Rb

lamp) must operate at a controlled temperature of at least 85C to insure temp-
erature and, hence, frequency stability over the full environmental temperature
range. As the temperature of the resonance and filter cell increases above
85C, the increased Rb density attenutates the transmitted Rb light thus decreas-
ing the ^{87}Rb resonance signal levels and degrading ther short-term frequency
stability. This effect can be mitigated by decreasing the length of the reso-
nance and filter cells. In particular, however, an upper bound in the vicinity
of 90C is found. This leaves a rather narrow temperature window of 5C to oper-
ate the resonance and filter cells. The Rb lamp is not as sensitive to temper-
ature consideration because in practice it is operated in the 110C to 130C
range. Litton rejected the scheme of operating the resonance and/or filter
cells at reduced temperatures with thermoelectric coolers on the basis that
too much power was required and magnetic shielding complexity was increased.
Another technique, that of reducing the Rb density in the temperature window
by adding a second alkali element in addition to the Rb[1], while increasing the
short-term stability, leads to possible long-term stability problems as well
as increasing the cell fabrication complexity and cost. Both of these
approaches were rejected in favor of a Rb frequency standard of the separate
filter cell type operated in the 5C temperature window.

Long-term stability of a Rb frequency standard can be achieved only if
sensitivity to light amplitude and temperature variation can be reduced to some
minimum level, while short-term stability is accomplished through attainment of
an appropriate signal-to-noise ratio. To reduce the temperature and light
amplitude sensitivity, it is imperative to observe the effects of the buffer
gases on the ^{87}Rb clock transition frequency. The buffer gas is needed to
reduce the relaxation rate experienced by optically pumped rubidium atoms upon

collision with the cell walls. Nitrogen is used as the buffer gas almost exclusively in rubidium devices. In addition to the buffering action, nitrogen molecules quench the rubidium excited state reducing the number of spontaneously emitted photons that would, if not quenced, cause a reduction in signal level.

It is known that buffer gases used in the resonance cell contribute to a change in the 6.8 GHz rubidium resonance frequency. The fractional frequency shift of the rubidium resonance due to nitrogen molecules is $+8.4 \times 10^{-8}$/torr and -9.3×10^{-9}/torr for argon.[2] This pressure shift has an associated temperature dependence which is approximately linear with temperature over the temperature span of interest here. The temperature dependence for nitrogen and argon, in units of fractional frequency shift per degree celsius per torr of gas, is $+7.9 \times 10^{-11}$ and -5.1×10^{-11}, respectively. Ideally, with the proper nitrogen/argon ratio, one would obtain a Rb frequency standard whose frequency was independent of all temperature variations. Unfortunately this ideal situation does not prevail, and a residual temperature-dependent shift, which is primarily a function of the intensity and spectral character of the Rb light, is always observed.

The variation in ^{87}Rb resonant frequency with Rb light intensity and spectral character (as large as several parts in 10^9) is known as light shift.[3] To build a practical Rb standard then, the temperature dependence at the operating conditions is reduced to an acceptably low level (temperature turning point) by adjusting the available parameters: lamp, resonance cell, filter cell temperature, buffer gas type and pressure both in the resonance cell and in the filter cell, and length of those cells. In order to operate

the FSU with reduced frequency sensitivity to the inevitable long-term variation in Rb light, the choice of parameters must be consistent with those that lead to a reduced light sensitivity at the operating temperature (light turning point).

Successful physics parameter design of a Rb FSU largely depends on whether the two important parameters, temperature turning point and light turning point, can be made to occur simultaneously. If this can be accomplished, the Rb FSU can be made insensitive to cell and lamp temperature perturbations.

Despite the importance of the temperature turning point and light turning point, no complete explanation of the dependence is yet available. Physics of optical pumping and relaxation of Rb atom offers explanation of first order effects, typically, in the order of a few parts in 10^{-9} in units of fractional frequency stability. In order to realize a Rb FSU that is stable in a few parts in 10^{-11}, extension of the theory into the higher order effects is therefore inevitable. Several workers have developed empirical formulae to explain their experimental observations, yet they often fail to explain the work of others.

The physics parameter design activities at Litton are divided into two subtasks, empirical approach and analytical approach. The empirical approach is the subject of this report. Analytical approach is an extension of basic theory of Rb FSU physics and should provide eventual improvements beyond those provided by the empirical approach.

To date, a viable choice of operating parameters has been found empirically that leads to acceptably low frequency variations as a function of the Rb light and cell temperature variations over long periods of time and all environmental conditions.

2.2 PRELIMINARY EXPERIMENTS

Fractional frequency shifts caused by the parameter changes cited in the previous section are in the order of, at the largest, a few parts in 10^{-10}. Experimental observation of such small effects is often hindered by minute asymmetry present in the detected rubidium resonance curve. The asymmetry arises from such parameters as dc magnetic field, rf distribution in the microwave cavity, temperature gradient across the cell, and spatial distribution of Rb light intensity, all of which deviate from the ideal, uniform conditions.[4] Although many of these parameters could be made nearly uniform in a laboratory set-up, such ideal conditions do not prevail in a practical Rb FSU where the size and other considerations are of primary concern. It is emphasized here that, due to the presence of minute asymmetry in the detected resonance signal, the measured Rb resonance frequencies represent the frequency of "the center of gravity," i.e., at the peak of the absorption resonance curve or, equivalently, at the zero dc point of the dispersion curve, rather than the frequency of "true" rubidium resonance. The work reported here was performed utilizing the Litton physics package (Figure 2-1) unless otherwise noted explicitly.

2.2.1 Experimental Set-Up

^{87}Rb Resonance Lamp

The lamp producing Rb resonance radiation is necessary for both optical pumping and detection of the 6.834 GHz clock transition. The lamp consists of a 1720 glass blank, 1/2 mm wall, of cylindrical shape 9 mm diameter and 10 mm overall length with a slight convex exit window and pinchoff at the opposite end. About 100 micrograms of isotopically pure ^{87}Rb is filled with 2.5 torr of Xe buffer gas. The lamp is excited in a helical resonator driven by a modified

16708-5
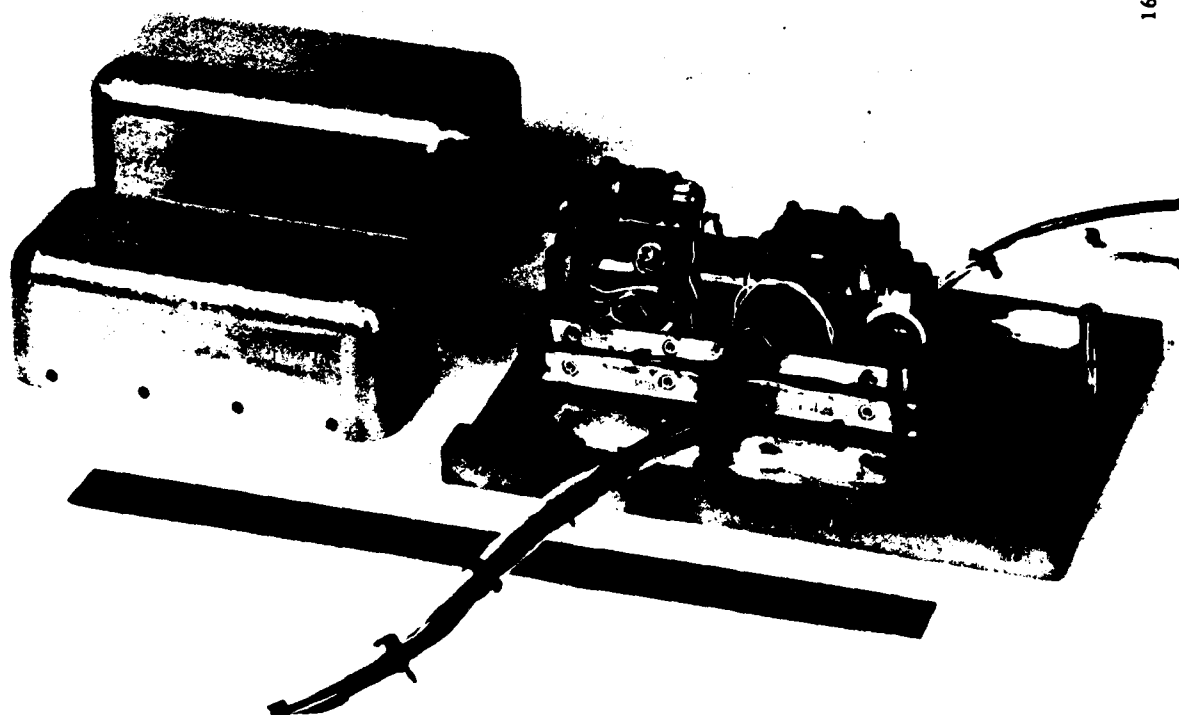
Figure 2-1. Litton Engineering Model Physics Package with Shields

Colpitts oscillator at $\sim$90 MHz. Lamp luminance for D_1 and D_2 radiation increases with lamp temperature over the range of interest, here 100°C to 120°C. Lamp temperature is monitored and controlled closely to maintain a constant spectral output. The resonance radiations of ^{87}Rb D_1 and ^{87}Rb D_2, as they are observed through a Fabry-Perot interferometer, are shown in Figures 2-2 and 2-3, respectively.

Filter Cell

Due to the severe restrictions of size and operating temperature imposed on the physics package of a tactical Rb FSU, a separate filter cell configuration would give better performance here than would the integrated filter-resonance cell approach. Filter cells used in this study are made from 12 mm diameter 1 mm wall glass tubing cut to length with 1 mm glass disks attached as end windows. The fill stem is attached on the side wall of the filter. Filter cells used in this work range from 7 mm to 9 mm overall length and are filled with isotopically pure ^{85}Rb and either Ar, N_2 or both gases. The filter cell temperature is controlled and monitored in the range 85°C to 92°C. This temperature range is dictated by thermal and steady-state power considerations imposed by the performance requirements. The filter cell serves two primary functions. One is to establish enough preferential optical pumping of the F=1 hyperfine level over the F=2 level for sufficient signal to noise ratio. The second function is to establish a spectral condition for minimum dependence of clock frequency on light intensity. This process will be discussed in detail in another section.

Resonance Cell

Due to the thermal design of the physics package and environmental considerations, the resonance cell must operate in the vicinity of 83C. At this
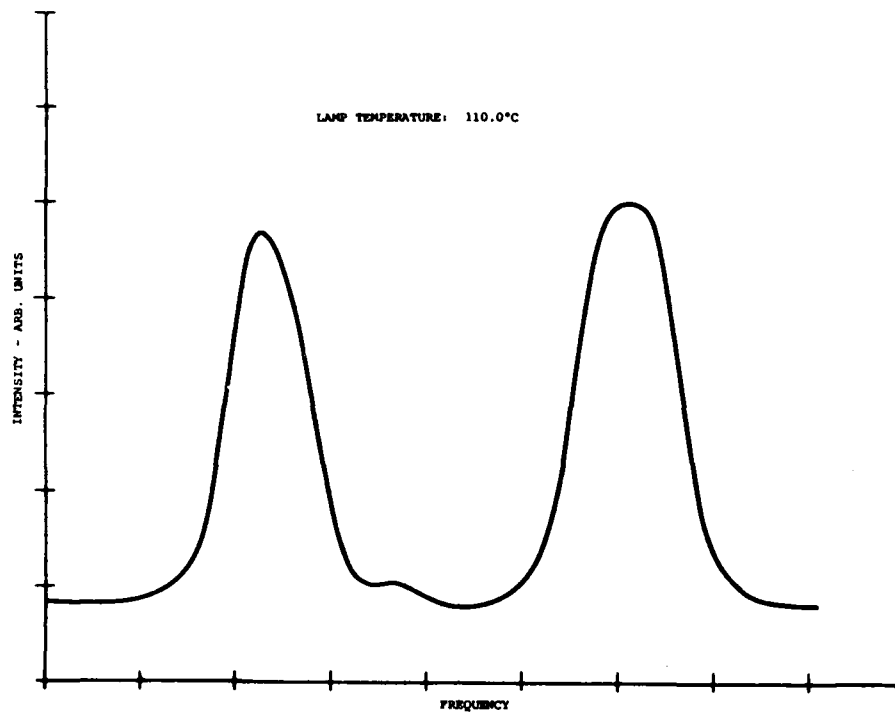
Figure 2-2. Spectral Profile of ^{87}Rb D_1 Light
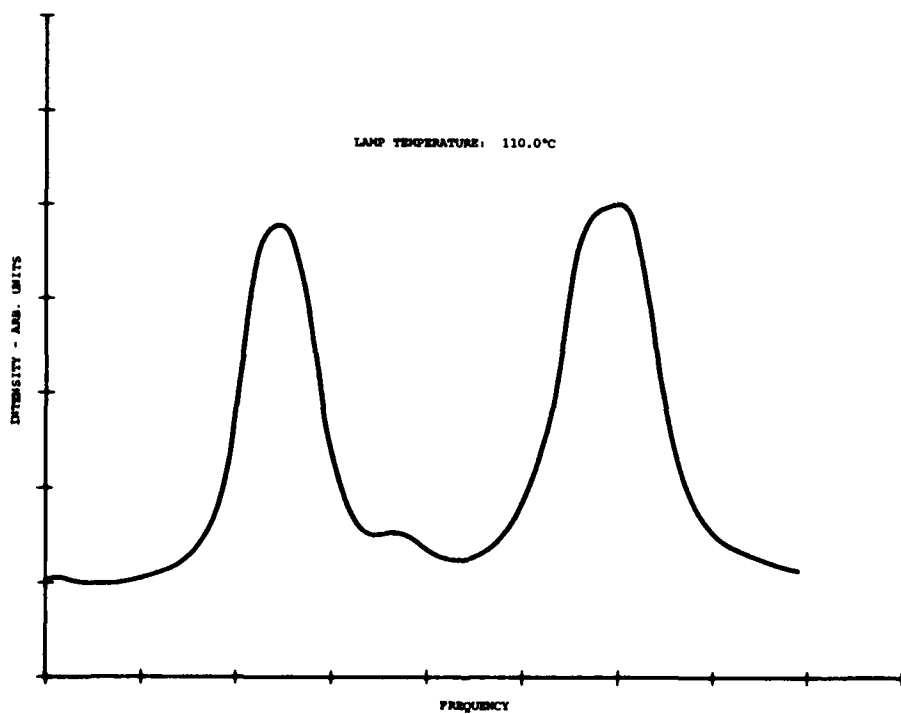
Figure 2-3. Spectral Profile of ^{87}Rb D_2 Light

2-8

temperature the Rb density is $8.4 \times 10^{11}/cm^3$ which is considerably higher, by a factor of 2 to 4, than at the lower temperture operating point of a conventional Rb FSU. This results in increased light absorption at our temperatures. In order to maintain the optimum ratio of transmitted to incident light for maximum FSU stability the resonance cell is made shorter in length than the cells found in conventional FSU's. Resonance cells used in this work are made of glass in a fashion identical to our filter cells. These cells range from 8 mm to 10.5 mm in length and are filled with isotopically pure ^{87}Rb and varying amounts of N_2 and Ar with total pressure in the 25 torr range.

Microwave Cavity

The cell is placed in a small rectangular microwave cavity operating in the TE_{101} mode. The cavity is partially loaded with a low loss dielectric slab.[5] A 0.3" diameter hole in each end of the cavity allows light to pass through the resonance cell and be collected at a photo cell mounted on the outside of the cavity. Two 10 mm diameter plano-convex lenses are placed in the cavity to optimize the optical process. The cavity is excited at 6.8 GHz resonant frequency by a step recovery diode (SRD) located in the cavity.

Experimental Appartus

The experimental set-up is shown in Figure 2-4. The physics package is placed inside a large cylindrical mu-metal shield. A pair of helmholtz coils located inside of the shield provides the static dc magnetic field. 10 MHz signal from a Cs frequency standard provides the reference to the frequency synthesizer and the input to the frequency mutliplier. Outputs of the multiplier, 120 MHz, and of the synthesizer, f_1 approximately 5.3 MHz, are mixed at a mixer to generate $f_2 = 120$ MHz $\pm f_1$.

Cs FREQ.
STANDARD
(FTS4050)

10 MHz

X12 FREQ.
MULTIPLIER

5.3 MHz
SYNTHESIZER
(HP 3325A)

MODULATION
FREQ., f_m

MIXER

120 MHz

f_1

SWEEP

PHYSICS PACKAGE

f_2

f_3

LOCK-IN
AMPLIFIER
(ITHACO 393)

Y AXIS

X AXIS

LAMP   FILTER   RESONANCE
       CELL   CELL

MAGNETIC
FIELD
CURRENT

TEMPERATURE CONTROLLER

X-Y RECORDER
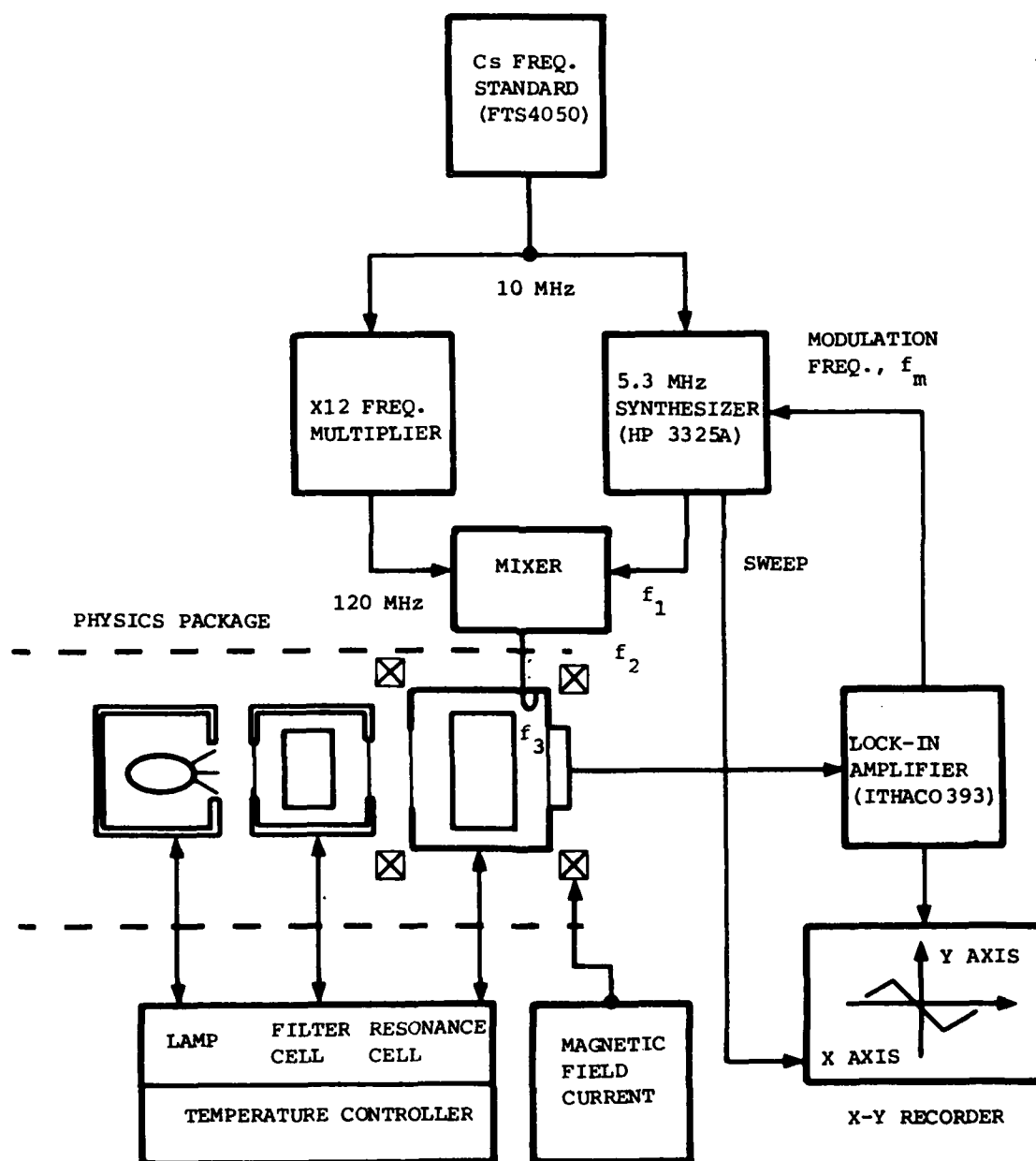
Figure 2-4.   Experimental Apparatus

In order to interrogate the atomic resonance at 6.8 GHz, the frequency f_2 is further multiplied by a step recovery diode in the microwave cavity. The cavity is tuned to select the lower sideband, f_3, of the 57th harmonics of f_2, i.e., $f_3 = 57 \times 120$ MHz $- f_1$. For f_1 being 5,312,500 Hz, f_3 becomes 6,834,678,500 Hz. In this set-up, the interrogation frequency can be varied by varying the synthesized frequency f_2. Phase modulation of the interrogation frequency is accomplished by modulating f_2 at the frequency synthesizer. Both frequency f_m and depth of modulation are readily adjustable at the lock-in amplifier. The resonance signal detected in the photodiode contains both in-phase and quadrature-phase components with respect to the modulation.[6] The quadrature signal is detected at the lock-in amplifier. The ^{87}Rb resonance dispersion curve is obtained in a x-y recorder by plotting the signal amplitude as a function of the interrogation frequency f_3.

2.2.2 Preliminary Results

Empirical design of physics parameters depends heavily on the systematic characterization of the physics elements for a given design of physics package. The experimental results reported here are not necessarily reproducible to the minute details in the physics packages of others. The reason for this is because several parameters of importance are closely interrelated to each other to the extent that no physical parameter can be varied without affecting the others.

Such an interdependence is exemplified in Figure 2-5, where a situation of varying lamp temperature is illustrated. The lamp temperature is varied typically in the case where varying amount of light intensity is desired. An increased lamp temperature, for example, results in an increased rubidium density as expected, however, such an increase is seen as a load change by the
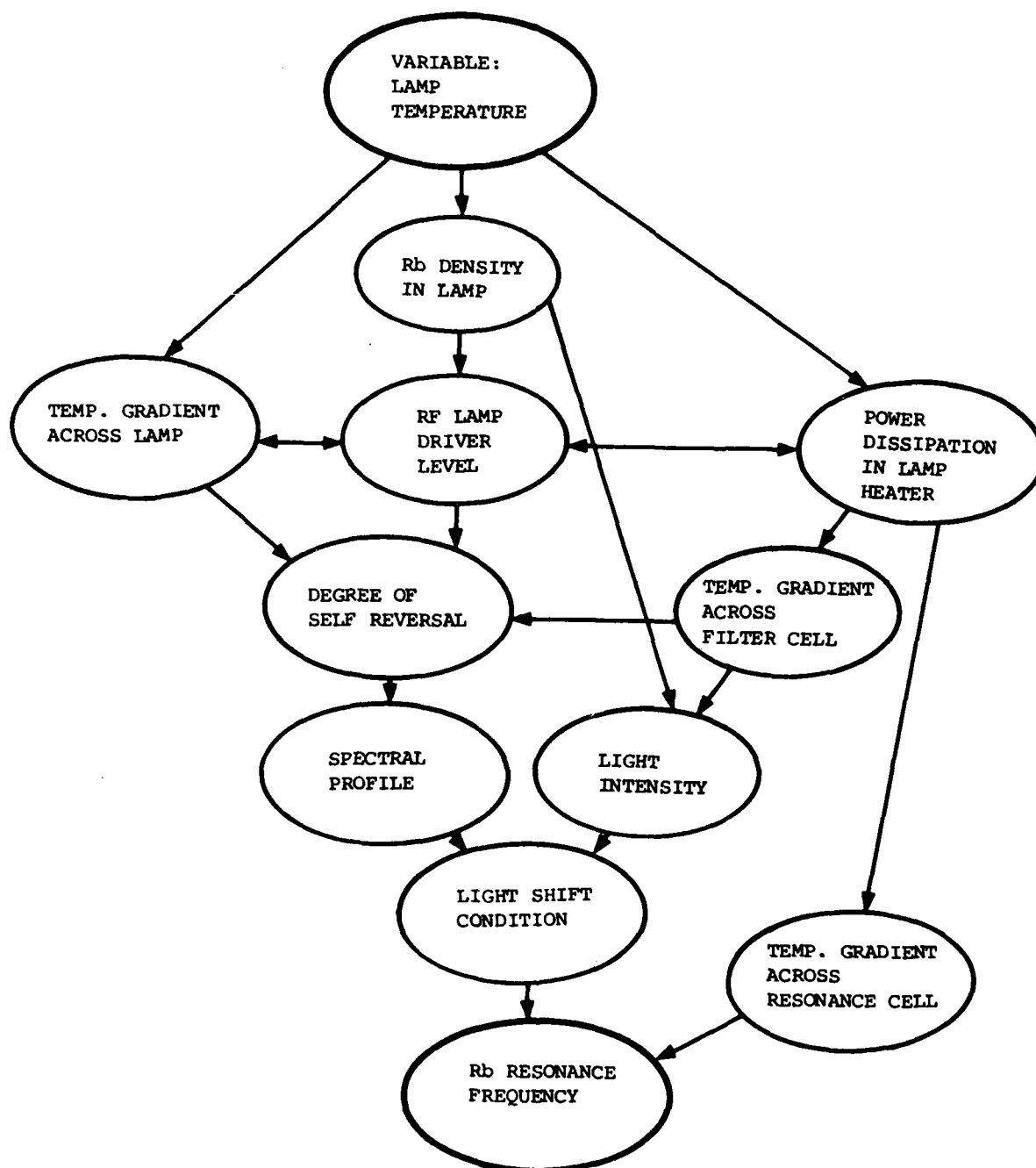
Figure 2-5. Parameters Affected by Lamp Temperature Variation

rf lamp driver. Depending on the driver design, it may mean a reduced rf power experienced by rubidium atoms which could result in a modified spectral profile due to different degree of self reversal. In a typical design of temperature control/heater driver, the temperature is monitored and controlled at one point where the control sensor element, such as an RTD, is located. Temperature of the rest of the heated object is dictated by the thermal conductivity, heat capacity of and by heat dissipation from the object. A temperature gradient is, therefore, established across the heated object. The extent of temperature gradient is a function of the temperature being controlled. Varying degrees of power dissipation resulting from variations in lamp temperature cause varying degrees of temperature gradient across the fiter cell. This is because there exists thermal cross-talk between the two adjacent heated objects. Figure 2-5 indicates how the Rb resonance fequency is affected by variations in the lamp temperature though differeant mechanisms. The data presented in this section are taken from the physics package designed for the Litton engineering model FSU.

Presented in this section are the results of preliminary experiments that have ultimately led to the optimum design of physics parameters utilizing the double buffer gas Rb resonance cell. The data are organized into three subsections (lamp, filter cell, and resonance cell), in order to emphasize each specific element of the physics package. Table II-1 lists the sample cells quoted in this section.

1. Lamp

Presented here are the results of experiments in which the lamp parameters, light intensity and lamp temperature, are varied. Input power to the RF lamp driver is held fixed during the measurements.

TABLE II-1
LIST OF CELLS USED IN THIS WORK

Cell Designation	Type*	Length (mm)	Buffer Fill[†]	Notes
1-921	RC	8.5	N_2, Ar	Increasing N_2/Ar Ratio
1-319	RC	10.5	N_2, Ar	
1-923	RC	9.2	N_2, Ar	
2-1283	FC	7.0	90 t.Ar	
1-1013	FC	8.3	60 t.N_2/60 t.Ar	
#3	FC	8.3	90 t.N_2	
2-1012	FC	8.0	120 t.Ar	
1-712	FC	8.5	185 t.N_2	

*RC: Resonance Cell, FC: Filter Cell

[†]t indicates pressure in torr

An important parameter characterizing the FSU is its sensitivity to changes in lamp intensity, i.e., the magnitude and direction of a frequency shift with light intensity. The desirable FSU operating point is where clock frequency is insensitive to light intensity. This condition is called a light turning point (LTP). The desirability of operating at the LTP lies in the fact that both short and long term frequency stability are improved. Intensity fluctuations other than those described by shot noise, if translated into frequency, can degrade the spectral purity of the clock output frequency. Long term stability is affected through "aging" of the lamp over its lifetime which is characterized by a significant decrease in lamp intensity. This would produce a frequency drift when the operating conditions do not give a LTP. In practice, frequency sensitivity to light is measured here by inserting a

neutral density filter of 85% transmission between the lamp and filter cell and noting the resulting change in clock frequency. This change can be positive, negative or zero depending on the total system operating point, and is referred to for convenience, as "light shift." It is emphasized that the term, light shift, used in this report is not necessarily the light shift as it is understood in the scientific community.[3] A positive light shift is defined here as a decrease in frequency with decrease in light intensity.

Figure 2-6 shows the slope of the ^{87}Rb resonance dispersion curve at resonance as a function of lamp temperature for the resonance cell 1-923. Since the VCXO frequency is steered to the Rb resonance by the amplitude of the dispersion curve, the slope at resonance is considered as signal-to-noise ratio in the FSU.[6] The steeper the slope is, the better the short-term stabilities are. The data shown in Figure 2-6 demonstrates that it is desired to operate the lamp near the high end of the temperature range in order to realize excellent short-term stability.

Figure 2-7 shows how clock frequency changes with lamp temperature. Clock frequency is plotted here as frequency offset not as an absolute frequency. Figure 2-8 shows the variation in light shift with lamp temperature. Comparing the bottom curve (filter at 89.7°C) and Figure 2-7 shows how clock frequency and light shift are related, an increasingly positive light shift with an increasing clock frequency. The LTP is shown in 2-8 at 117°C lamp temperature when the filter is 89.7°C and at 112°C when the filter is 87.4°C. Figures 2-9 and 2-10 show variation of light shift with lamp temperature for several filter cells and filter temperatures. These curves show a general trend of a positive increasing light shift with increasing lamp temperature in the vicinity of a LTP. When conditions are such that a large negative light

16801-5
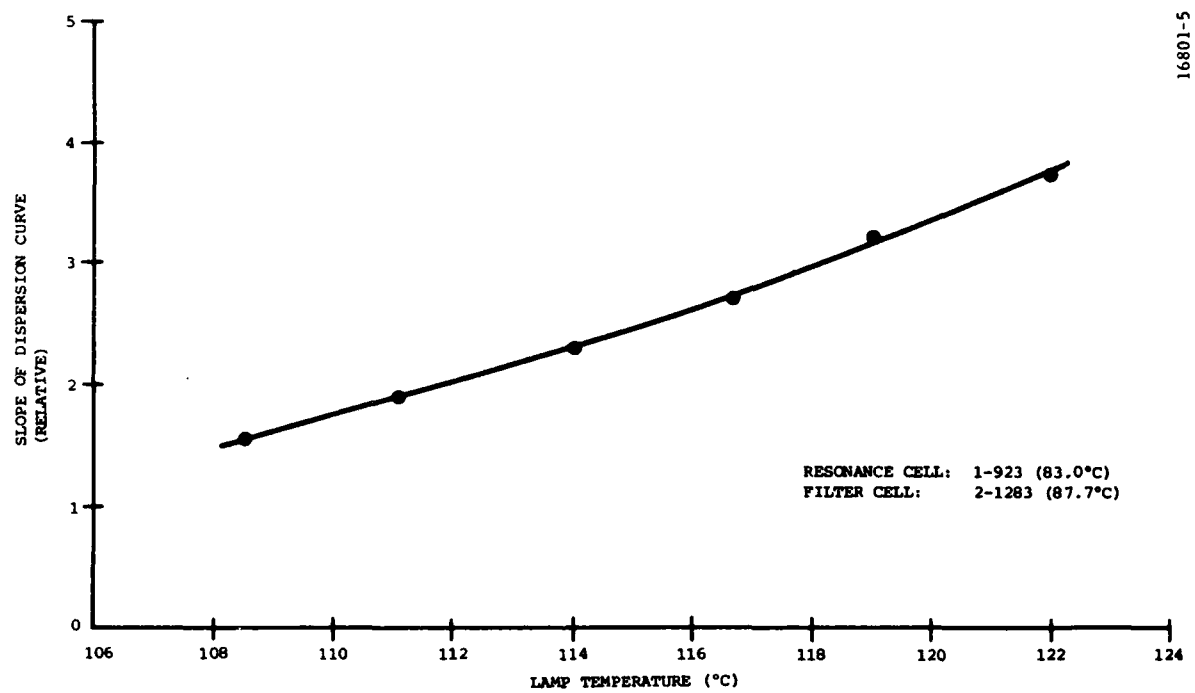
Figure 2-6. Slope of ^{87}Rb Resonance Dispersion
Curve vs Lamp Temperature
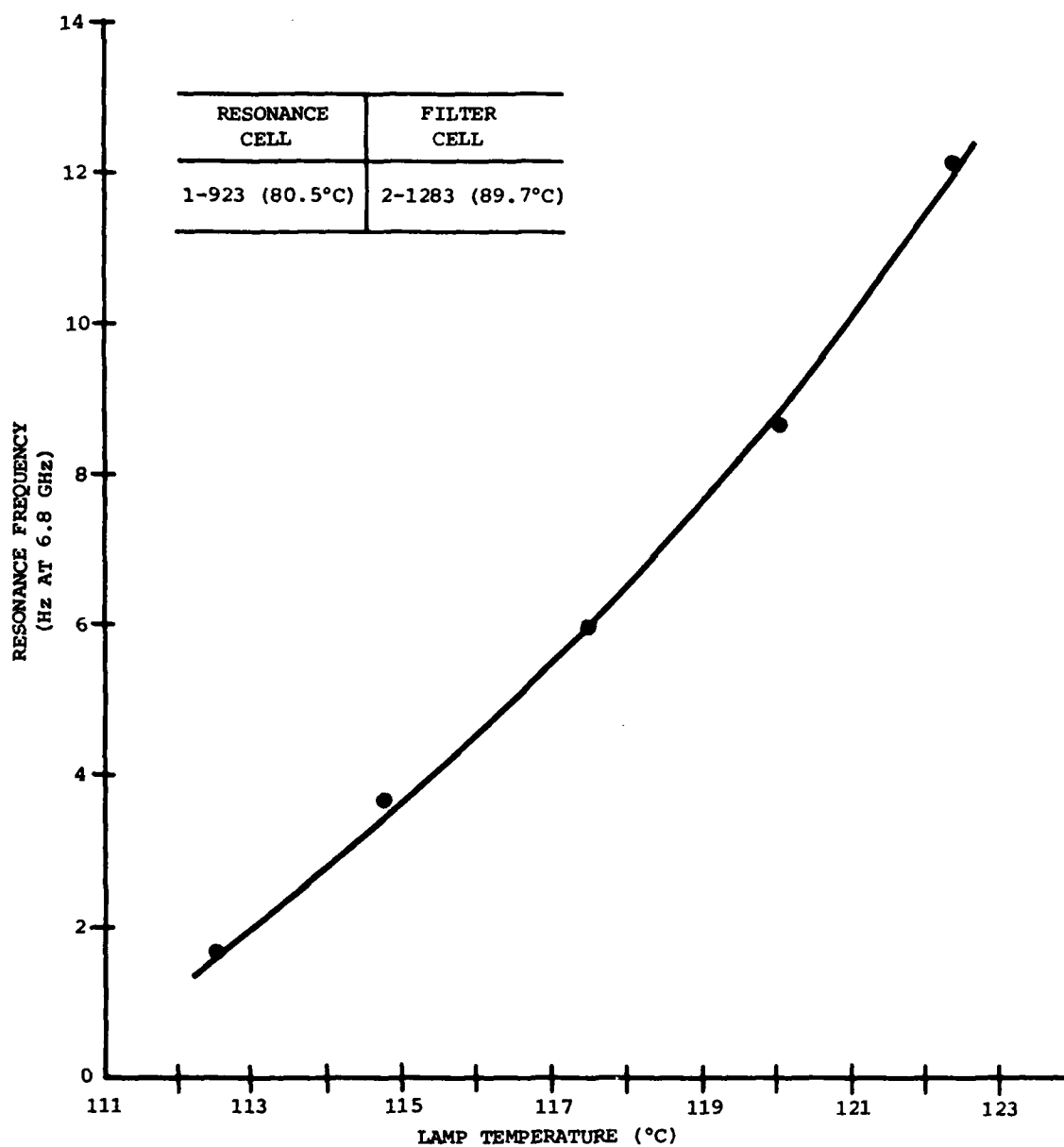
Figure 2-7. ^{87}Rb Resonance Frequency vs Lamp Temperature
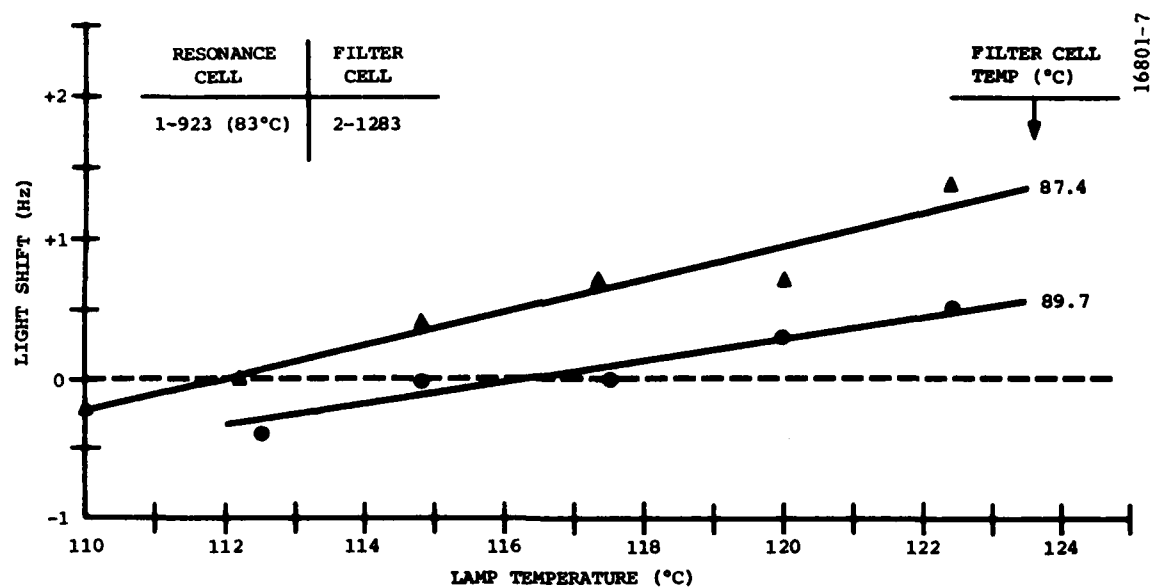
Figure 2-8. Light Shift vs Lamp Temperature
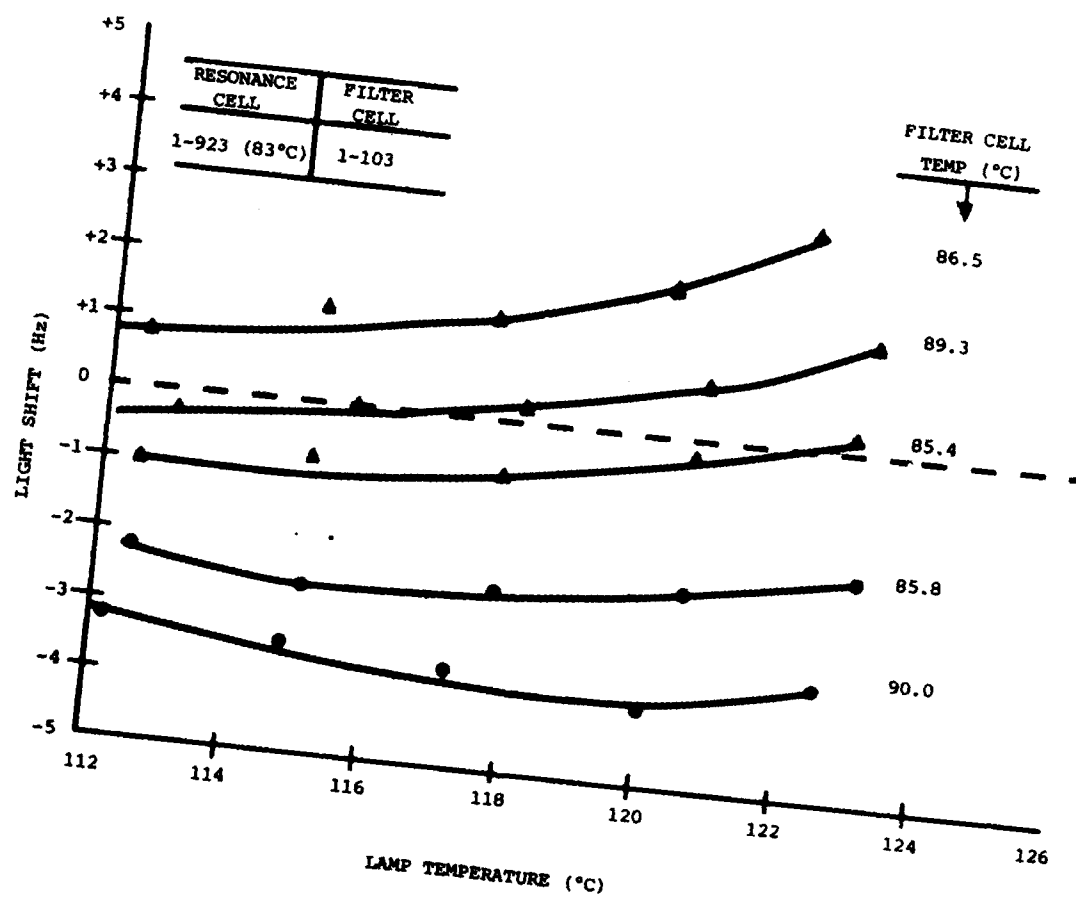
Figure 2-9. Light Shift vs Lamp Temperature
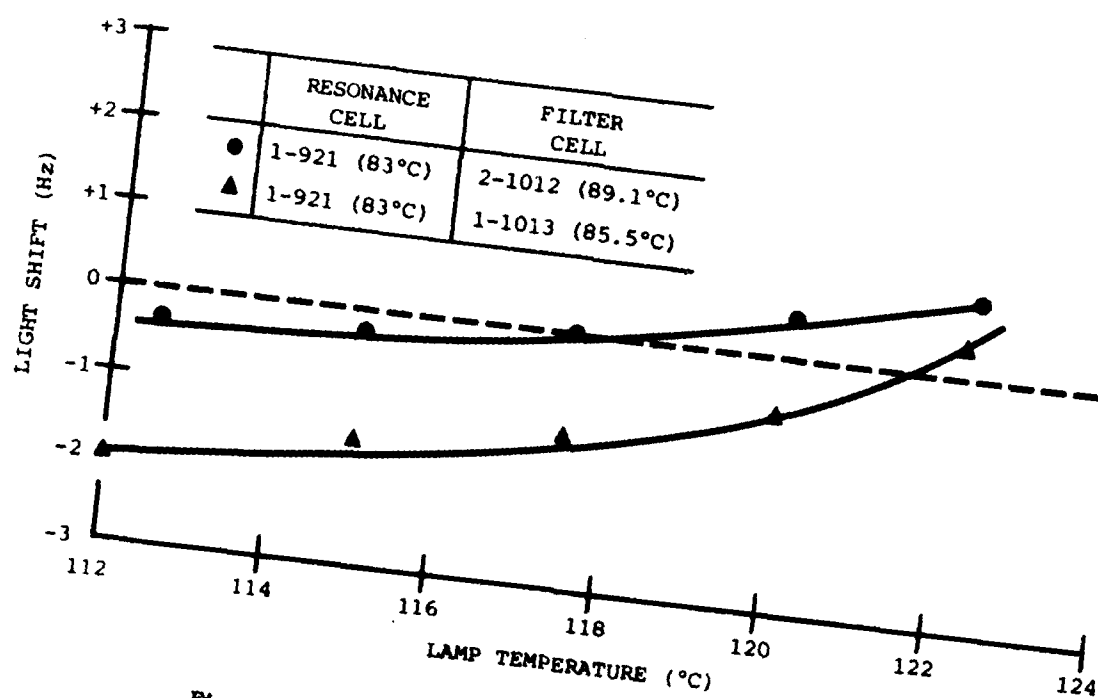
Figure 2-10. Light Shift vs Lamp Temperature

16801-9

2-20

shift is present, as would result from using a filter cell with insufficient buffer pressure, then increasing lamp temperature results in a negative increasing light shift (see Figure 2-11). An intermediate behavior is shown in the bottom curve of Figure 2-9. Since we are restricted to operate over a narrow temperature window, data shown here will be for that range only.

Figure 2-12 shows light shift for three resonance cells of similar buffer pressures but varying length, and indicates the nonlinear fashion in which light spectrum is integrated over the resonance cell to produce the net light shift. The strong effect of lamp temperature on light spectrum and hence light shift that we see here is probably related to the increasing amount of self-reversal seen in our lamps with increasing temperature.

2. Filter Cell

In this section we demonstrate how buffer gas pressure, length, and temperature of the filter cell are adjusted in order to obtain the desired LTP at the FSU operating conditions.

Figure 2-13 shows light shift versus filter temperature for three different filter cells. Throughout this measurement, the resonance cell 1-923 is used, and the temperatures of lamp and the resonance cell were held constant. From curve 2 of Figure 2-13, the LTP is found with the filter cell 2-1283 at 87.7°C.

Figure 2-14 shows the light shift dependence on lamp temperatures as a function of filter cell temperature. It demonstrates that more than one LTP can be realized by adjusting both lamp and filter cell temperatures simultaneously. The negative slope of the curves shown in Figures 2-13 and 2-14 are typical of our design.
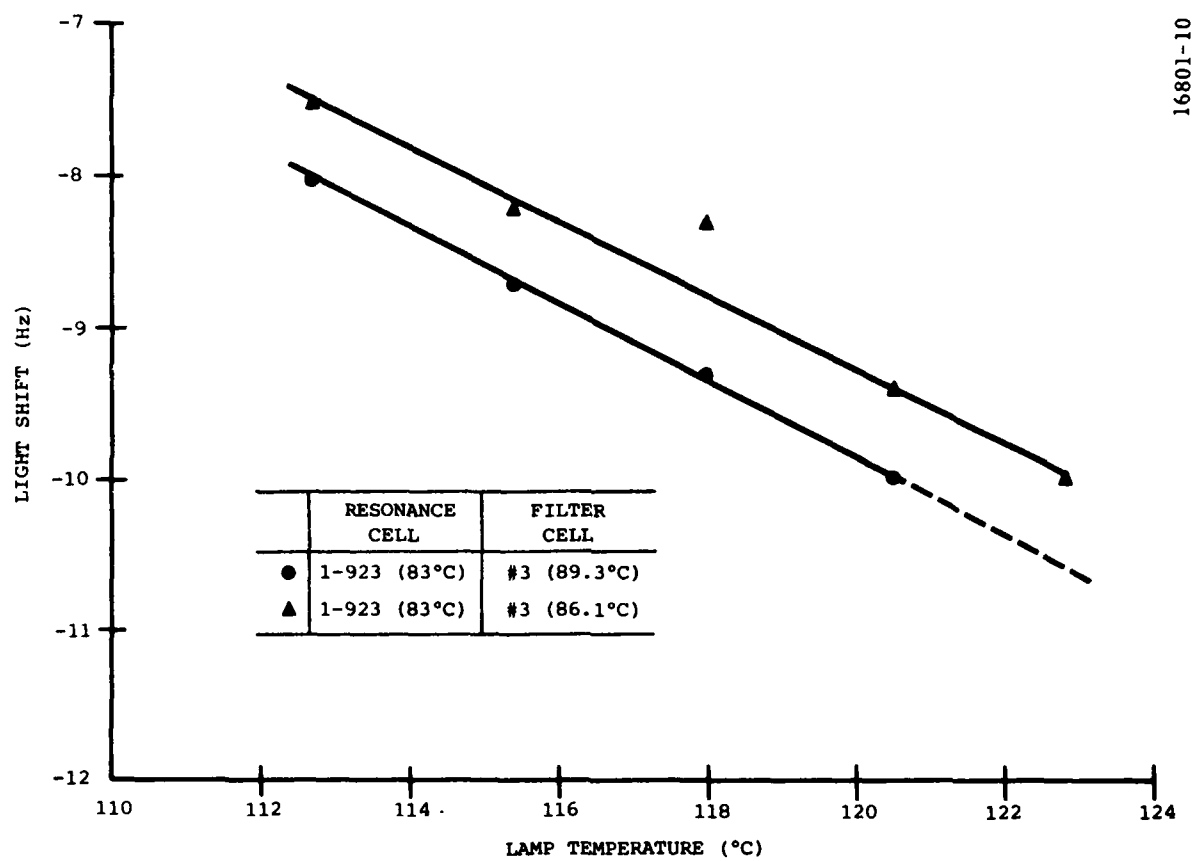
Figure 2-11. Light Shift vs Lamp Temperature
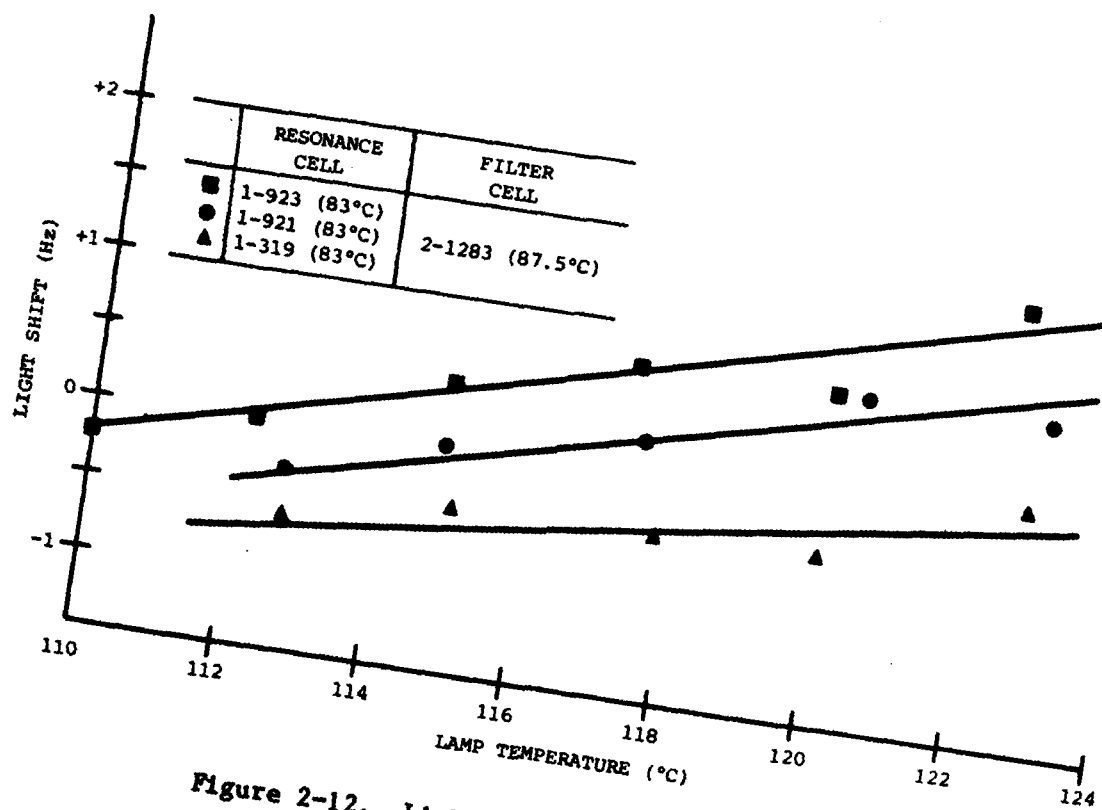
Figure 2-12. Light Shift vs Lamp Temperature

	RESONANCE CELL	FILTER CELL
■	1-923 (83°C)	
●	1-921 (83°C)	
▲	1-319 (83°C)	2-1283 (87.5°C)

16801-11
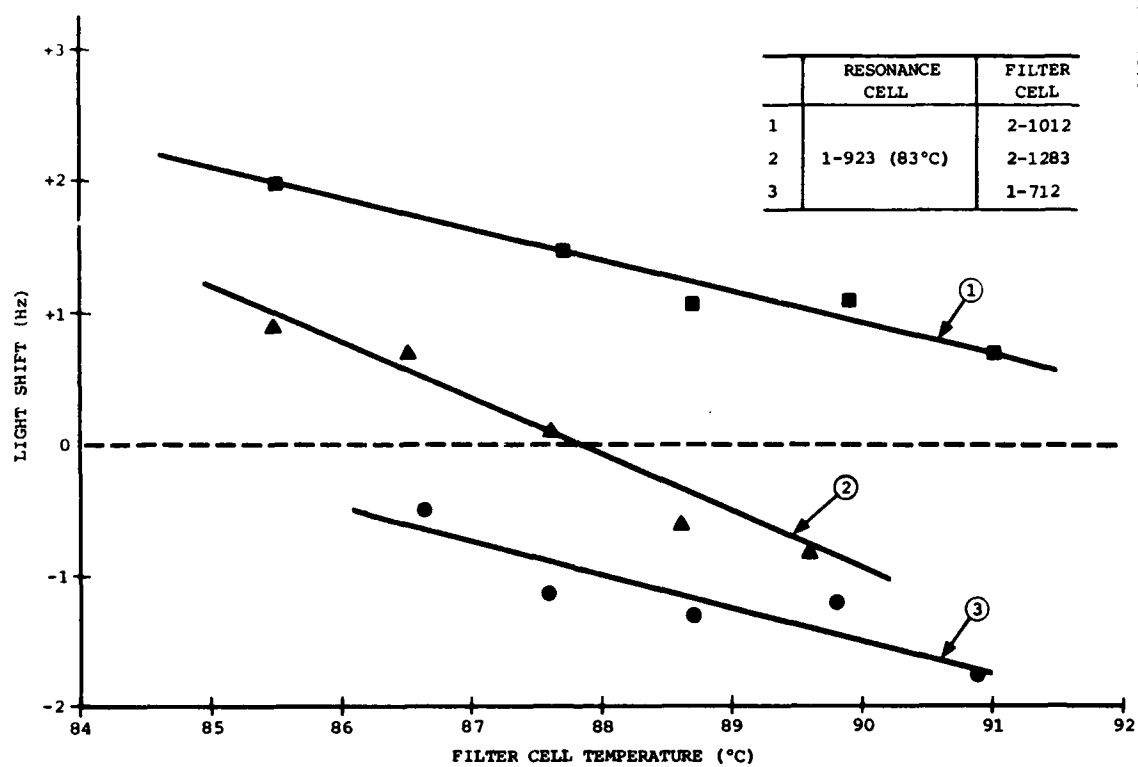
Figure 2-13. Light Shift vs Filter Cell Temperature

2-24
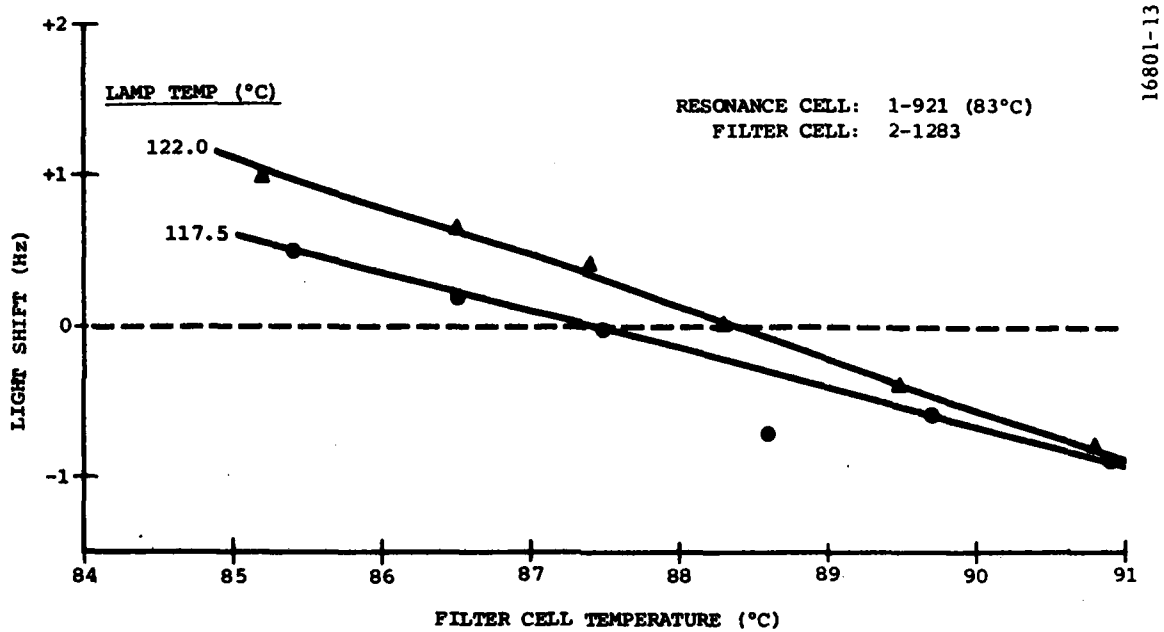
Figure 2-14. Light Shift vs Filter Cell Temperature

16801-13

2-25

In Figures 2-15 and 2-16, the light shift is plotted as a function of N_2 and Ar pressures, respectively, in the filter cell. In general, for a fixed filter cell length and fill pressures greater than 30 torr, the light shift increases with increasing buffer pressure from large negative through zero to positive values. This behavior is found for both N_2 and Ar. In order to realize the zero light shift condition, twice as much N_2 pressure as that of Ar is required. This is related to the fact that the physical constants such as spectral shift and broadening which determine the filtering of ^{87}Rb light by the ^{85}Rb filter are different for Ar and N_2.

For a fixed buffer gas pressure in the filter cell, the light shift increases monotonically with decrease in the filter cell length (Figure 2-17). This is thought to be caused by the decrease in optical thickness, similar to the previous effect that light shift increases as temperature of the filter cell decreases. The filtering action by the filter cell for each spectral component of the light can be analytically described by the form of exp (-kL), where L is the filter length and k an absorption coefficient. From this, we see that temperature and length enter the same way into the spectral filtering (and hence the light shift).

For filter pressures less than 30 torr, the opposite behavior is observed with light shift increasing in a positive sense with decreasing filter buffer pressure. A zero light shift condition is realized in the vicinity of 10 torr buffer pressure. This LTP could be a candidate for our use except that the signal to noise given by a 10 torr filter is significantly less than given by the higher pressure filters. This LTP observed with a 10 torr filter cell is analogous to that obtained in the "integrated filter" type of Rb FSU.
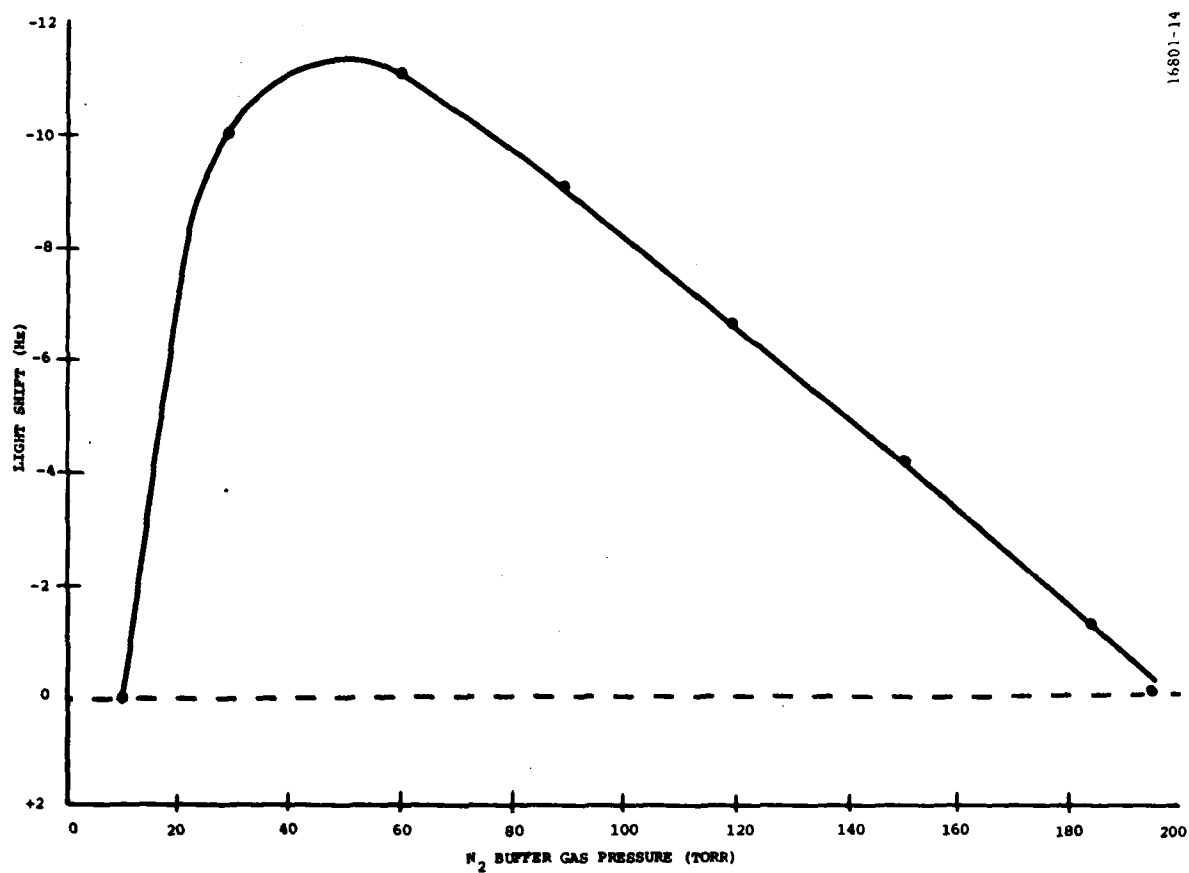
Figure 2-15. Light Shift vs N_2 Buffer Gas
Pressure of Filter Cell
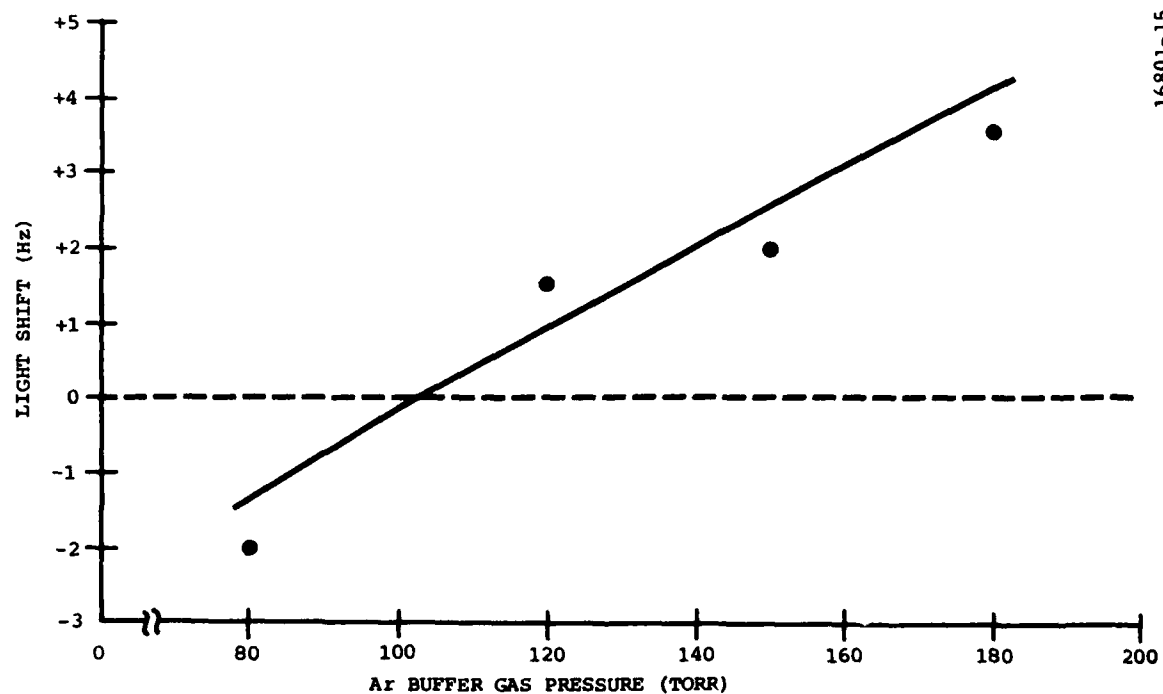
Figure 2-16. Light Shift vs Ar Buffer Gas
Pressure of Filter Cell
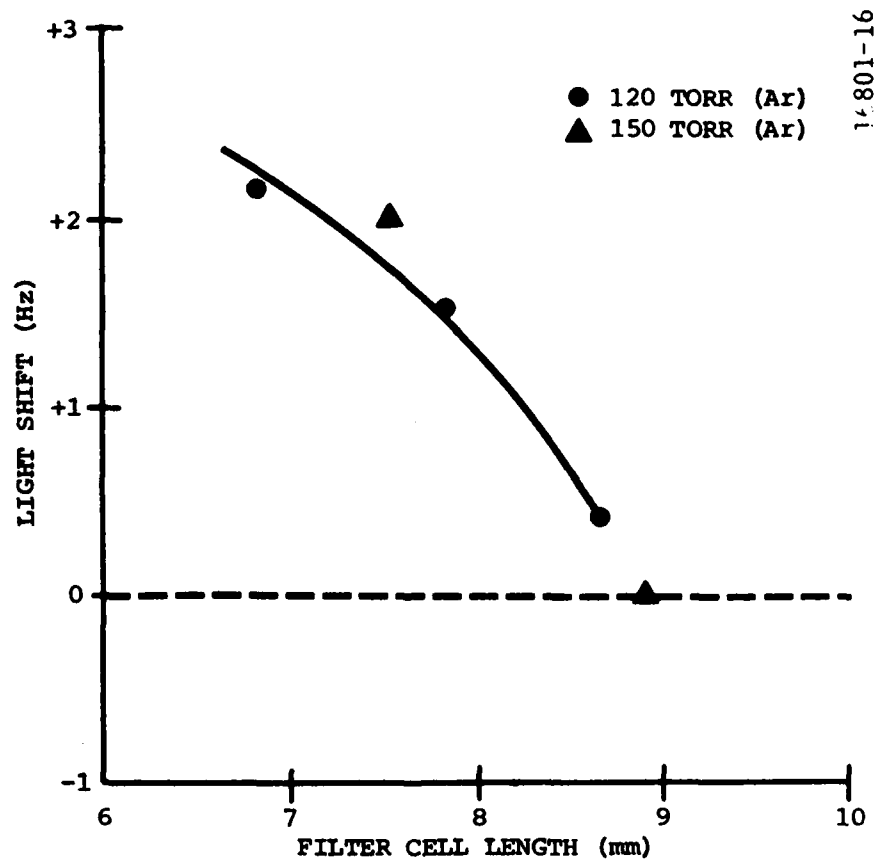
Figure 2-17. Light Shift vs Filter Cell Length

Figure 2-18 is the plot of ^{87}Rb clock transition frequencies at the oper-
ating conditions corresponding to those of Figure 2-14. As the light shift
becomes less positive, the clock frequency decreases. The FSU output frequency
sensitivity to the fitler cell temperature is obtained from the slope of curves
in Figure 2-18 at the operating temperature.

3. Resonance Cell

In the preceding sections of this report we have shown how clock fre-
quency is strongly dependent on the Rb light spectrum integrated over the
resonance cell. This integrated spectrum is determined by lamp temperature,
filter cell design and temperature and to a lesser extent the resonance cell
itself. Not only is clock frequency itself altered by the light shift phenom-
ena but also the temperature coefficient of the resonance cell, i.e., change
in frequency with temperature. Figures 2-19 through 2-21 show the change in
resonant frequency of three different resonance cells with the same filter
cell. The data in all cases was taken at or very near the LTP's. More than
one LTP is possible by adjusting both lamp and filter temperatures appropri-
ately. Here each curve represents different LTP conditions.

The FSU output frequency sensitivity to the resonance cell temperature
is obtained from the slope of curves shown in Figures 2-19 through 2-21. The
temperature sensitivity of a resonance cell arises from the pressure shift of
the ^{87}Rb hyperfine transition frequency. This effect gives a contribution, υ_B,
to the resonant frequency and to the resonance cell temperature coefficient,
$T_c B$. At 83°C, they are shown to be[2]:

$$\upsilon_B \text{ (Hz)} = 572\ P_{N_2} - 63\ P_{Ar} \tag{1}$$
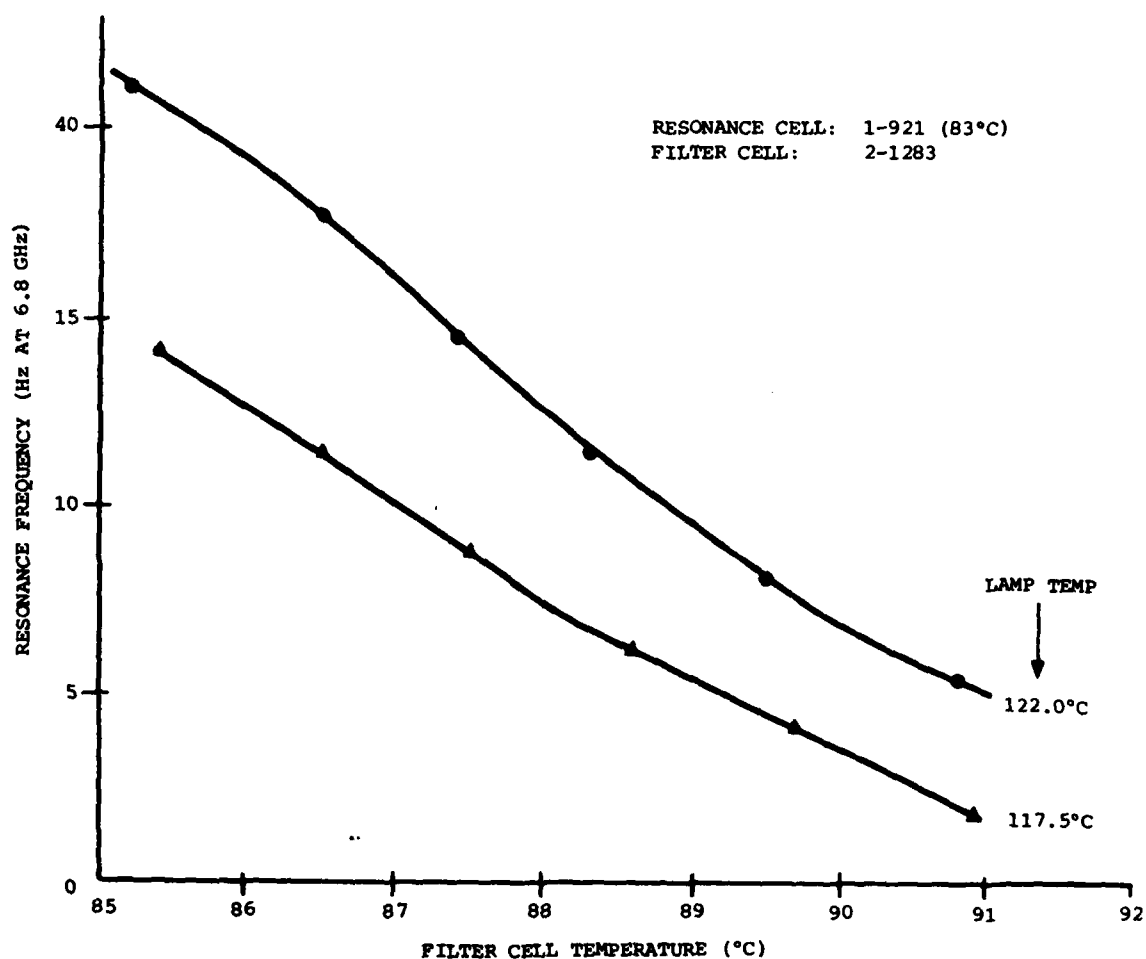
Figure 2-18. ^{87}Rb Resonance Frequency vs Filter Cell Temperature
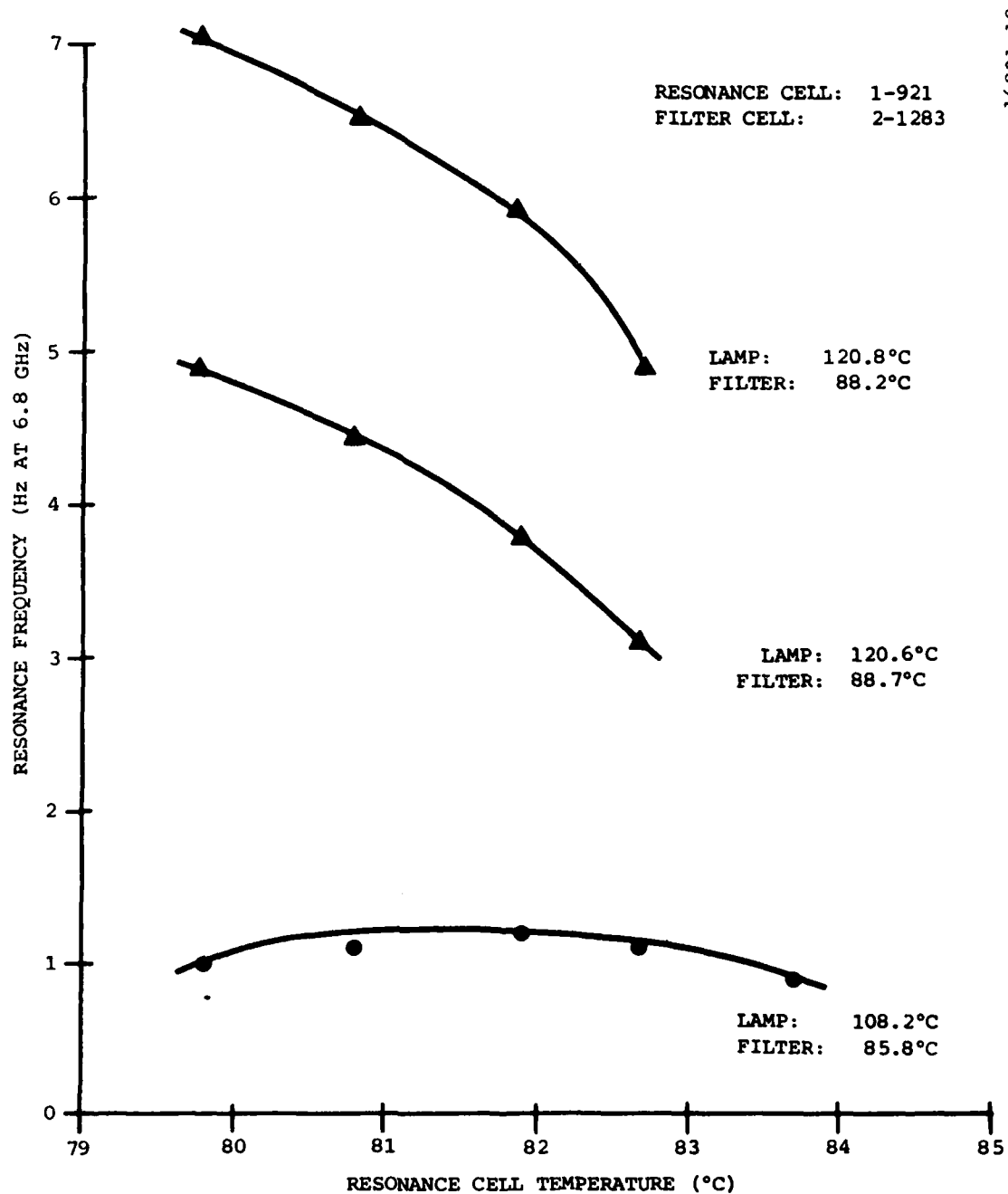
Figure 2-19. ^{87}Rb Resonance Frequency vs Resonance Cell Temperature
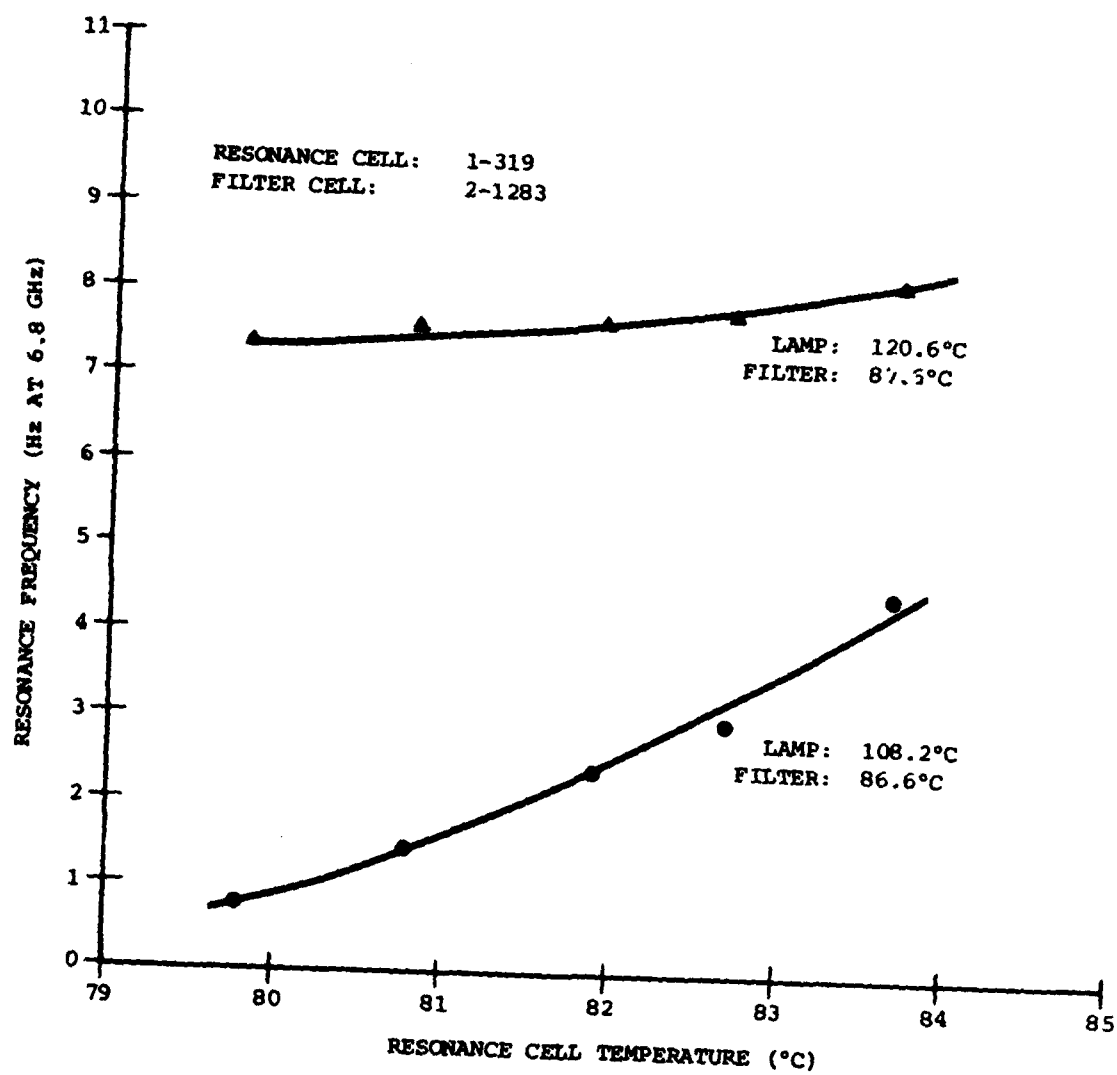
Figure 2-20. ^{87}Rb Resonance Frequency vs Resonance
Cell Temperature
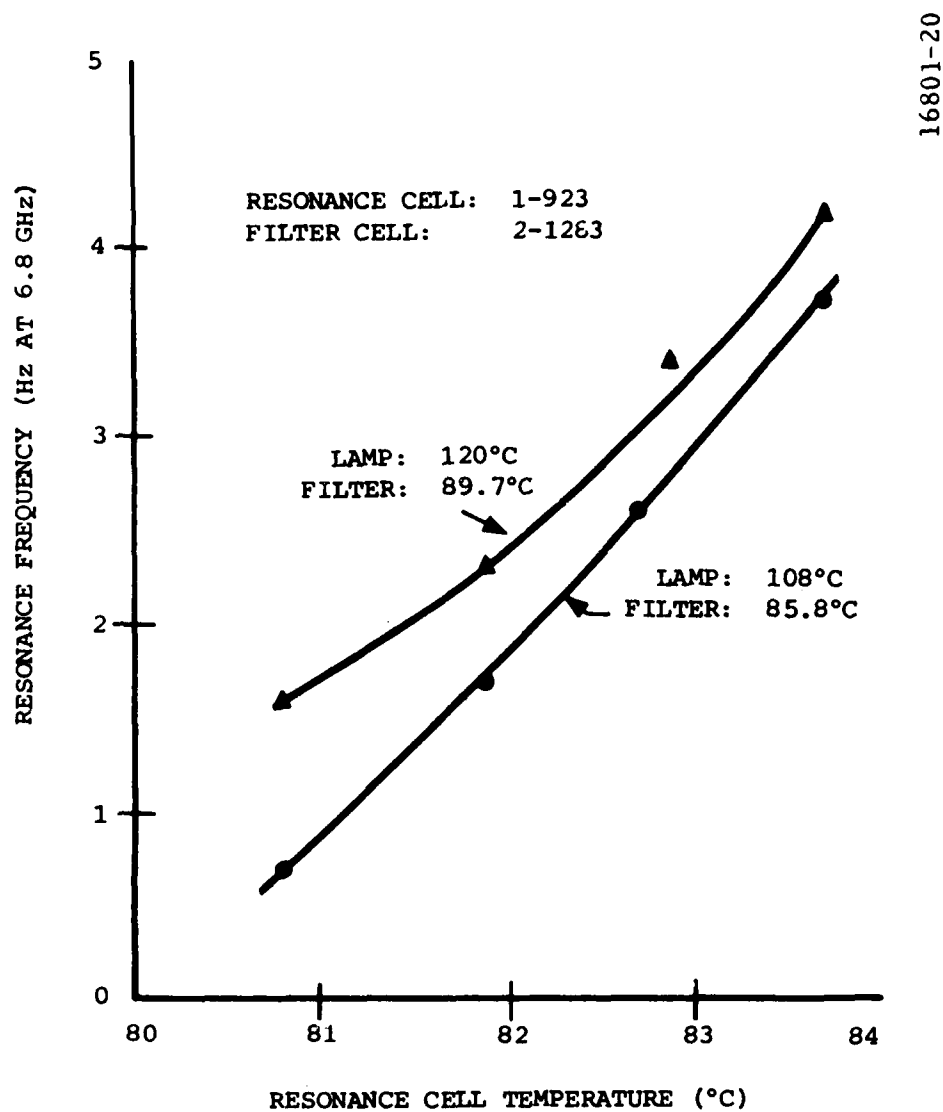
Figure 2-21. ^{87}Rb Resonance Frequency vs Resonance
Cell Temperature

16801-20

2-34

$$T_c{}^B \text{ (Hz/°C)} = 0.54\ P_{N_2} - 0.35\ P_{Ar} \tag{2}$$

where P_{N_2} and P_{Ar} are the buffer gas pressures of N_2 and Ar, respectively, in units of torr. Equations (1) and (2) demonstrate that there exists the freedom to independently adjust υ_B and $T_c{}^B$.

The clock transition frequency, υ_0, is shown to be:

$$\upsilon_0 = 6{,}834{,}682{,}613. + \upsilon_B + \upsilon_H + \upsilon_L \tag{3}$$

where υ_H is the contribution from the static dc field and υ_L is the light shift residual. The 6.8 GHz frequency synthesizer of Litton design provides $\upsilon_0 = 6{,}834{,}687{,}500.$ Hz which is chosen primarily due to simplicity of the circuit design. For the static field of 350 m Gauss, the cell is filled with buffer gases to give $\upsilon_B \approx 4835$ Hz. Among the infinite number of pressure combinations that would result in the designed υ_B, the particular combination is chosen through the requirement for $T_c{}^B$. Such conditions are satisfied when $P_{N_2} \approx 10$ torr and $P_{Ar} \approx 14$ torr.

Figures 2-19 through 2-21 correspond to the cells with increasing buffer gas ratio of P_{N_2}/P_{Ar}. Examination of the figures indicate that $T_c{}^B$ could be made acceptably small at the particular mixture ratio for a given operating condition. This feature is not found in the single buffer gas resonance cell in the temperature range of interest.

An added constraint on the resonance cell buffer gases is that there be sufficient N_2 pressure to quench the re-emission of Rb resonance radiation. At the higher cell temperature range, this constraint is more severe. Figure 2-22 shows how the discriminator curve slope increases with N_2 pressure. At our operating fill of near 10 torr N_2 the re-emission is fairly well "quenched."
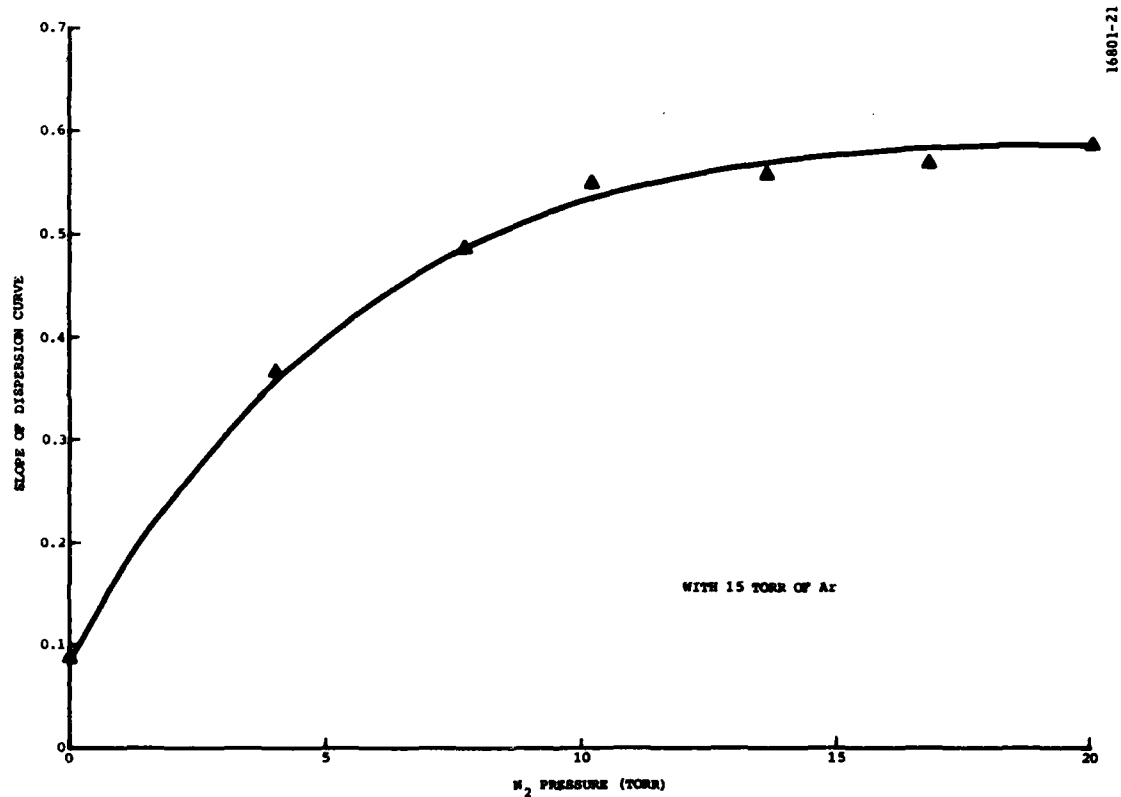
Figure 2-22. Slope of ^{87}Rb Resonance Dispersion Curve vs
N_2 Buffer Gas Pressure of Resonance Cell

2.2.3 Parameter Optimization

As mentioned previously, the physics package must be designed to meet a variety of criteria. Lamp temperature should be less than 120°C to maximize lifetime, but above 115°C to produce sufficient signal to noise. The filter cell should operate above 85°C due to the restrictions in the thermal design. For the same reason the resonance cell should operate in the vicinity of 83°C. The physics package as a whole should operate at a LTP. This LTP should extend over as wide a range as possible to allow for environmentally induced changes in system operating point. Temperature coefficients of the three physics elements should be as low as possible.

Figures 2-23 and 2-24 show physics package parameters at several candidate operating points for the combination of resonance cell 1-921 and filter cell 2-1283. The lamp temperatures are held constant, 109.8C for Figures 2-23 and 116.8C for Figure 2-24. The figures at the top are the plots of ^{87}Rb clock transition frequency versus resonance cell temperature as a function of filter cell temperature. The slope of the curves at the operating resonance cell temperature represents the frequency sensitivity of the resonance cell to the temperatures. The differences in frequency for the two curves in the same figure result in the frequency sensitivity of the filter cell to temperature. By comparing the frequencies in Figure 2-23(a) with those in Figure 2-24(a), the frequency sensitivity of the lamp to temperature is obtained. The light shifts are shown in the bottom figures.

In Figure 2-23, the lamp temperature (109.8C) is too low for optimum signal, but gives a broad LTP for filter cell temperatures near 88.8°C. The resonance cell temperature coefficient at this filter temperature is sufficiently low to be acceptable, −0.2 Hz/°C, near 83°C resonance cell temperature. The
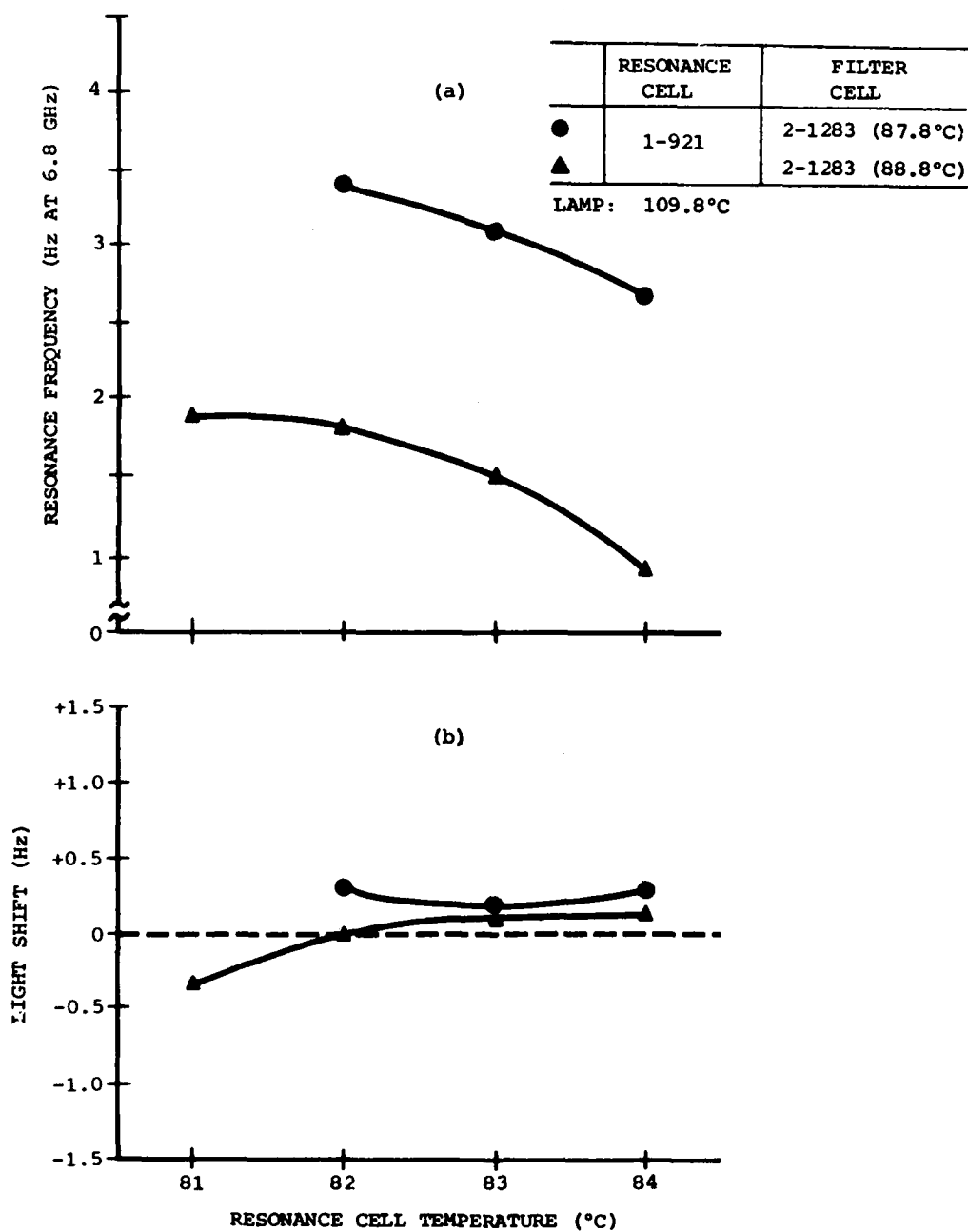
Figure 2-23. (a) ^{87}Rb Resonance Frequency and (b) Light
Shift vs Resonance Cell Temperature

	RESONANCE CELL	FILTER CELL
0	1-921	2-1283 (89.8°C)
X		2-1283 (90.8°C)

LAMP: 116.8°C

16801-23

(a)

RESONANCE FREQUENCY (Hz AT 6.8 GHz)

(b)

LIGHT SHIFT (Hz)

RESONANCE CELL TEMPERATURE (°C)

Figure 2-24.   (a) ^{87}Rb Resonance Frequency and (b) Light
Shift vs Resonance Cell Temperature

microwave sensitivity for the operating point is also acceptably low,
+0.2 Hz/db. Filter cell and lamp temperature coefficients, however, are quite
high, -1.5 Hz/°C and +1.0 Hz/°C, and may not be acceptable.

Figure 2-24 shows improved LTP condition and microwave sensitivity over
those in Figure 2-23 but slightly degraded resonance and filter cell tempera-
ture coefficients, -0.5 Hz/°C and -1.7 Hz/°C, respectively.

Figure 2-25 shows physics package parameters at several FSU operating
points using resonance cell 1-319 and the filter cell used previously, 2-1283.
The buffer gas fill for this resonance cell has been adjusted to give an
increased positive T_c^B over cell 1-921. The operating point with lamp at
119.5C and filter at 86.5C shows a negligible resonance cell temperature coef-
ficient and a very broad LTP with changes in filter, lamp, and resonance cell
temperature. Light shifts are below 0.2 Hz in this region. The filter and
lamp temperature coefficients are again quite high, -2.5 Hz/°C and +1.5 Hz/°C
respectively. The microwave sensitivity has increased over the cell 1-921 to
+0.5 Hz/db.

Figures 2-26 and 2-27 are given for resonance cell 1-923 filled with buf-
fer gas to give a further increase in T_c^B over the previous cells. The optimum
system operating point among those shown here is with a lamp temperature of
116.7C and filter at 89.8C. Microwave level sensitivity is still quite high
here at 0.4 Hz/db. The lamp temperature coefficient is about +1.0 Hz/°C and the
filter cell coefficient is -2.2 Hz/°C.

In summary, we have shown through the data presented that most of the
design criteria can be achieved with the physics elements operating in the tem-
perature range of the Litton design. Double buffer gas fills in the resonance

2-40
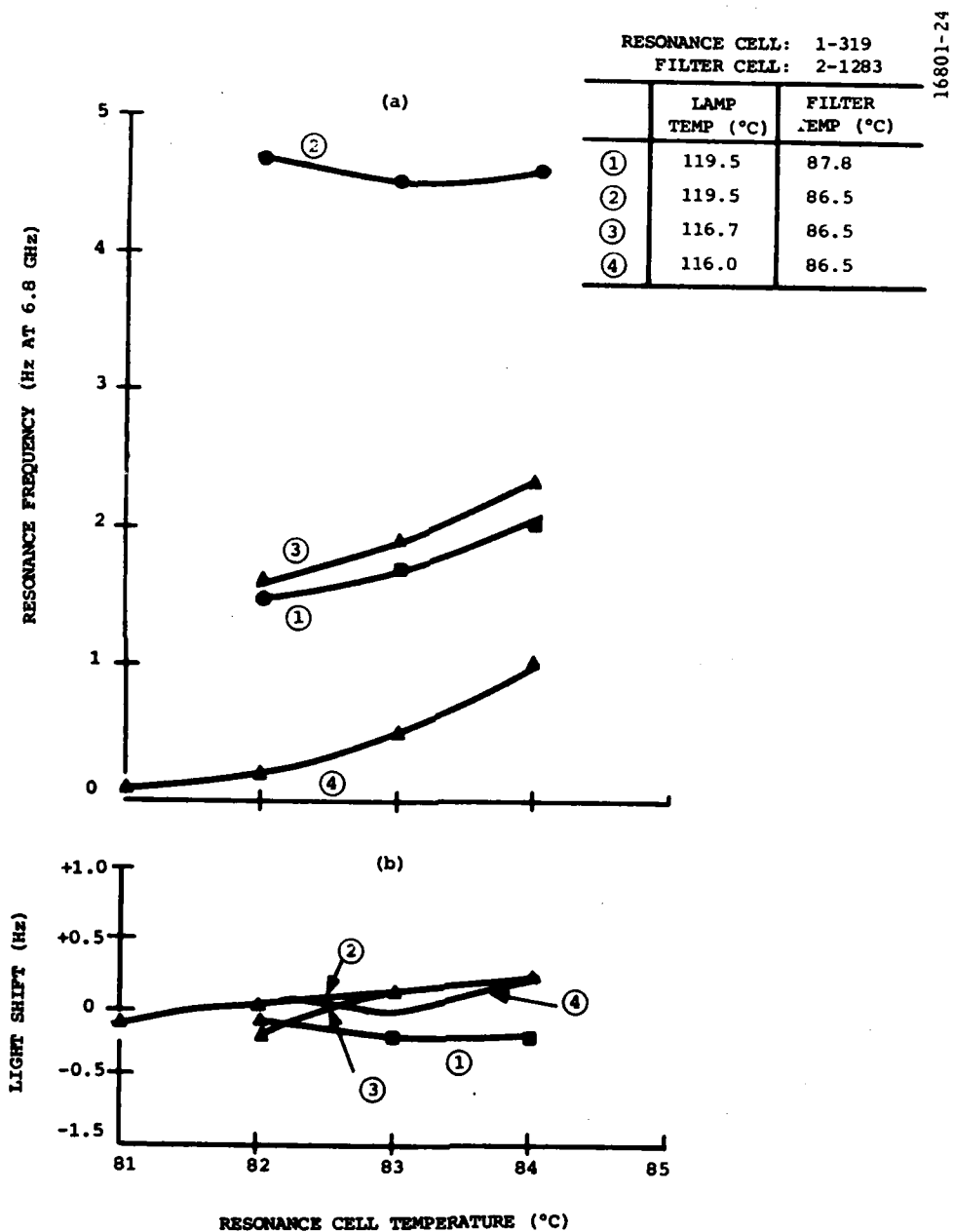
Figure 2-25. (a) ^{87}Rb Resonance Frequency and (b) Light
Shift vs Resonance Cell Temperature
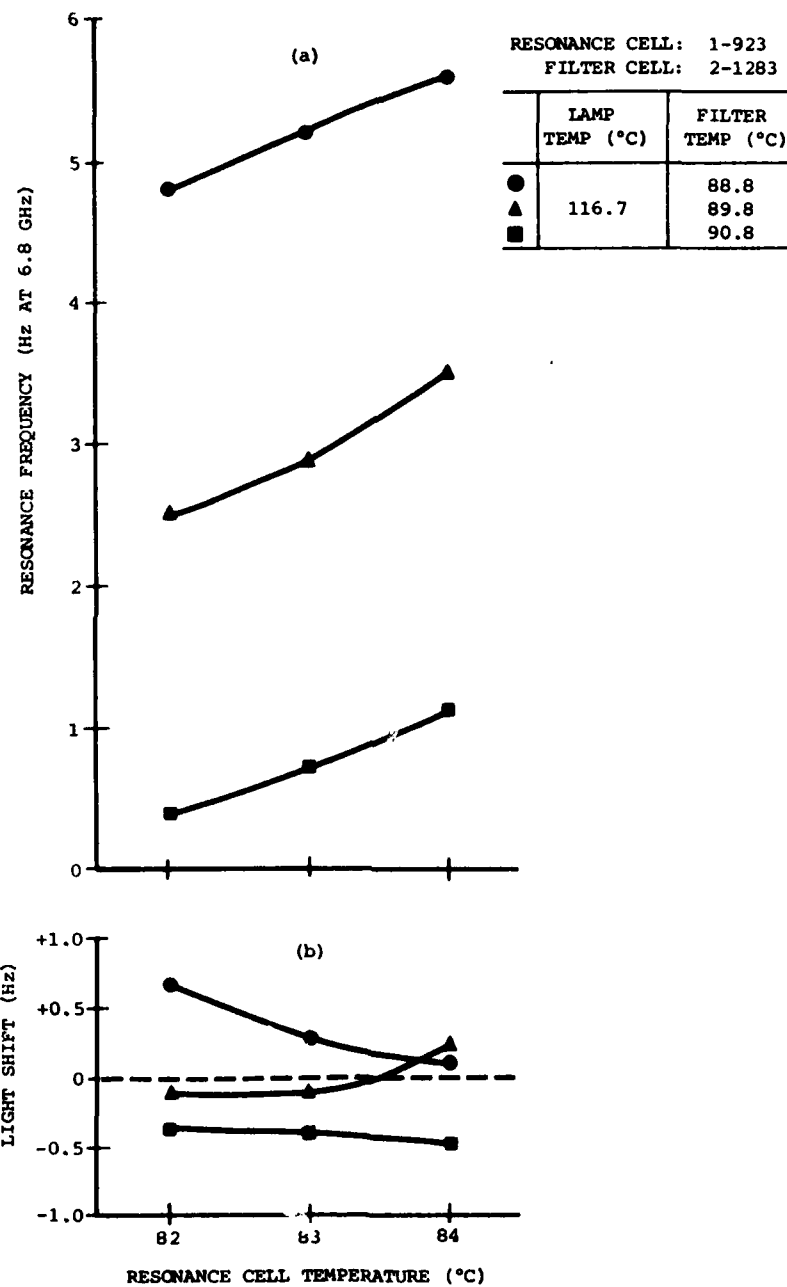
Figure 2-26. (a) ^{87}Rb Resonance Frequency and (b) Light
Shift vs Resonance Cell Temperature

RESONANCE CELL: 1-923
FILTER CELL: 2-1283

I801-26

	LAMP TEMP (°C)	FILTER TEMP (°C)
●		87.8
	109.8	
▲		88.8

RESONANCE FREQUENCY (Hz AT 6.8 GHz)

LIGHT SHIFT (Hz)

RESONANCE CELL TEMPERATURE °C)
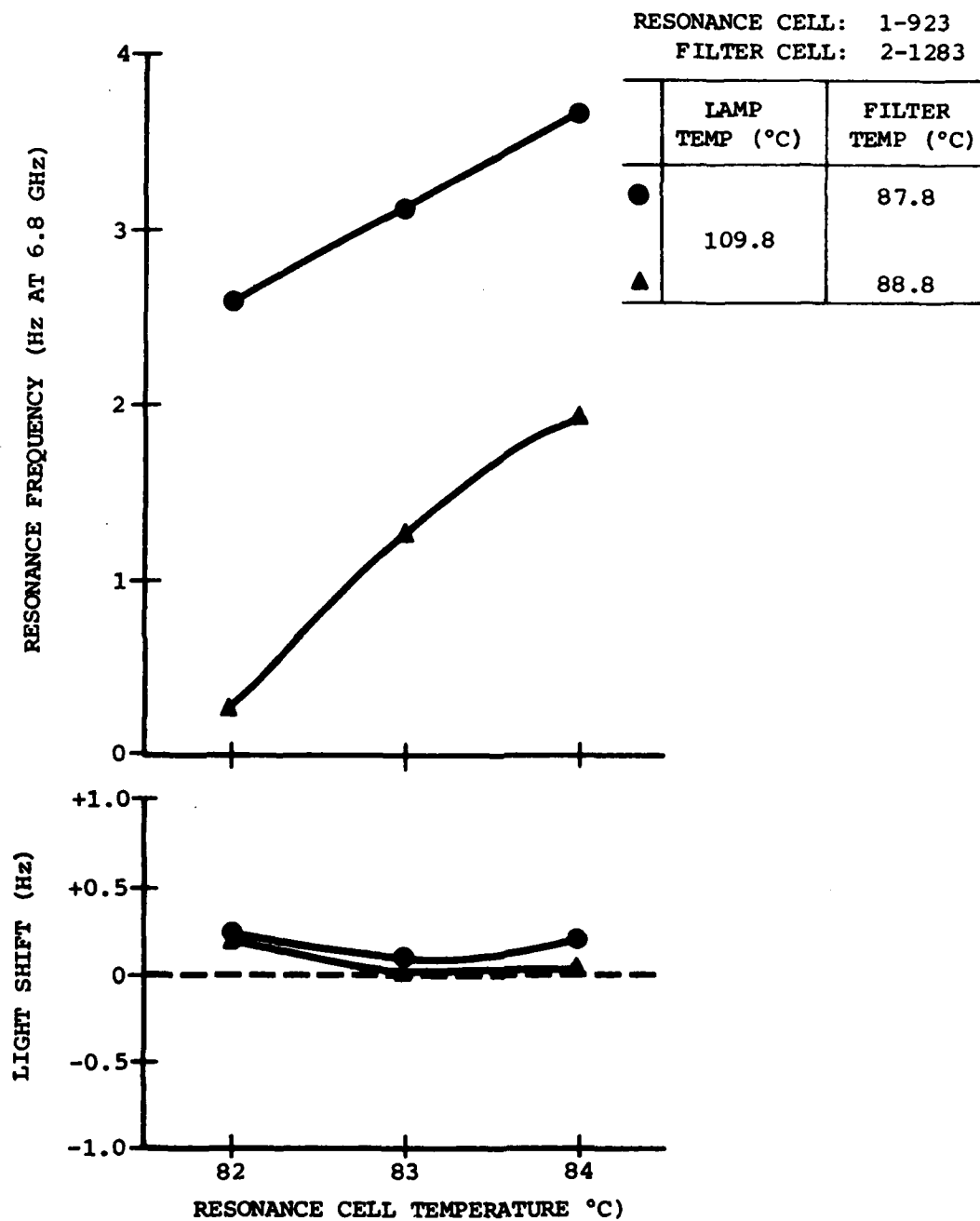
Figure 2-27. (a) ^{87}Rb Resonance Frequency and (b) Light
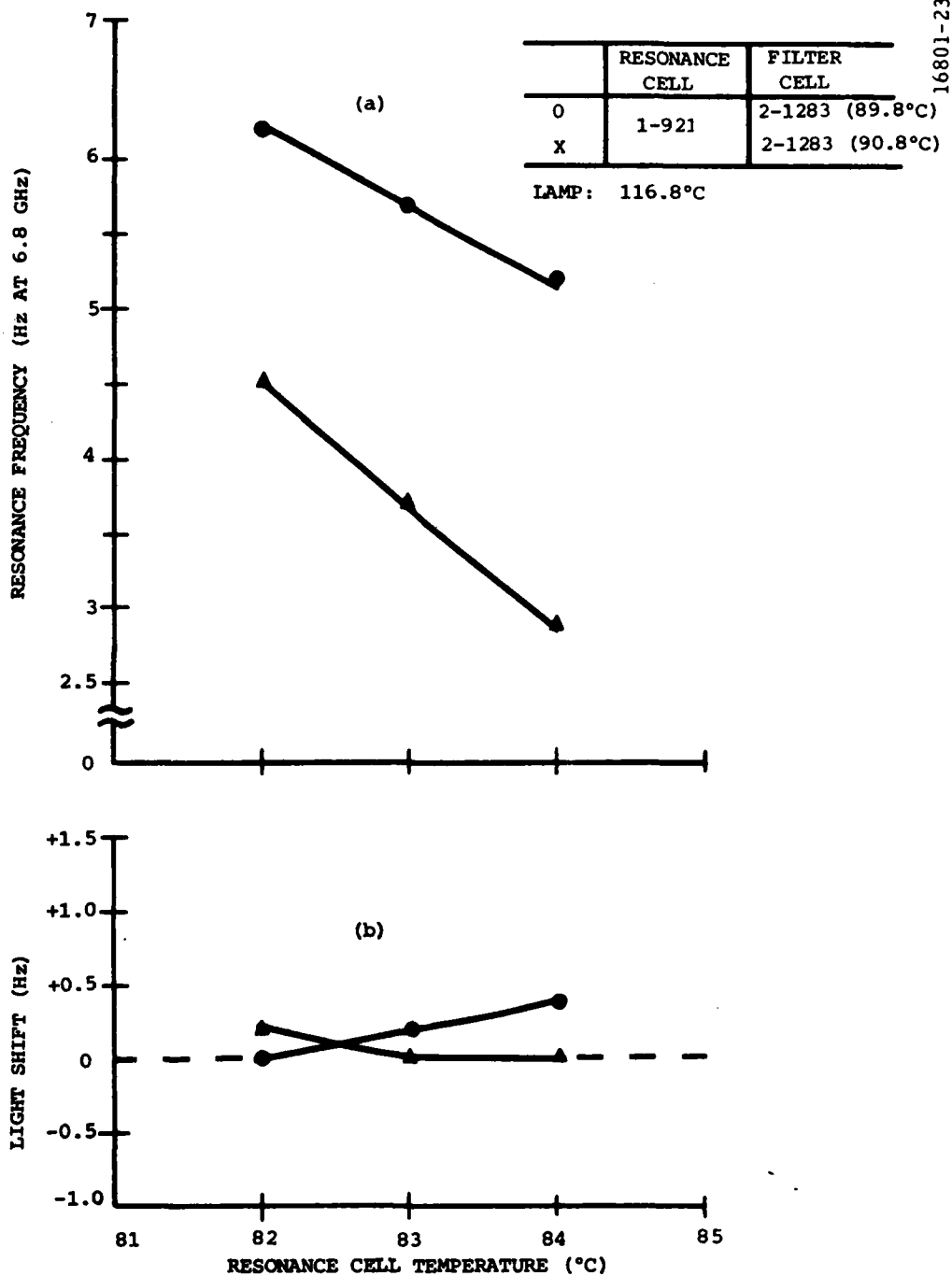Shift vs Resonance Cell Temperature

2-43

cell are shown to be capable of producing the net resonance cell temperature coefficient that exceeds the performance goal of a tactical Rb FSU. A broad region of low light sensitivity is obtained. The large negative filter cell coefficient -2 Hz/°C remains as a potential limiting source for obtaining the required FSU performance over the environmental range.

2.3 PHYSICS PARAMETERS FOR TACTICAL Rb FSU

The preliminary experimental results presented in the previous sections have led to the optimum design parameters for the physics package that exceeds the performance goal for a tactical Rb FSU.

The optimum design configuration of the physics package consists of ^{87}Rb lamp, filter cell 245 and resonance cell 241. The 6.8 GHz microwave cavity is of Litton design as described previously.

The filter cell 245 is 8 mm in overall length and is filled with 115.0 torr of Ar. The double buffer gas scheme implemented in the resonance cell 241 consists of N_2 and Ar. The cell is filled first with 10 torr of N_2 to produce the ^{87}Rb resonance frequency of 6,834,688,049. Hz under a local earth magnetic field environment. After the N_2 fill, 14 torr of Ar is added to obtain the net resonance frequency of 6,834,687,351. Hz before the cell is sealed off. After the cell is aged for several days at 80°C, the desired frequency of 6,834,687,500. Hz is obtained under the static magnetic field of 630 mG. The lamp is of conventional design filled with 2.5 torr of Xe.

The optimum operating temperatures are as follows:

Lamp: 116 - 117 °C

Filter Cell: 90.5 - 91.0°C

Resonance Cell: 82.7 - 83.2°C

Figure 2-28 demonstrates existence of the light turning point at the operating temperatures. In the figure, the ^{87}Rb clock transition frequency is plotted as a function of filter cell temperature for two different light intensities, 100% and 85%. The point that the two curves cross each other represents the LTP.

The measured temperature sensitivities at the operating conditions are summarized in the following:

Lamp: $\approx 2 \times 10^{-11}/°C$

Filter Cell: $\approx -1.9 \times 10^{-10}/°C$

Resonance Cell: $<2 \times 10^{-11}/°C$

Figure 2-29 is the typical performance of the entire physics package when it is subjected to the environmental temperature chamber. The 10 MHz output of the Litton FSU is plotted as the chamber temperature is varied from -55C to +60°C. The data are contiguous, and show the frequency behavior at the temperature transient. The noise spike shown when the chamber temperature is raised from -9C to +31C is due to the moisture collected on the circuits that were not conformally coated at the time of this test. The maximum frequency excursion shown in the figure is $<1.8 \times 10^{-10}$, and represents a typical performance. Maximum frequency excursion of less than 1×10^{-10} over the entire operating ambient temperture range has been measured on a similar physics package to that reported here. Litton believes that the performance of the finalized physics package design is adequate for use in a tactical Rb FSU with comfortable margin.
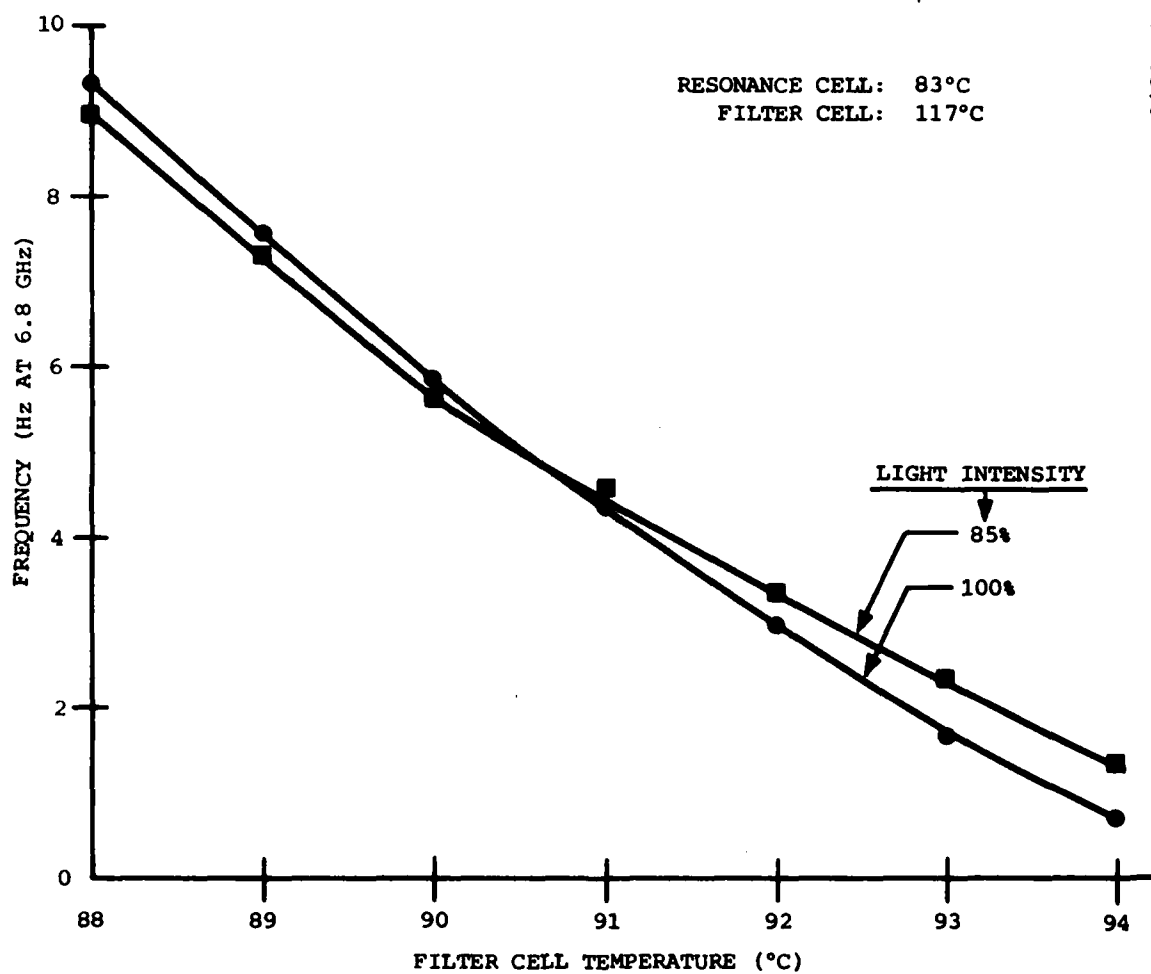
Figure 2-28. ^{87}Rb Resonance Frequency vs Filter Cell Temperature

2-46
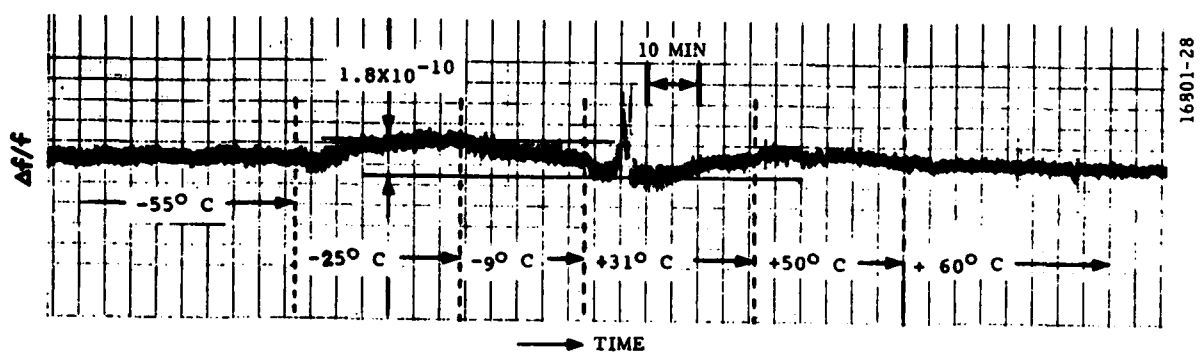
Figure 2-29. Ambient Temperature Test Result of
Litton Physics Package

REFERENCES

1. Leon Malnar and Henri Brun, "Optical Resonance Cells Containing an Alloy of an Alkali Metal with Another Metal," U.S. Patent No. 3577069, February 5, 1968.

2. G. Missout and J. Vanier, IEEE Trans. Instr. Meas. $\underline{24}$ 180 (1975)

3. B.S. Mathur, H. Tang, and W. Happer, Phys. Rev. $\underline{171}$ 11 (1968)

4. J.C. Camparo, R.P. Frueholtz, and C.H. Volk, Phys. Rev. A $\underline{27}$ 1914 (1983)

5. H.E. Williams, T.M. Kwon, and T. McClelland, Proc. 37th Ann. Symp. Freq. Contrl. (to be published)

6. G. Missout and J. Vanier, Can. J. Phys. $\underline{53}$ 1030 (1975)

SECTION III

BUFFER GAS ADSORPTION PROCESS

3.1 INTRODUCTION

The essential feature of any atomic frequency standard is to realize excellent long-term frequency stability beyond the level that crystal oscillators can offer. The long-term stability, commonly known as frequency aging, is probably the least understood phenomena in the art of the Rb FSU.

The inherent stability of the ^{87}Rb clock transition frequency which steers the VCXO output depends on many parameters. Such parameters may be classified into three functional catagories; electrical, mechanical, and physics parameters. Examples of electrical parameters are the set points of operating temperatures of physics package, the level of rf discharge of the lamp, 6.8 GHz microwave power level, and the magnetic field current, all of which are subject to long-term variations. Mechanical components and material, particularly, those used inside the 6.8 GHz microwave cavity, may age in time resulting in a long-term drift.

The work reported in this section investigated the frequency aging due to the long-term variations of physics parameters. Specifically addressed is the buffer gas adsorption onto the glass cell wall, which is manifested as long-term frequency variations. As will be discussed later in this section, the adsorption characteristics of the glass surface have not been well understood to date. The frequency aging due to physics parameter variations appear to be dependent on the type of glass material, origin and history of the glass, and the resonance cell fabrication processes. Perhaps, lack of understanding on the subject has led to speculation that the fabrication of resonance cells is a kind of "magic". This investigation is intended to be the first step toward the understanding of physics parameter variations in the resonance cell.

3.2 EXPERIMENTAL RESULTS

In order to investigate the nature of the buffer gas adsorption process, two types of experiments were conducted. In a first type of experiment, the 6.8 GHz Rb clock transition frequency of a resonance cell operating at 82°C is monitored in a FSU starting immediately after the cell is sealed off from the cell processing vacuum station. The frequency measurements are continued, typically for several days, until the frequency appears to have reached an equilibrium. In order to distinguish the different conditions of the cell before and after the measurements, we refer to them as "fresh" and "aged" resonance cells, respectively. In a second type of experiment, an aged cell is placed first in a controlled temperature environment where the cell tip region containing Rb reservoir is held at a low temperature while the rest of the cell wall is maintained at an elevated temperature. The intent in this process is to disturb the equilibrium conditions that the fresh cell has attained. Following such disturbances, the cell is installed in a FSU in order to monitor the 6.8 GHz clock transition frequency until it reaches an equilibrium.

Results of the first type of experiments are summarized in Figures 3-1 and 3-2, in which the 6.8 GHz resonance frequency of ^{87}Rb is plotted as a function of time, for an N_2 cell and three all Ar cells, respectively. The initial fill pressures are 10 torr for N_2 and 15 torr for Ar.

Monotonic frequency decrease of ~26 Hz is observed in the all N_2 cell until the frequency appears to have reached an equilibrium after a period of ~40 hours. No such monotonic frequency variation is observed, however, in the all Ar cells. Three different cells, each with the identical fill pressures of Ar, are shown in Figure 3-2. The frequencies of the all Ar cells increase for the first one hour period and subsequently decrease gradually in time. The

3-2

Figure 3-1. ^{87}Rb Clock Transition Frequency of Fresh
All N$_2$ Cell vs Elapsed Time
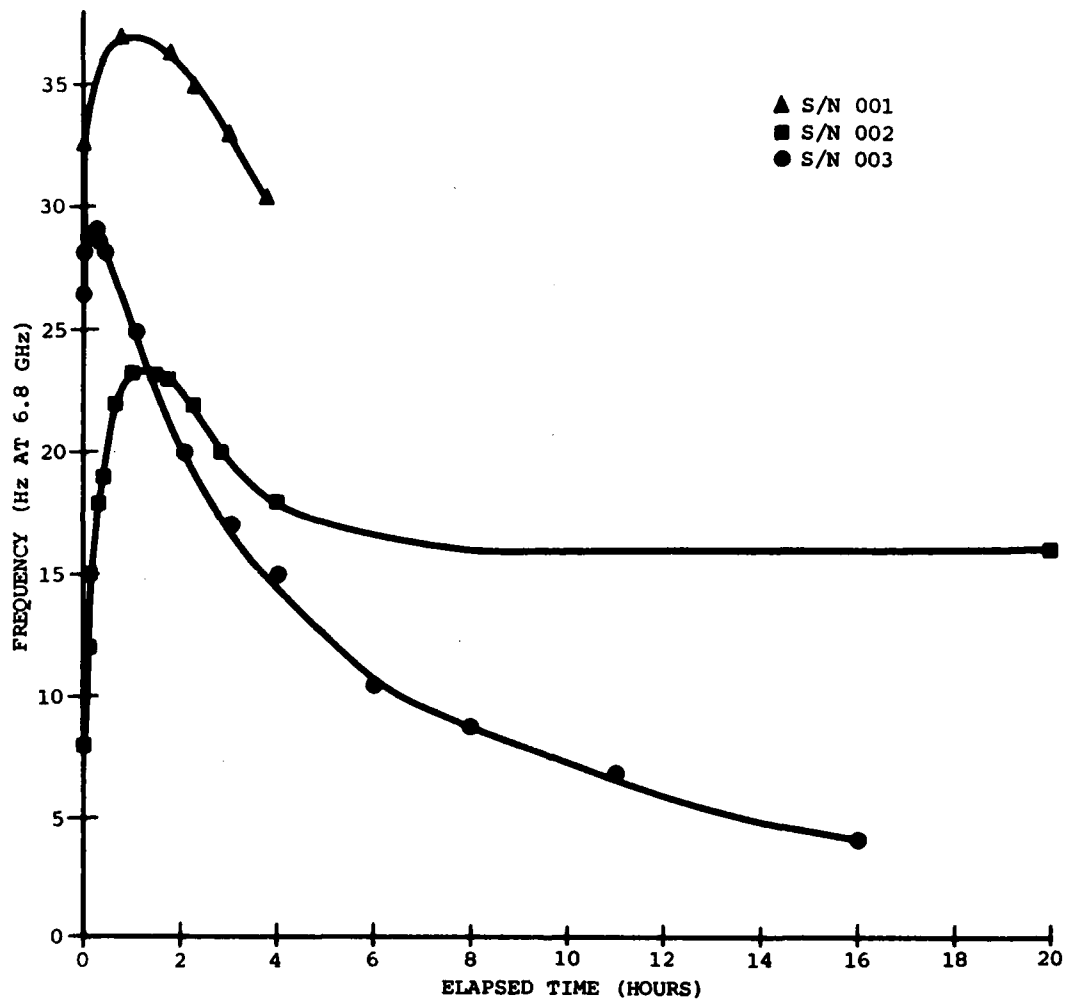
Figure 3-2. ^{87}Rb Clock Transition Frequency of Fresh
All Ar Cell vs Elapsed Time

16801-30

3-4

initial frequency increase ranges from 3 Hz to 15 Hz. The differences in the magnitude of frequency increase from cell to cell are probably due to the differences in time that it took to process the cells on the cell processing vacuum system. The cell processing procedures are described later in Section 3.3. Following the initial increase, the frequency of the all Ar cells decreases gradually by about 25 Hz during the next 15 hour period until an equilibrium is finally established.

The second type of experiments are summarized in Figures 3-3 and 3-4 for an all N_2 cell and for an all Ar cell, respectively. The resonance frequency of 87_{Rb} are plotted in the figures as a function of elapsed time after the cell wall is disturbed as described earlier. The two results show monotonic frequency behavior; decreasing frequency by ~4 Hz for the all N_2 cell and increasing frequency by ~4.5 Hz for the all Ar cell. The all N_2 cell has reached equilibrium in ~8 hours, while the all Ar cell required only an hour to reach frequency equilibrium.

The experimental observations described above are summarized in the following:

1. The all N_2 cell, fresh or aged, shows monotonic frequency decrease. The magnitudes of decrease are ~25 Hz and ~4 Hz with equilibrium times of 40 hours and 8 hours for the fresh and the aged cells, respectively.

2. The fresh, all Ar cells show increase in frequency, the magnitudes of which vary between 3 to 15 Hz depending on the cell processing conditions during the first one hour period.

3. Following the initial increase (No. 2 above), the frequency of the all Ar cells decrease gradually as much as 25 Hz during the next 15 hour period.
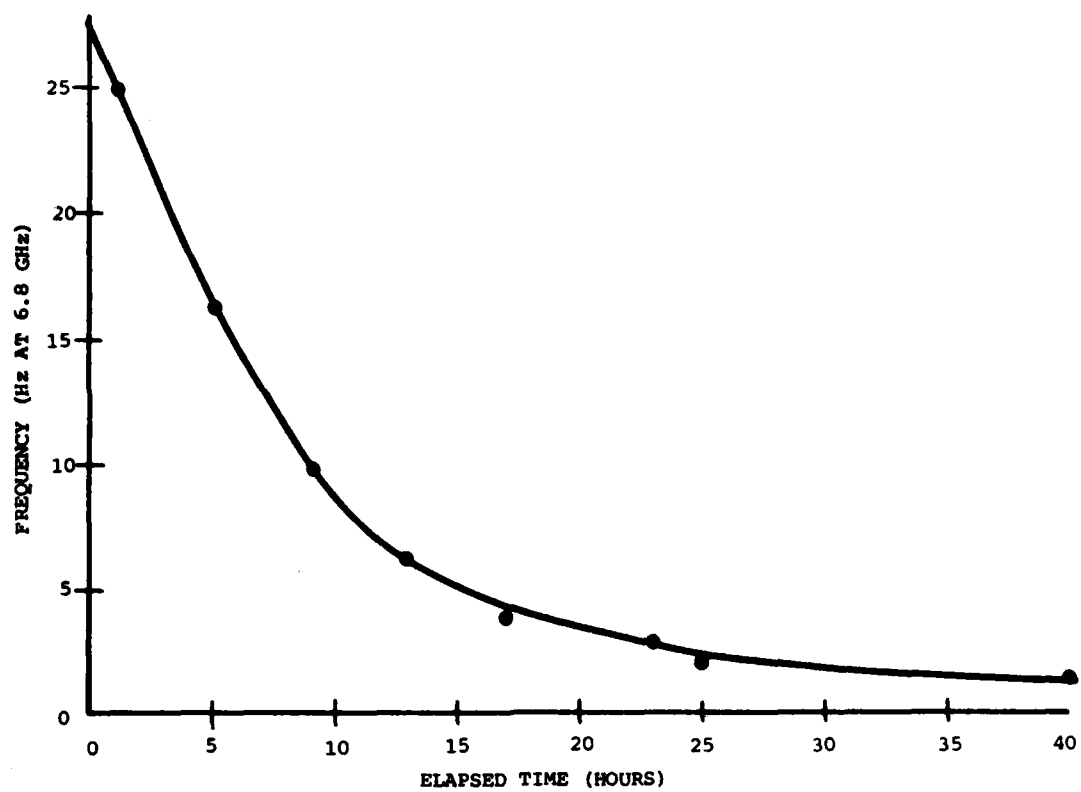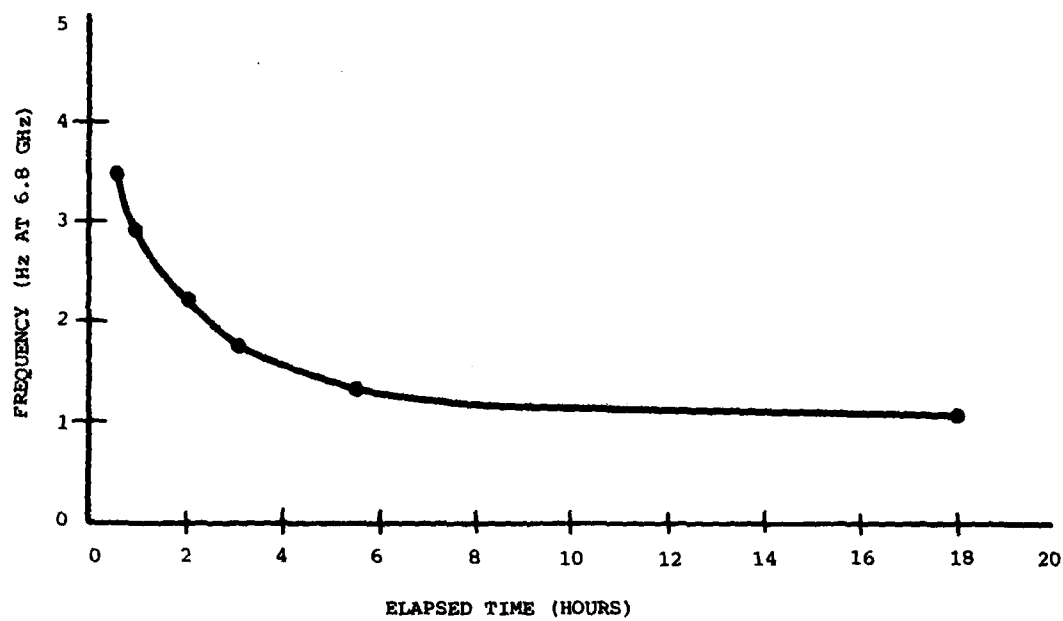
Figure 3-3. ^{87}Rb Clock Transition Frequency of Aged
All N_2 Cell vs Elapsed Time
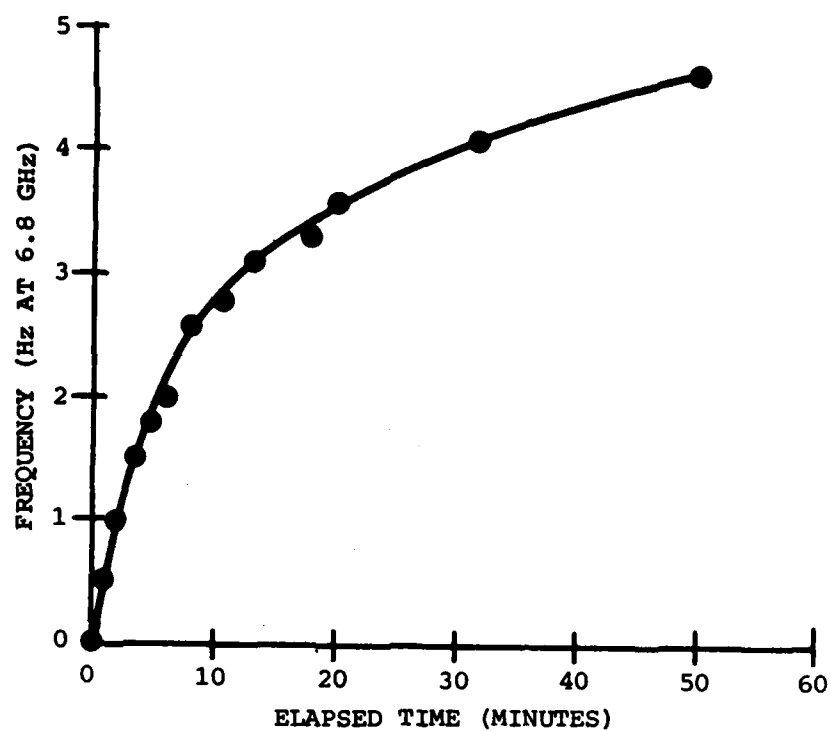
Figure 3-4. ^{87}Rb Clock Transition Frequency of Aged
All Ar Cell vs Elapsed Time

4. In the aged, all Ar cell, only monotonic frequency increase is observed. The magnitude of increase is ~4.5 Hz with equilibrium time of 1 hour.

5. All aged cells (both N_2 and Ar) are characterized by magnitudes of frequency variation which are several times smaller than those of the fresh cells.

6. In the case of the all N_2 cell, the observed equilibrium time for a fresh cell is several times longer than that of an aged cell.

7. The fresh, all N_2 cell does not show directional change in the frequency variation analogous to the condition No. 3 above observed from the fresh, all Ar cells.

3.3 DISCUSSIONS

It is reiterated here that the presence of N_2 buffer increases the ^{87}Rb clock transition frequency, and that the Ar buffer results in a decreased frequency. The decreased frequency observed from both the first and the second type of experiments for the all N_2 cell (Figures 3-1 and 3-3, respectively), and the increased frequency for the all Ar cells (the first one hour data in Figure 3-2 and the data shown in Figure 3-4) are interpreted as results of decreased buffer gas pressure.

Interpretation of the data from the first type of experiment requires understanding of how the resonance cells are processed. The resonance cells are sealed off from the cell processing vacuum station after the buffer gas pressure is precisely adjusted in order to produce a desired resonance frequency of the cell. The pressure adjustments are done, while the cell is still attached to the vacuum manifold, by installing the cell in a test fixture which is essentially a physics package operating as a laboratory version of the FSU.

3-8

The test fixture enables precise pressure adjustments by monitoring the Rb resonance frequency. Repetitive introduction of small pressure increments may be required to reach the desired final pressure. The entire buffer gas filling procedure may take a few hours.

It is expected that the physical process(es) which are responsible for the buffer gas pressure drop have started as soon as the gas is introduced into the vacuum manifold. In fact, when N_2 buffer is introduced, continually decreasing frequency of 87_{Rb} resonance is observed. Repetitive introduction of N_2 in small increments is necessary in order to bring the resonance frequency back up to the desired value. The cell is sealed off when the rate of frequency decrease is manageably small. The frequency variations observed in the sealed cells could well be, therefore, the results of a continuing process of this nature.

The result No. 1 of Section 3.2 for the N_2 cell corresponds to N_2 pressure drops of 0.05 and 0.007 torrs for the fresh and the aged cells respectively. The initial frequency increase, result No. 2, for the fresh all Ar cells corresponds to the Ar pressure drop of between 0.05 and 0.24 torrs. Result No. 4 for the aged all Ar cell amounts to a pressure drop of 0.07 torr. We note here that the pressure drops in Ar are about an order of magnitude larger than those in N_2.

Buffer gas pressure drop is considered to be a result of physical phenomena related to the surface adsorption. The buffer gas absorption, i.e., diffusion into the cell wall material is a long-term process measured in weeks and months, and is not considered here.

Both chemisorption and physical adsorption could cause decrease in the buffer gas pressure. Because of the inert nature of the buffer gases, the chemisorption of high activation energy should not contribute significantly to this process. An attempt is made here to see if the frequency variations could be interpreted on the basis of a simple picture of physical adsorption.

From the kinetic theory, the number of atoms (molecules), σ, on the unit surface area in equilibrium with the gas phase atoms has been shown to be[1]:

$$\sigma = N_c \tau, \tag{1}$$

where N_c is the number of atoms that strike a unit surface area per unit time and that remain there for an average time τ. N_c is given by:[2]

$$N_c = \frac{1}{4} n \overline{V}, \tag{2}$$

where n is the gas phase density and $\overline{V}$ is the mean gas velocity. For 10 torr of N_2 and 15 torr of Ar at 80°C, Eq. (2) is calculated to be:

$$N_c(N_2) = 3.4 \times 10^{21}/cm^2 \ sec \tag{3a}$$

$$N_c(Ar) = 4.2 \times 10^{21}/cm^2 \ sec \tag{3b}$$

Based on the size of the numbers in Eq's (3a) and (3b), adsorption equilibrium is considered to be establed in a very short time ,[1,2] certainly short compared to the time necessary to fill the cells with the buffer gases. The equilibrium times on the order of hours, as we observed in our experiments, can not be explained by a simple surface coverage. It suggests that, in addition to the simple surface coverage, a type of transport mechanism is taking place on the cell wall.

3-10

The adsorption time, τ, in Eq. (1) is shown to be of the form:[3]

$$\tau = \tau_o e^{Q/kT} \qquad (4)$$

where τ_o is the sticking time corresponding to the simple reflections of the incident gas atoms at the surface in the high temperature limit. Q is the adsorption energy, i.e., the amount of energy liberated when the atom is brought from the gaseous state to the adsorbed state.

The exact magnitude of τ_o depends on the translation and vibration modes of freedom of the atomic spieces at the adsorbed site. Values for τ_o between $10^{-12} \sim 10^{-13}$ sec are reported.[1]

Determination of adsorption energy Q requires knowledge of the real surface. The real surface is considered to consist of many adsorption sites each with different adsorption energy.[4] This reflects the condition that the adsorption tends to occur first at sites with the highest Q, with subsequent adsorption associated with lower values of Q. Values of Q's ranging from 0.5 to 10 K cal/mole are reported for Ar and N_2 on the pyrex surface when the surface coverage is less than a complete monolayer.[2,5-7]

Assuming the values of

$$\tau_o = 1 \times 10^{-12} \text{ sec and} \qquad (5a)$$

$$Q = 4 \text{ K cal/mole}, \qquad (5b)$$

the surface density of adsorbed atoms in equilibrium with the gaseous phase are calculated from Eq's (1) through (4) to be:

$$\sigma (N_2) \approx 8.8 \times 10^{11} \text{ molecules/cm}^2 \qquad (6a)$$

$$\sigma (Ar) \approx 1.1 \times 10^{12} \text{ atoms/cm}^2 \qquad (6b)$$

We note here that Eq. (6) represents orders of magnitude less in magnitude than that of the monolayer coverage. The surface density, σ_m, for the monolayer coverage is shown to be:[6]

$$\sigma_m\ (N_2) = 6.2 \times 10^{14}\ \text{molecules/cm}^2 \tag{7a}$$

$$\sigma_m\ (Ar) = 7.0 \times 10^{13}\ \text{atoms/cm}^2 \tag{7b}$$

The total number of atoms, N, adsorbed on the surface is calculated from Eq. (1):

$$N = \gamma A \sigma \tag{8}$$

where γ is a measure of surface roughness, namely the ratio of true surface area to apparent geometric surface area, A. Typically, the true surface area is much larger than the geometric area. The surface roughness appears to depend on its origin and history. Published data taken from pyrex seem to indicate that its surface is nearly flat and non-porous.[6,8] For a certain type of quartz glass, the ratio of as large as 1×10^3 has been reported.[9] We assume the true surface area of the resonance cell reported here to be ≈10 times larger than the geometric area. With $A = 5.0\ \text{cm}^2$, the total number of atoms, N, adsorbed on the glass cell wall is calculated from Eq's. (6) and (8) to be:

$$N\ (N_2) \approx 4.4 \times 10^{13}\ \text{molecules} \tag{9a}$$

$$N\ (Ar) \approx 5.4 \times 10^{13}\ \text{atoms} \tag{9b}$$

Taking the cell volume of $0.7\ \text{cm}^3$, Eqs. (9) are translated into the pressure drop $\Delta\rho$:

$$\Delta\rho\ (N_2) \approx 2.3 \times 10^{-3}\ \text{torr} \tag{10a}$$

$$\Delta\rho\ (Ar) \approx 2.9 \times 10^{-3}\ \text{torr} \tag{10b}$$

and into the shifts in the ^{87}Rb clock transition frequency, Δf:

$$\Delta f\ (N_2) \approx -1.3\ \text{Hz} \tag{11a}$$

$$\Delta f\ (Ar) \approx +0.2\ \text{Hz} \tag{11b}$$

3-12

The agreement between Eq. (11a) and the experimental result, $\Delta f \approx +4.5$ Hz, from the aged, all N_2 cell may be considered in good agreement in view of the assumptions made here. Eq. (10b) predicts that Ar pressure drop would be of the same order of magnitude to that of N_2, and, as a result, the frequency shift would be one sixth of that of N_2. Experimental results show, however, that the two frequency shifts on the aged cells are of the same magnitude (result No. 1 and result No. 4 of Section 3.2). In terms of pressure this would mean that pressure drop is an order of magnitude larger than that in N_2. In order to describe such differences between Ar and N_2, one is forced to assume:

- Surface adsorption energy for Ar is higher than that of N_2, and/or

- Effective adsorption surface for Ar is larger than that of N_2.

Both assumptions appear to be physically acceptable.

One may picture the cell wall having mountains and valleys of many different sizes. The Ar atom may creep into some deep and narrow valleys where N_2 molecules could not because of its larger physical size. This would result in the differences of effective surface area and/or of adsorption energy between Ar and N_2.

Much larger frequency shift observed from the fresh, all N_2 cell, result No. 1 of Section 3.2, than that of the aged, all N_2 cell may also be interpreted with higher adsorption energy or larger surface area than those assumed. It would mean that the cell surface conditions for the fresh cells are substantially different from those of the aged cell. Results shown in No's 5 and 6 of Section 3.2 supports this argument.

The evolving wall adsorption characteristics in time can best be described in an example of Rb resonance cells used in the nucler magnetic resonance (NMR) gyro developed in this laboratory. The NMR cell contains, in addition to ^{87}Rb and buffer gases, one or two noble gas spieces with half integer value of nuclear magnetic moments. The NMR signal is observed from the noble gas nuclear moments precessing about the quantization axis. The role of ^{87}Rb and buffer gas is to align the magnetic moments by optical means and to detect the nuclear signal by mechanizing the Rb system as an atomic magnetometer. The magnitude of precessing noble gas moments decreases exponentially in time with the char- acteristic time equal to the relaxation time. Study indicates the interaction of the noble gas moments with the glass cell wall is seen as a significant source of relaxation. The wall interaction is primarily caused by the noble gas adsorption on the glass surface. The magnetic moments of noble gas aligned initially by the optical means are disoriented while the gas is being adsorbed on the wall causing a decrease in the signal amplitude. The degree of dis- orientation is a function of, among others, the sticking time shown in Eq. (4). The NMR study of relaxation phenomena provides therefore a convenient way of investigating noble gas adsorption onto the Rb resonance cell wall. The study is qualitative in nature, and only limited success has been made to date in the qualitative analysis.

The noble gas signal, as it is measured when the cell is fresh from the cell processing vacuum station, is extremely small, and relaxes rapidly in the order of 10 seconds. As the cell is "aged", however, in a matter of a day or two in an oven at ~80°C, one observes increasing signal as well as increasing relaxation time up to several hundred seconds. The increasing relaxation time in the NMR cells indicates that the noble gas sticking time is decreasing as

3-14

they are aged. Through Eq. (4), this is interpreted as decreasing magnitude of wall adsorption energy. The aging process described above is common for most cells, and is observed routinely in this laboratory and others.[8]

Variations of the wall adsorption energy are manifested as variations in the relaxation time in the NMR study, whereas in the FSU they result in resonance frequency shifts. A question remains here as to the physical mechanism(s) common to both FSU and NMR cells that are responsible for the evolving wall adsorption characteristics in time.

Investigations conducted at Columbia University reveal that as the rubidium resonance cells are aged, the glass wall is gradually coated with a thin layer of Rb metal.[8] This conclusion is drawn from a cell that had two electrodes protruding into the inner cell space for measuring electrical conductivity. In a matter of a few days at room temperature, the cell wall became conductive, although no Rb film was visible.

The presence of Rb metal coating on the cell wall characterizes the aged cells. Data indicate that the noble gas adsorption energy is smaller in magnitude on the alkali metal surface than on the bare glass wall.

As the metal film is formed, the mountains and valleys present in the fresh glass surface tend to be smoothed out. Ar atoms that were imbedded deeply in the narrow valleys may be gradually desorbed as the Rb atoms adhere in the valleys. Displacement of one adsorbed atomic spieces by another has been reported for noble gas systems contained in a pyrex flask.[9,10] The increase in frequencies followed by gradual decrease observed in the fresh, all Ar cell (result No's 2 and 3) may be considered qualitatively due to the desorbed atoms as the Rb metal coating is formed. Desorption of N_2 molecules is also

3-15

conceivable, but is considered to be in a small effect because the effective adsorption surface area compared to that of Ar (Summary No. 7 of Section 3.2) is small.

3.4 SUMMARY AND RECOMMENDATIONS

Variations of the ^{87}Rb clock transition frequency evolving in time have been reported. The experimental results are interpreted on the basis of a simple picture of physical adsorption of buffer gas atoms. Qualitative arguments presented here appear to be physically reasonable. Due to short supply of quantitative information on the real glass surface, only a limited analysis was performed. Nevertheless, the work reported here clearly points out the significance of buffer gas adsorption processes as a source of frequency aging of a Rb FSU.

Results of this work point out strongly the possibility of cell fabrication procedures being responsible for varying degrees of frequency aging from unit to unit. This is because the fabrication technique may actually modify the adsorption characteristics. One important step in the fabrication are the procedures of cleaning the glass cell surface. Combination of chemical cleaning, ozone cleaning, and/or plasma cleaning may be applied. During the cleaning process, however, caution should be exercised so that such a process does not modify the wall characteristics beyond an acceptable level.

In view of the impact of the cell surface parameters on the long-term frequency stability of a FSU, continued effort in this area is highly desired. We believe the work reported here provides momentum needed toward further understanding of the "magical" nature of frequency aging in a Rubidium Frequency Standard.

3-16

REFERENCES

1. J.H. de Boer, "The Dynamic Character of Adsorption," Oxford Press, 1968.

2. S. Brunauer, "The Adsorption of Gases and Vapors," Princeton Univ. Press, 1945.

3. J. Frenkel, Z. Physik, 26, 117 (1924).

4. J.P. Hobson, Can. J. Physics, 43, 1941 (1965).

5. Y. Tuzi, T. Saito, J. Vac. Sci. & Tech. 6, 238 (1969).

6. J.P. Hobson, R.A. Armstrong, J. Phys. Chem., 67, 2000 (1963).

7. J.P. Hobson, J. Chem. Phys, 34, 1851 (1961)

8. W. Happer (Private Communication).

9. Y. Tuzi, M. Kobayashi, K. Asao, J. Vac. Sci. Tech., 9, 248 (1971).

10. B.G. Baker, L.A. Bruce, P.G. Fox, Trans. Far. Soc., 64, 477 (1968).

SECTION IV
VIBRATION SENSITIVITY INVESTIGATIONS

4.1 INTRODUCTION

The challenging design goal for the tactical Rb FSU is its performance under severe environments. No Rb FSU available to date meets all the tactical environmental specifications. A particularly challenging requirement is its performance under shock and vibration.

In view of the growing demand for the tactical Rb FSU's, Litton has investigated the vibration sensitivities that are inherent to the mechanization of a passive atomic frequency standard. Presented in this section is the preliminary result of analytical investigations of the vibration sensitivities. Litton believes that this work is the first compreshensive study to date and represents significant progress for the development of a tactical atomic oscillator.

4.2 SOURCES OF VIBRATION SENSITIVITY

The output frequency of an Rb FSU is that of a voltage controlled crystal oscillator (VCXO), which is servo-controlled with reference to the atomic resonance of Rb. Figure 4-1 illustrates a typical Rb FSU configuration. The Rb atomic resonance takes place in the subassembly consisting of an rf excited rubidium lamp, a filter cell, and a rubidium resonance cell in a microwave cavity. This subassembly is commonly referred to as the "physics package." The atomic resonance is interrogated by applying microwave power to the resonance cell, the frequency of which (~6.8) GHz is derived, through frequency multiplication and synthesis, from that of the VCXO. The resonance signal is detected in a form of light intensity variations at the photodetector. Typical of resonance detection is the use of a phase sensitive detection technique.
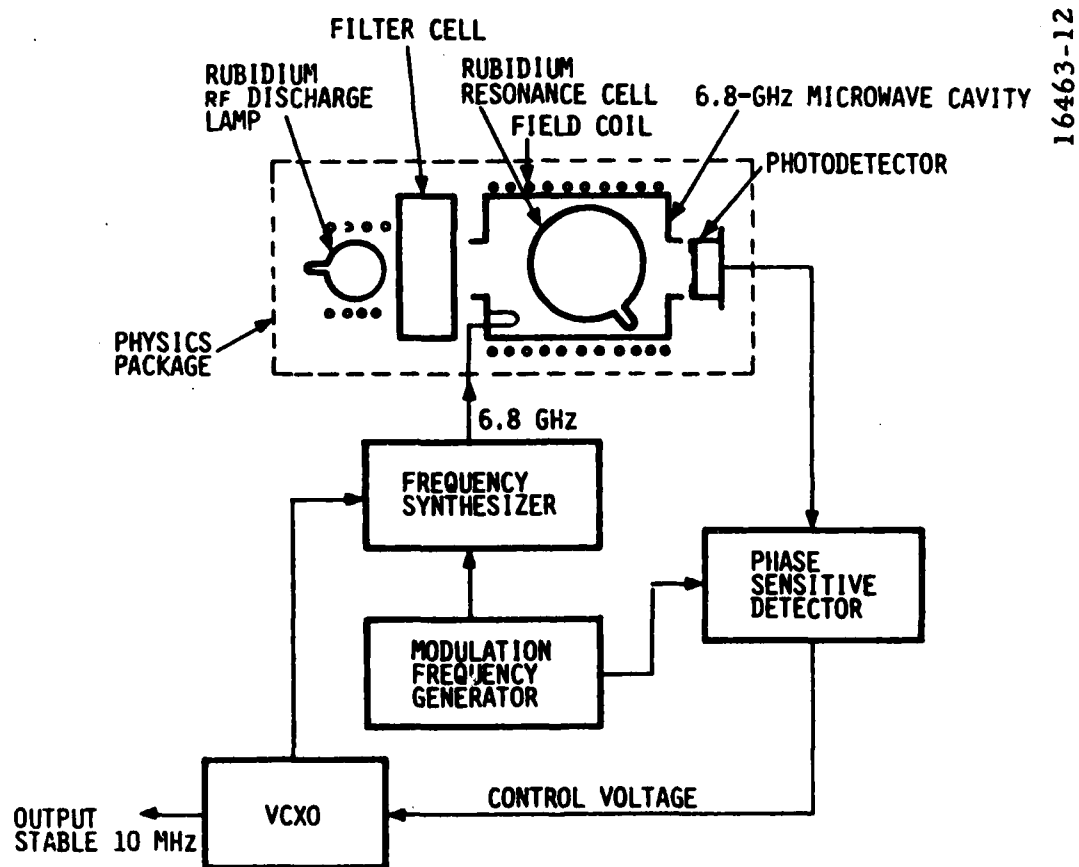
Figure 4-1. Functional Schematic of Rubidium Frequency Standard

The microwave frequency is modulated, and resulting variations in the light intensity are demodulated to obtain the resonance information. This information is used to determine if the frequency of the interrogating microwave (6.8 GHz), therefore, the output of VCXO, is lower than, exactly equal to, or higher than the frequency of the atomic resonance, and subsequently send an appropriate control voltage to the VCXO. The VCXO frequency is then said to be locked to the rubidium resonance.

Preliminary experimental results indicate that both the physics package and the VCXO generate vibration-induced spurious interference signals that perturb the servo control loop. Such perturbations are manifested as frequency instabilities and/or frequency shift in a Rb FSU.

4.2.1 Physics Package Vibration

The physics package is subject to vibration sensitivities from a number of inherent design features. The significant potential source of vibration sensitivity is mechanical translation of physics elements resulting in a change of detected light intensity, for example:

- Relative position of the rubidium lamp envelope with respect to the rf discharge coil

- Motion of the lamp assembly with respect to the resonance cell and/or the filter cell

- Translation of the resonance cell in the 6.8 GHz microwave cavity

- Microphonics of the photodetector and signal leads

Reduction of the physics package vibration sensitivity is paramount to an acceptable design of a rubidium frequency standard. Of particular concern are the tradeoffs that must be considered between the fine thermal balance required

by the rubidium devices necessitating minimal thermal mass and the desire to eliminate relative dynamic motion among the physics package elements by rigid mechanical structure.

The preliminary experiment shows that the output frequency instabilities due to the mechanical vibrations of the physics package are most pronounced at the vibration frequencies close to the servo loop modulation frequency.

The reason the servo loop modulation frequency is significant is that the basic signal mechanism used to detect the error between the multiplied VCXO signal the rubidium hyperfine resonance, i.e. the VCXO-to-rubidium resonance error signal exists in the servo loop as a light intensity variation at the modulation frequency. If the light intensity modulation due to the atomic resonance is perturbed by mechanical resonance, the servo loop generates an erroneous control voltage to the voltage controlled crystal oscillator (VCXO). The worst-case situation occurs when the physics package vibrates exactly at the modulation frequency.

4.2.2 VCXO Vibration

The voltage-controlled crystal oscillator (VCXO) is inherently vibration sensitive.[1,2] It is used, however, in all atomic frequency standards because of its excellent low noise characteristics. The VCXO provides the output signal of a rubidium frequency standard directly. As a result of this primary functional employment and its inherent characteristics, it is the most vibration-sensitive component of a rubidium frequency standard.

It has been shown that the fractional frequency shift of the output frequency of an ideal crystal oscillator is proportional to the change in acceleration that it experiences.[2] The proportionality constant is a function of the

4-4

direction of the acceleration with respect to a set of axes fixed to the oscillator.

The frequency of a crystal oscillator, f_1, is written as:

$$\frac{f_1 - f}{f} = \vec{\gamma} \cdot \vec{A} - \vec{A}_o \qquad (1a)$$

where f is the nominal frequency of the crystal oscillator corresponding to the acceleration $\vec{A}_0$, and $\vec{A}$ is the acceleration corresponding to the output frequency f_1. The proportionality constant, $\vec{\gamma}$, is called the g-sensitivity of a crystal oscillator. For simplicity, A_0 is assumed to be zero. f is therefore the static frequency. Eq. (1a) can then be rewritten as:

$$\frac{f_1 - f}{f} \equiv \frac{\Delta f}{f} = \left[\overleftarrow{\gamma} \cdot \vec{A} \right] \qquad (1b)$$

For a fixed direction, Eq. (1b) reduces to:

$$\frac{\Delta f}{f} = \gamma \cdot A \qquad (1c)$$

Eq. (1c) predicts that the output frequency of a crystal oscillator is frequency modulated at a rate equal to that of the vibration frequency with maximum fractional frequency deviation of:

$$\frac{\Delta f}{f} = \gamma A_p \qquad (2)$$

where A_p is the peak acceleration of the vibration.

An elaborate analysis demonstrates that such a frequency modulation is exhibited as "vibration-induced" sidebands about the carrier (the nominal oscillator frequency, for example, 10 MHz) at a displacement from the carrier which is equal to the vibration frequency. For small modulation index which

is the case for the vibration induced frequency modulations, the ratio of the amount of power, $\mathcal{L}_v$, carried by the sideband relative to that of carrier is shown to be: [2]

$$\mathcal{L}_v = 20 \log \left(\frac{\gamma A_p f}{2 f_v} \right) \tag{3}$$

in units of dBc, where f_v is the vibration frequency.

In many situations, the crystal oscillator is subject to random vibrations. the worst-case condition is usually described by a power spectral density of the vibration envelope. Using the same argument as used in deriving Eq. (3), the level of noise power has been obtained analytically.[2]

Typical g-sensitivities of off-the-shelf crystal oscillators are ~2 × 10^{-9}/g for both AT- and SC-cut crystals. Under a vibration of 5g peak, the fractional frequency deviation for such an oscillator becomes as large as 1×10^{-8}. This could well be outside of the specification requirement for a tactical frequency standard.

Eq. (1b) above suggests a possibility of compensating actively the g-sensitivity of a crystal oscillator by sensing the acceleration.[3-6] Active compensation however, has shown only a moderate improvement in a limited vibration frequency range under well-regulated sinusoidal vibration conditions. A crucial question of whether such a compensation scheme, once implemented, would be repeatable and stable over time has yet to be investigated.

The descripton of the vibration effect presented in the previous section has assumed an "ideal" crystal oscillator where its vibration sensitivity arises only from that of the quartz resonator. In order to electrically excite it, the quartz resonator is mounted in a set of electrodes. Such mounting structures are also susceptable to external vibration, since the dynamics of

4-6

mechanical resonances in the mounting structure are seen as added vibrations. Rearrangement of mechanical stresses in the mounting structure and/or the bondings may well result in variations of the direction of the g-sensitivity vector over time. Hence it is emphasized here that, for the reasons stated above, the accelerometer compensation technique is still not mature.

Recent research and development activity has resulted in a crystal ocsillator with superior (lower) vibration sensitivities to that of off-the-shelf oscillators.[7] To date the 5 MHz fifth overtone SC-cut crystals mounted at three points by thermo-compression have consistently shown the best g-sensitivities, $2 \sim 3 \times 10^{-10}/g$. When accurately mounted, the reported yield rate of such oscillators is as high as 50%. The 3-point mount of the crystal has shown a moderate mechanical resonance rise above 3 kHz whereas the conventional 2-point mount of the 10 MHz third overtone AT-cut has mechanical resonances in the frequency range of 400 to 1000 Hz. The presence of the mechanical resonance rise above 3 kHz is determined to be acceptable on the basis that the peak-to-peak displacement at such a high frequency produces no significant sidebands.

Figure 4-2 shows the peak amplitude of vibration-induced sidebands, Eq. (3), in a free running VCXO with two different g-sensitivities, $\gamma = 3 \times 10^{-10}/g$ and $3 \times 10^{-9}/g$. A ± 5 peak acceleration is used throughout the vibration spectrum.

4.3 ESTIMATES OF VIBRATION INDUCED ERRORS

As described above, the primary effects of vibration in the rubidium frequency standard are amplitude modulation of the photocurrent signal in the physics package and frequency modulation of the VCXO due to the inherent acceleration sensitivity of the quartz crystal. The effect of these vibration induced
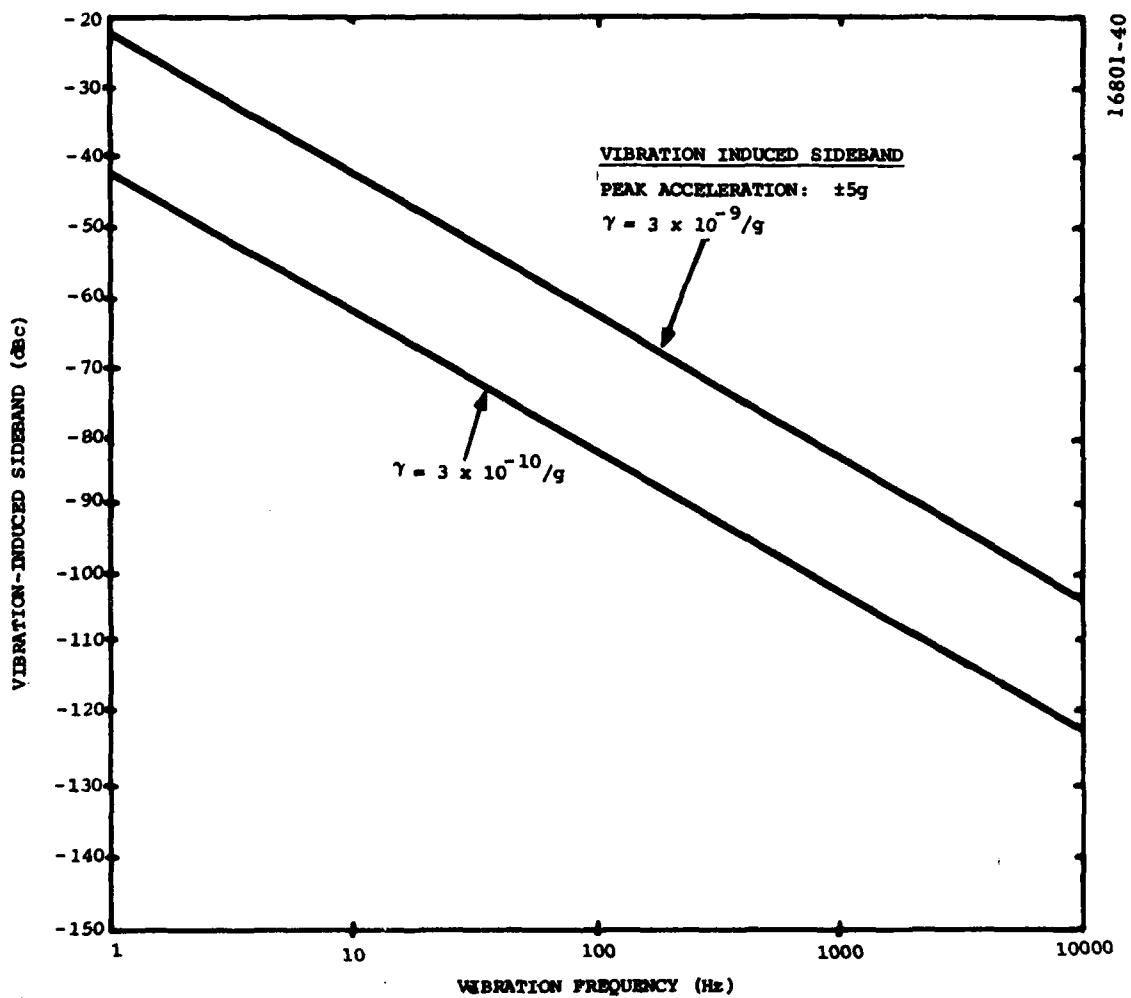
Figure 4-2. Vibration-Induced Sidebands for
Two Different VCXO g-Sensitivities

signals on the output frequency stability and phase noise is best explained by reference to the vibration error model diagram in Figure 4-3.

In a static environment, the VCXO output frequency (f_o = 10 MHz) is electronically multiplied to the rubidium resonance frequency (f_R = 6.84 GHz) and is also phase modulated at the modulation frequency (f_m) such that the instantaneous frequency (f) applied to the microwave resonant cavity in the physics package is sinusoidally swept across the resonance absorption curve of the rubidium cell. The resulting absorption modulation of the light level (I_o) at the photodetector in the physics package produces a signal (ΔI) containing ac components at the modulation frequency (f_m) and its harmonics. The signal (ΔI) is coherently demodulated ($\bar{s}$) and amplified by the loop transfer function G(s) to produce a control voltage at the VCXO input. If the output frequency (f_o) drifts, a correction voltage is applied to the VCXO to null the drift error.

In order to estimate the magnitude of vibration induced errors, an error signal expression which shows the relative interdependence of the quiescent vibration free error and the vibration induced components is required. In the quasi-static case of small modulation frequency and small deviation about the resonance line center, a simple quadratic expansion of the modulation/absorption process gives the signal expression for the fundamental:

$$\Delta I = KI_o \; (2 \; \epsilon A) \; \sin \; (\omega_m t + \phi) \tag{4}$$

where: I_o = dc photocurrent

K = physics conversion gain Hz^{-2}

ϵ = $\overline{f_R - f}$ = mean frequency error Hz

A = peak frequency deviation Hz

and the instantaneous frequency difference is:
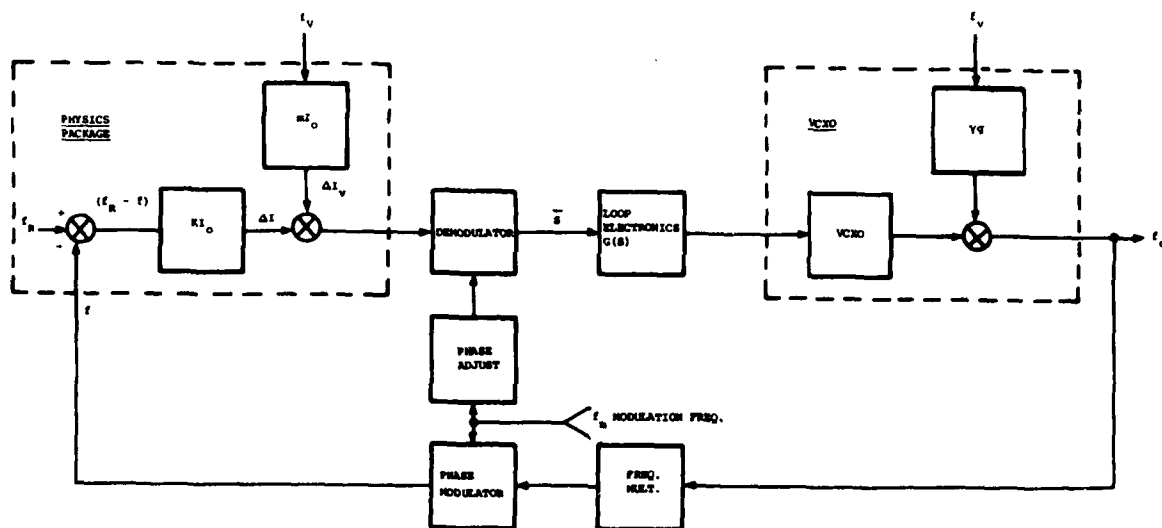
$$(f_R - f) = \epsilon + A \sin \omega_m t$$

Figure 4-3.   Model of Vibration Induced Error in
Frequency Control Loop

This limiting case is easily extended for the actual situation where the peak deviation A approaches the half line width λ by including higher order terms in the expansion, however, since $\varepsilon \ll (\lambda, A)$ we need only consider terms to first order in ε. The higher order harmonic terms in ω_m are rejected in the electronics. The net result then of increasing the peak deviation A to about equal to the half-line width is to modify the conversion gain K.

To extend the signal expression for the dynamic case of large modulation frequency, we refer to the work of Missout and Vanier,[8] and Audoin, et al,[9] which show both analytically and experimentally that as the modulation frequency is increased to approximately the half-line width, the principal effect is simply an increase in the phase lag of the fundamental signal which is accounted for by proper reference phase adjustment at the demodulator. The conversion gain remains relatively constant within a few percent as the modulation frequency is increased to the half-line width value.

The conversion gain factor K is dependent on operational parameters such as microwave power level, absorption line width and depth and modulation frequency and deviation. The conversion gain has been measured experimentally on the operating FSU system and exhibits a typical value of about $1.5 \ (10^{-9})$. Note that the amplitude of the fundamental is to first order proportional to both the mean frequency error ε and the peak deviation A which is typically adjusted to about equal to the half-line width (≈ 500 Hz).

The signal (ΔI) is coherently detected with the demodulator reference phase adjusted for the phase lag (ϕ) to produce the loop error signal:

$$\overline{s} = K \ I_0 \ A \ \varepsilon \tag{5}$$

which is driven toward zero by the second order closed loop response.

When the physics package and the $\overline{VC}XO$ are subjected to mechanical vibration at frequency (f_v) the signal (ΔI) at the physics package output contains an additional interference term:

$$\Delta I_v = mI_o \sin (2 \pi f_v t) \qquad (6)$$

where: $m = G \times F (f_v)$ fractional modulation of I_o

$G =$ vibration input level

$F (f_v) =$ frequency selective g-sensitivity of the physics package

and the output frequency (f_o) of the VCXO is modulated as:

$$f_o (1 + \gamma G \sin (2 \pi f_v t))$$

producing an instantaneous frequency difference in the physics package:

$$(f_R - f) = \epsilon + A \sin (\omega_m t) + B \sin (\omega_v t) \qquad (7)$$

with $B = \gamma G f_R$

$\gamma =$ fractional frequency g-sensitivity of VCXO

Again in the signal expansion, since $B \ll (\lambda, A)$, we retain only terms linear in B. The resultant demodulated signal now contains additional terms (retaining only dc and low frequency components):

$$\overline{s} = I_o \left[\frac{m}{2} \cos (\omega_m - \omega_v)t + K \left\{ A \epsilon + B \epsilon \cos (\omega_m - \omega_v)t + \frac{AB}{2} \sin (2 \omega_m - \omega_v)t + AB \sin (\omega_v t) \right\} \right] \qquad (8)$$

The closed servo loop attempts to force $\overline{s} \rightarrow 0$ and assuming the values,

$$m = (10^{-5}) = 10 \text{ ppm}$$

$$K = 1.5 (10^{-9}) \text{ Hz}^{-2}$$

$$A = 500 \text{ Hz}$$

$$\gamma = 4 \ (10^{-10}), \quad G = 1g, \quad f_R = 6.84 \ (10^9) \ \text{Hz}$$

$$B = \gamma \ G \ f_R = 2.74 \ \text{Hz/1g}$$

the principal output frequency errors can be estimated as follows.

4.3.1 Physics Package Vibration

Vibration induced modulation of the photocurrent creates an input control loop signal having an equivalent error magnitude of

$$|\epsilon| = \frac{m}{2KA} \cos (\omega_m - \omega_v)t$$

$$= (6.7 \ \text{Hz}) \cos (\omega_m - \omega_v)t \tag{9}$$

which is passed to the output in accordance with the closed loop transfer function. The resultant fractional frequency error when $f_v = f_m$ or the difference frequency is within the closed loop bandwidth has a magnitude of:

$$\left| \frac{\Delta f}{f} \right| \approx 10^{-9}$$

for vibration induced relative modulation of 10 ppm.

4.3.2 VCXO Vibration

Vibration induced modulation of the VCXO results in frequency errors injected into the loop directly at the output point and are therefore modified by the closed loop error response function. The principal error effect occurs when the vibration frequency is twice the modulation frequency, $f_v = 2 \ f_m$. The equivalent loop error signal is:

$$| \epsilon| = \frac{B}{2} = 1.37 \ \text{Hz/g} \tag{10}$$

resulting in a fractional frequency error at the output of

$$\left| \frac{\Delta f}{f} \right| = 2 \ (10^{-10})/g$$

There are minor responses for vibration frequencies $f_v = f_m$ and at $f_v = \frac{1}{2} f_m$, however, these are of insignificant magnitude and are effectively masked by the system noise level.

The principal response at $f_v = 2 f_m$ indicates both the need for an improved oscillator having low g-sensitivity and for the use of vibration isolators to reduce the acceleration level in the high frequency region of the spectrum.

4.3.3 Vibration Isolation of the VCXO

As indicated above, vibration sensitivity of the VCXO is most critical at the second harmonic of the control loop modulation frequency. Typically, in the Litton design for the frequency standard, the hard mounted vibration input level at the second harmonic is 10 g's. Obviously, in order to provide the requisite frequency stability, the VCXO mounting must incorporate vibration isolators to attenuate the input g-spectrum to a tolerable level of 1g or less.

Ideally, a damped mechanical vibration isolator exhibits a transmissibility characteristic as shown in Figure 4-4. The amplification at the resonance rise is approximately equal to $1/2 \zeta$ where ζ is the damping coefficient of the isolator. With due consideration of the input vibration spectrum and the frequency characteristics of the electronics control loop, a set of isolators was selected for the VCXO mounting having the following characteristics:

Natural resonance   30 to 60 Hz

Resonance gain ≈ 3

VCXO design weight   0.5 pound

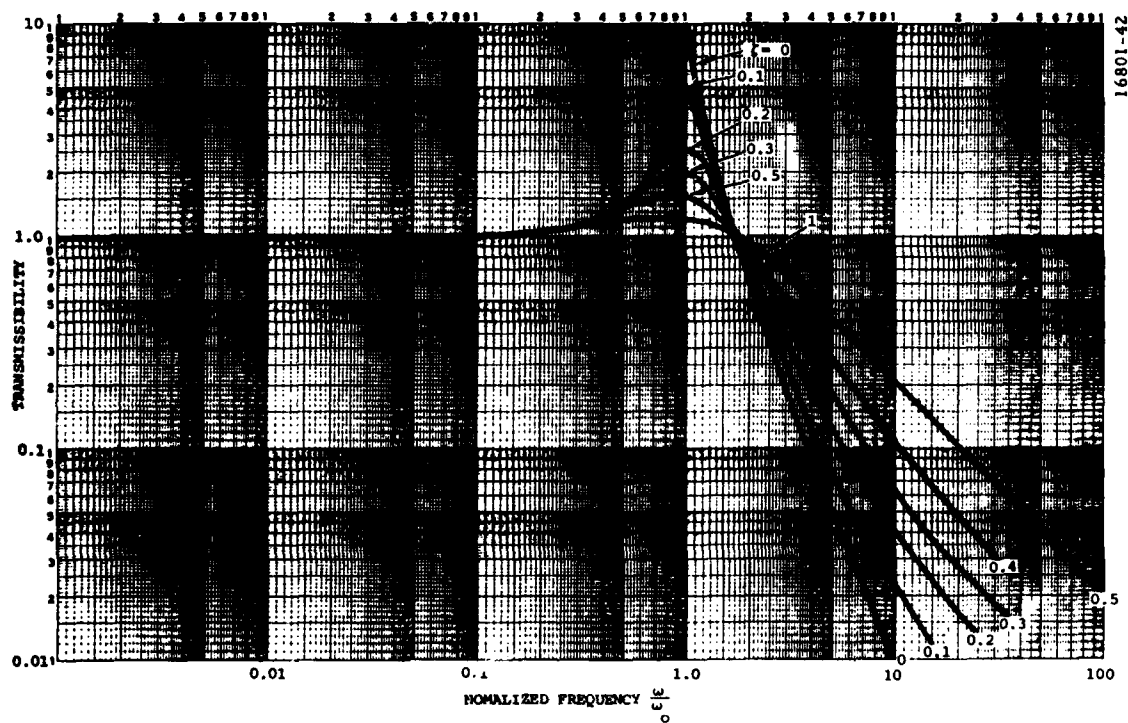Test results of this mechanical isolator are presented in Section V below.

4-14

Figure 4-4. Vibration Isolator Transmissibility

4.4 VIBRATION SIMULATION TESTS

The error effects of physics package vibration and VCXO vibration have been simulated by injection of variable frequency interference signals at appropriate points in the servo loop of the engineering model FSU.

4.4.1 Physics Package

Physics package vibration was simulated by injecting a sinusoidal interference signal at the output of the photodetector preamplifier in the closed loop. The frequency of the interference signal (derived from a HP frequency synthesizer) was swept slowly over a range of 5 Hz to 1000 Hz. The resulting error effect in the closed loop was monitored by recording the control voltage variations at the VCXO input control terminal. Using the known VCXO control voltage sensitivity (0.3 Hz/volt ÷ 3×10^{-8} ($\Delta f/f$/volt) the output frequency stability error can be directly inferred. A typical chart recording of the control voltage error is shown in Figure 4-5; in (a) the complete frequency span of 5 Hz to 1000 Hz is presented and demonstrates that the only significant error effect occurs at the modulation frequency and at adjacent frequencies within the servo loop bandwidth; in (b) the central frequency region is expanded to show more clearly the beat effect for interference frequencies adjacent to the modulation frequency.

Similar data were taken for input interference signal amplitudes ranging from 2.4 to 555 µvolts rms. The resulting error magnitudes were closely linear over this range and the effective relative frequency error sensitivity of the physics package can be expressed as:

$$\frac{\Delta f}{f} = 1.32 \ (10^{-4}) \ m$$

(A)

INPUT: 308 μV RMS
m = 90 PPM

$0.1 \text{ VOLT} = 3 \times 10^{-9} \ \Delta f / f$

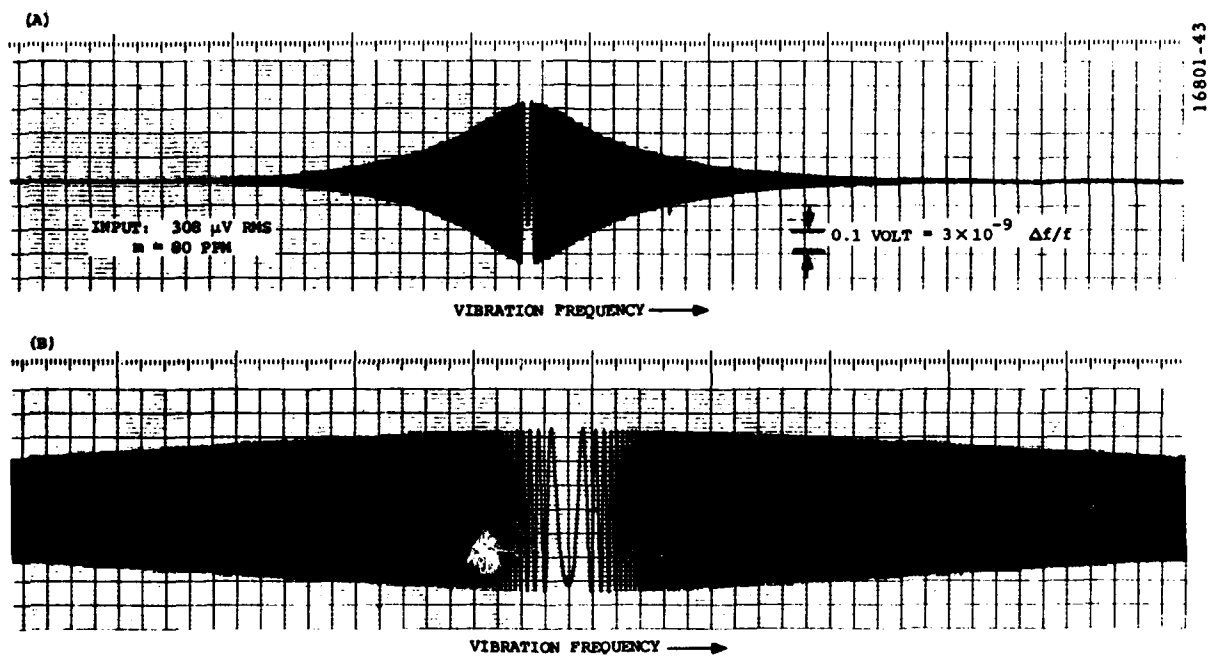VIBRATION FREQUENCY →

(B)

VIBRATION FREQUENCY →

Figure 4-5. Physics Package Simulated Vibration Test

where (m) is the amplitude of the interference signal relative to the dc photo-current level. Thus, if the relative frequency error due to physics package vibration is to be limited to $\pm 10^{-9}$, vibration induced modulation of the light level at the photodetector should be no greater than about ± 7.5 ppm. This sensitivity compares closely with the estimated interference level in Section 4.3.

It should be noted that the vibration sensitivity magnitude is not affected by the electronic gain in the servo loop, but is, however, dependent on the conversion gain (error signal amplitude per Hertz frequency offset) of the microwave power absorption process in the rubidium resonance cell. The physics conversion gain is in turn, dependent on operational parameters such as microwave power level, absorption line width and depth, and peak frequency deviation of the modulation. In order to minimize the physics package vibration sensitivity, the conversion gain should be made as large as possible.

4.4.2 VCXO

VCXO vibration was simulated by injecting a sinusoidal interference signal at the control voltage input terminal of the VCXO. The amplitude of the injected signal was adjusted to be equivalent to a 5 g vibration level for an oscillator $\gamma = 4 \times 10^{-10}/g$. The frequency of the interference signal was swept slowly and the residual error signal at the control input summing junction was observed on a chart recorder. From the known control sensitivity of the VCXO (Hz/volt) the resultant frequency deviation of the output can be calculated. A typical chart recording of the entire frequency span is shown in Figure 4-6, the lower trace is a direct continuation of the upper trace. At the low frequency end of the spectrum the linear rise of the error is in accordance with the error response of the closed loop servo which has a corner frequency at about 100 Hz. The

END
12-83

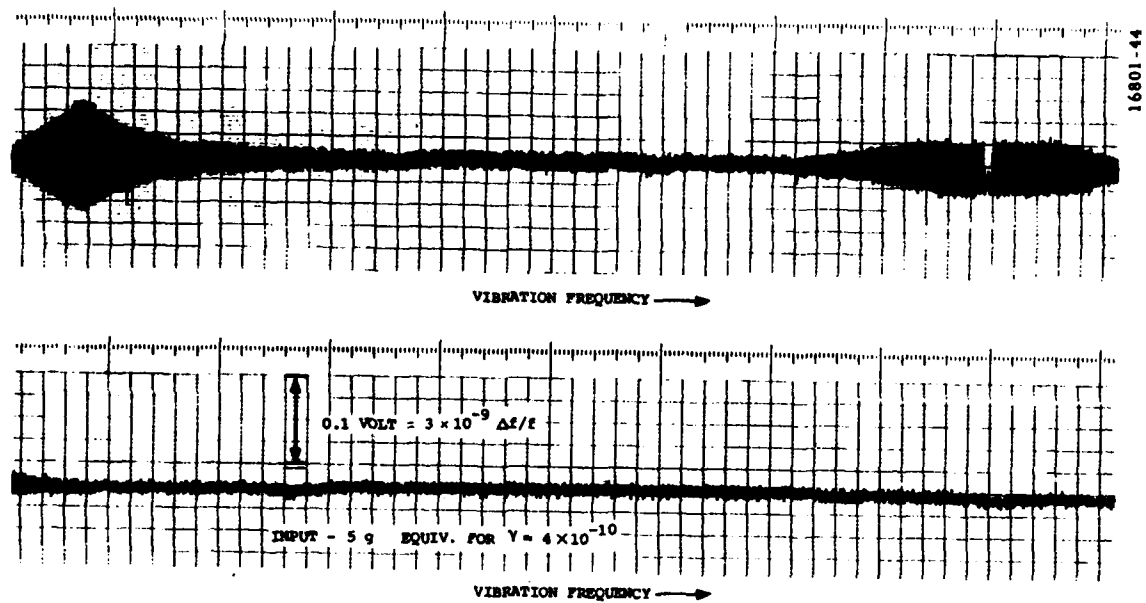MICROCOPY RESOLUTION TEST CHART

NATIONAL BUREAU OF STANDARDS-1963-A

Figure 4-6. VCXO Simulated Vibration Test

subsequent drop is due to limited frequency response of the recorder. If we observe the actual oscillator output frequency with a Tracor frequency difference meter having a time constant of the order of 1/2 second, the low frequency vibration effects are not observed i.e., the mean frequency stability is not affected by low frequency vibration.

The principal frequency error effect occurs when the vibration interference frequency is at twice the modulation frequency for which the offset error is:

$$\left| \frac{\Delta f}{f} \right| \approx 3.6 \times 10^{-10}/g$$

This value is within a factor of 2 larger than the predicted interference effect calculated in Section 4.3. The continuation of the frequency sweep up to 2 kHz shows no observable error effect at the fourth harmonic of the modulation frequency and confirms the error prediction hypothesis that only the quadratic terms in the expansion need to be considered.

4.5 PHYSICS PACKAGE VIBRATION TESTS

Vibration tests of the engineering model FSU physics package were made with the test fixture mounting shown in Figure 4-7. A resonance test with sensing accelerometer mounted on the microwave cavity indicated a low Q mechanical resonance at about 1400 Hz, well above the expected interference region around the modulation frequency. Subsequent vibration tests were performed in an operating mode in which the r-f discharge lamp was activated (both thermal control and r-f excitation) and the photodetector signal, amplified by a remote wide band preamplifier (not subject to vibration) was observed and recorded on a storage spectrum analyzer (HP-3582A).

The physics package was subjected to vibration test levels of 1g, 5g, and 10g in the three orthogonal case axes. For each acceleration level and each
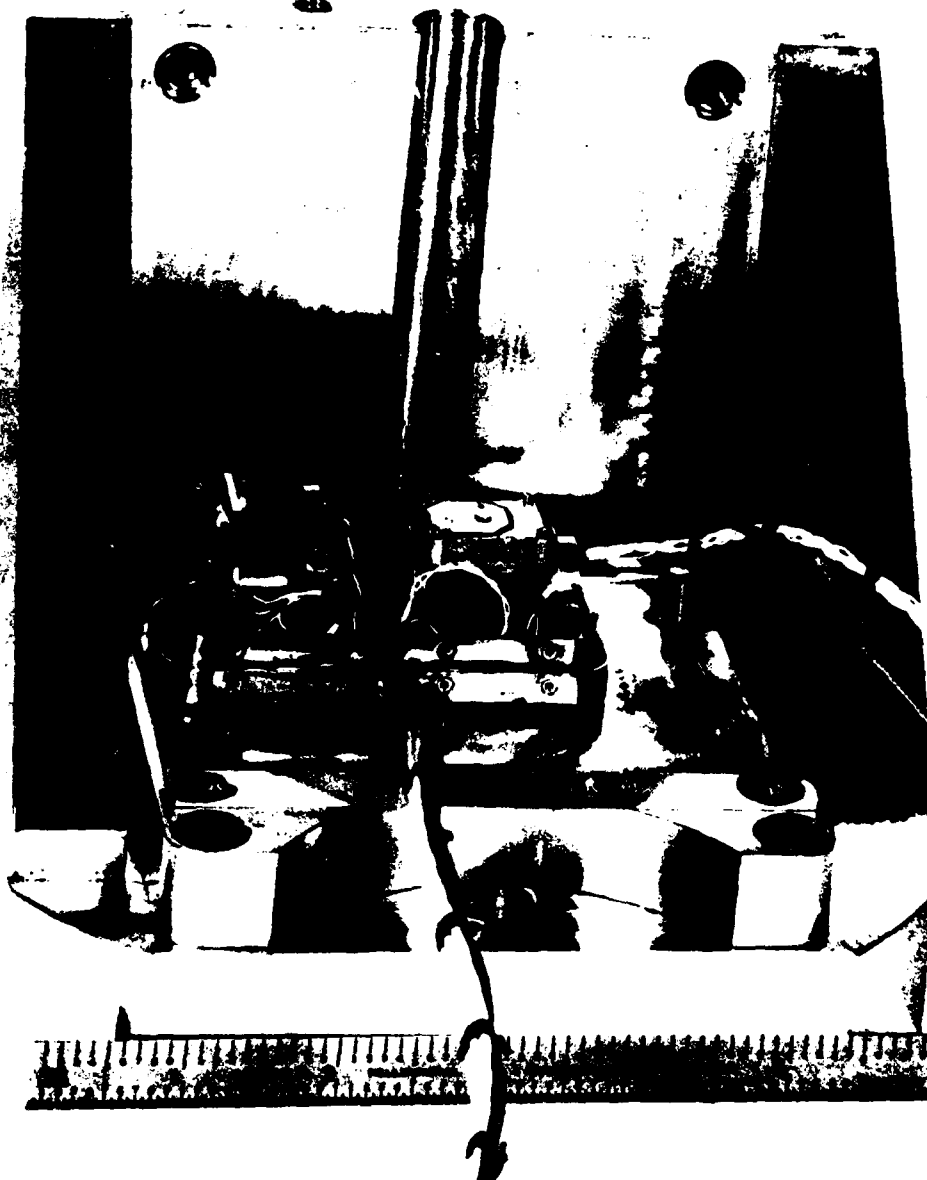
4-20

16708-7

Figure 4-7. Engineering Model Physics Package
Vibration Test Assembly

axis, the vibration frequency was swept slowly from about 20 Hz to 1000 Hz as the interference signal magnitudes were detected and stored by the spectrum analyzer and subsequently transferred to an x – y plotter. A typical record for the y axis is shown in Figure 4-8. Note that over most of the frequency range, the induced signal level is linear with input g-level and that there are no sharp resonances. In general in the low frequency region, the interference signal amplitudes fall off about inversely with increasing frequency with a minimum level at about 300 Hz and thereafter rise gradually with increasing frequency. Vibration data for the other axes exhibit similar features.

In order to separate and identify the probable sources of modulation of the photocurrent, the lamp was vibration tested directly with a photodetector (of the same design) firmly mounted to the front of the helical resonator lamp housing. A plot of the lamp vibration induced signals for the y axis is shown in Figure 4-9. The general characteristics of the spectra are similar to those obtained for the complete physics package but are at a lower level relative to the dc photocurrent.

As indicated by the vibration induced error predictions and by the simulated vibration tests, the critical frequency is about the modulation frequency in the electronics control loop. Accordingly, the vibration induced interference levels at the modulation frequency have been normalized relative to the dc photocurrent I_O and are presented in Figure 4-10. The result shows the relative interference modulation factor m as a function of vibration g level in the three case axes. The vibration test results and conclusions for the physics package are summarized as follows:
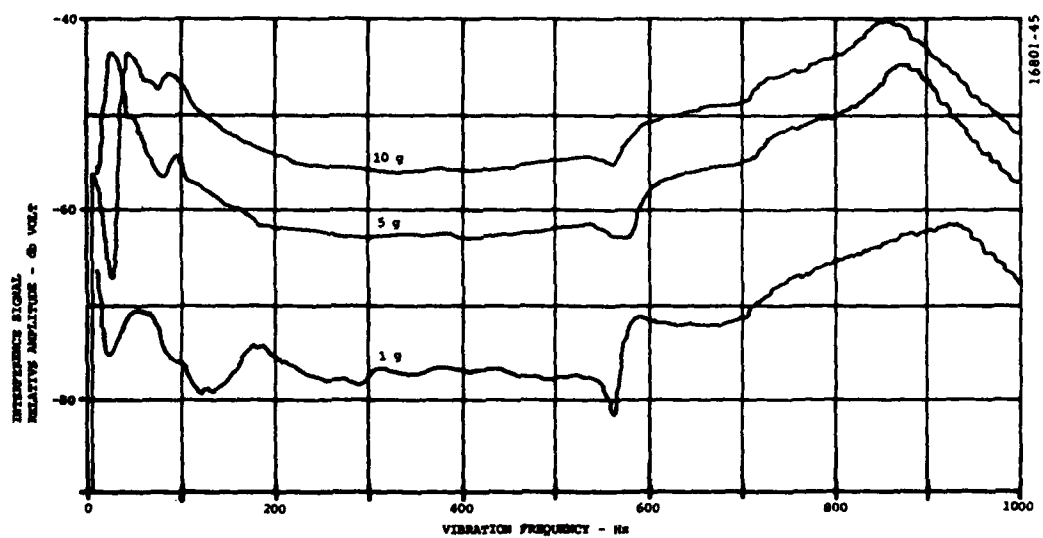
4-22

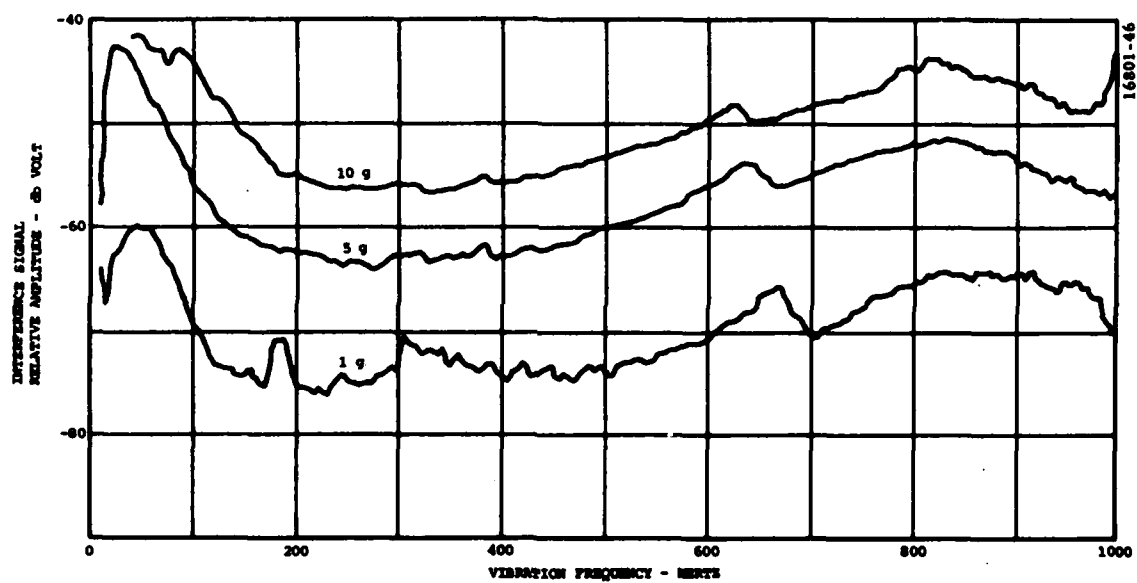Figure 4-8.   Physics Package Vibration Test
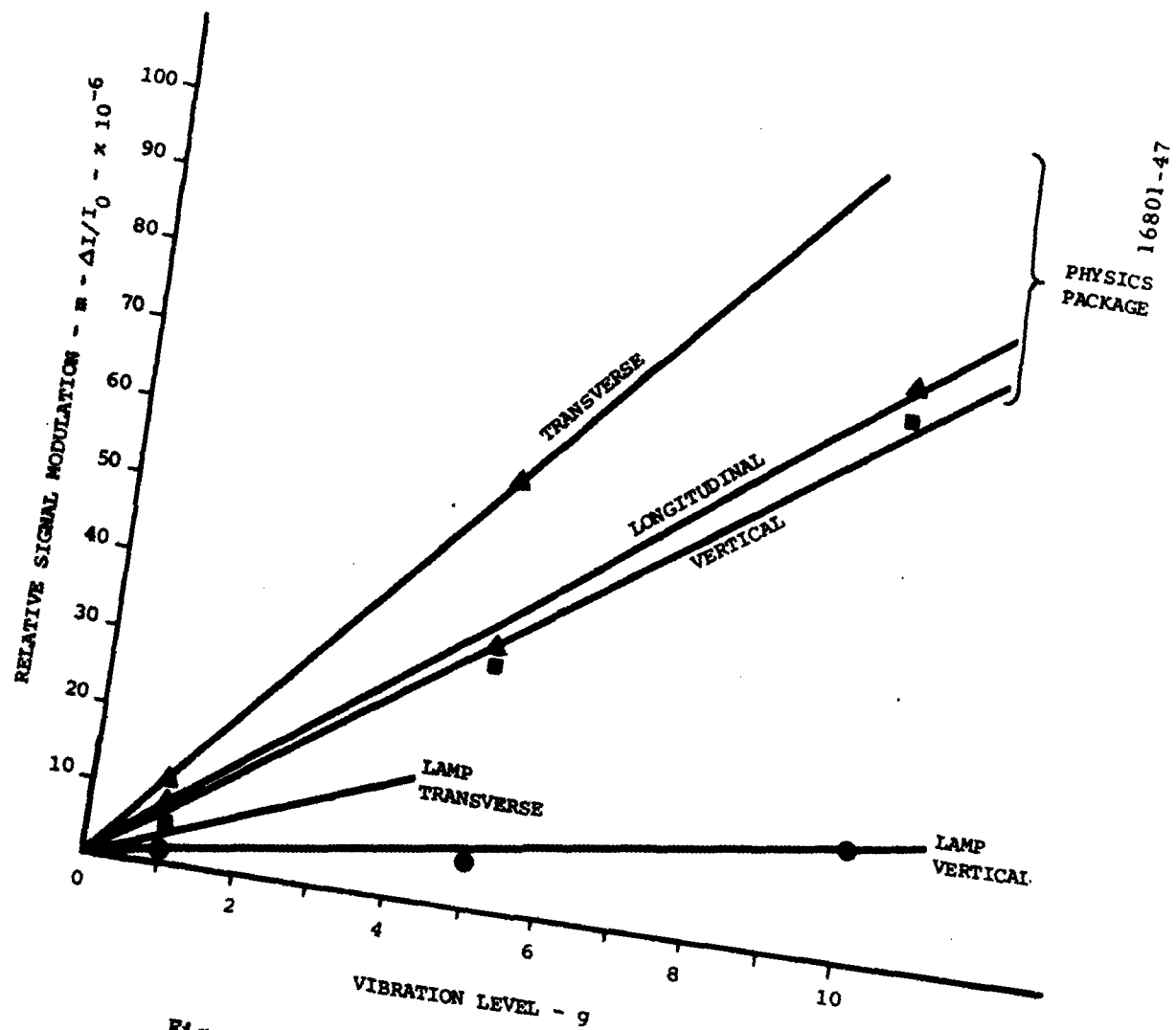
Figure 4-9. Vibration Test of Lamp

Figure 4-10. Physics Package and Lamp Vibration Sensitivity at Modulation Frequency

1. Vibration induced modulation of the light level I_o is essentially linear with g level up to 10g, except for transverse vibration at about 700 Hz which exhibits a non-linear response.

2. At the modulation frequency, the vertical and longitudinal vibration modulation is $\sim$ 7 ppm/g of which $\sim$ 2 ppm/g appears to be due to direct vibration effects in the lamp, photodetector and signal leads.

3. In the present physics package design, the vibration acceleration sensitivity vector is principally in the transverse direction which exhibits a modulation level of $\sim$ 10 ppm/g of which $\sim$ 5 ppm/g appears due to the lamp and photodetector above.

4. Attempts to further identify and reduce sources of vibration modulation by reduction of the entrance pupil aperture and focusing adjustment of the transfer optics did not reduce the relative modulation index.

5. We conclude that the principal part of the vibration induced light modulation is caused by small relative motion of the lamp and the resonance cavity containing the transfer optics and photodetector. The desired modulation sensitivity level based on the error estimates and simulated vibration tests is about 1 ppm/g. Reduction to this level requires design modification of the physics package to provide a stiffer mounting of the component parts relative to one another. Further investigation of the inherent vibration sensitivity of the lamp and its associated RF drive circuit is required to insure a lamp design free of interference.

4.6 SUMMARY AND CONCLUSIONS

The primary sources of vibration induced errors in the rubidium FSU are:
(1) amplitude modulation of the photocurrent signal in the physics package and,
(2) frequency modulation of the VCXO due to its inherent g-sensitivity. Both
theoretical analyses and experimental measurements identify and confirm the
principal errors of these two sources as:

- Physics Package: Only those vibration frequencies at or near the con-
  trol loop modulation frequency produce a significant error effect.
  Amplitude modulation of the dc photocurrent I_o of the order of 10 ppm
  will produce a fractional frequency error of about 10^{-9} when the
  vibration frequency is coherent with the modulation frequency; if the
  vibration frequency differs from the modulation frequency by an amount
  δf within the closed loop bandwidth, the VCXO will be frequency modu-
  lated with a corresponding side band phase noise level of $0.005/\delta f$
  (e.g. -66 dbc for $\delta f = 10$ Hz).

- VCXO: The significant induced error occurs when the vibration fre-
  quency equals twice the control loop modulation frequency, in which
  case, the fractional frequency error is $(\gamma G)/2$ (e.g. $3 \times 10^{-10}/g$ for
  an oscillator $\gamma = 6 \times 10^{-10}$). Low frequency vibration effects in
  the VCXO are attenuated in accordance with the closed loop error
  response.

Reduction and control of the vibration induced errors in the Engineering
Model FSU have been accomplished by a combination of techniques, including:
subcontract development of an improved VCXO having relatively low g-sensitivity;
the use of internal vibration isolators to attenuate the high frequency g-level
at the VCXO; the use of a high gain - wide bandwidth servo loop to attenuate the

low frequency vibration interference; mechanical design of the physics package
providing a relatively stiff structure avoiding low frequency mechanical reso-
nances and having inherently low g-sensitivity. Actual vibration test results
of the physics package indicate the need for design modification to provide
further reduction of the vibration induced interference signal levels in a hard
mounted - high g environment.

REFERENCES

1. W.L. Smith and W.J. Spencer, "Precision Crystal Frequency Standards," Proc. 15th Ann. Symp. Freq. Control, Fort Monmouth, N.J. 1961, p. 139

2. Raymond L. Filler, "The Effect of Vibration on Frequency Standards and Clocks," Proc. 35th Ann. Freq. Control Symposium, Ft. Monmouth, N.J. May 1981, p. 31

3. Michel M. Valdois and Armand B. Dupuy, U.S. Patent 4,100,512 granted on July 11, 1978.

4. J.M. Przyjemski, "A Compensation Technique for Accel. on-Induced Frequency Changes in Crystal Oscillators," NAECON '78 May 1978

5. Donald A. Emmons, "Acceleration Sensitivity Compensation in High Performance Crystal Oscillators," Proc. 10th Ann. PTTI Meeting, Nov. 1978

6. V.R. Rosati and R.L. Filler, "Reduction of the Effects of Vibration on SC-cut Quartz Crystal Oscillators," Proc. 35th Ann. Freq. Control Symp., Fort Monmouth, May 1981, p. 117

7. B. Goldfrank, J. Ho, and A. Warner, "Update of SC-cut Crystal Resonator Technology," Proc. 35th Ann. Freq. Control Symp., Fort Monmouth, May 1981, p. 92

8. G. Missout and J. Vanier, "Some Aspects of the Theory of Passive Rubidium Frequency Standards," Can. J. Phys, 53,1030 (1975)

9. C. Audoin et al, "Influence of Modulation Frequency in Rubidium Cell Frequency Standards," Proc. 14th Ann. PTTI Mtg, NASA GSFC, Greenbelt, MD, Nov., 1982, p. 87

SECTION V

SC-CUT VCXO CHARACTERIZATION

5.1 INTRODUCTION

The small size, vibration, g-sensitivity, and shock requirements, as well as thermal and response time considerations for a tactical FSU have defined state-of-the-art parameters for the voltage-controlled crystal oscillator (VCXO) module that do not currently exist in any off-the-shelf model VCXO. Based on analyses, part of which are exhibited in the foregoing sections, Litton has funded a subcontract with Frequency Electronics Inc. (FEI) of Mitchell Field, N.Y. to develop a modularized VCXO that will integrate into Litton's tactical FSU design to provide performance sufficient to meet the tactical requirements.

The choice of the appropriate quartz crystal is key to obtaining the required VCXO performance. Quartz crystal blanks for VCXO applications are cut from the bulk crystal along planes having a well-defined orientation relative to the principal crystalographic axes, Figure 5-1. Traditionally most VCXO's have employed quartz blanks having an AT-cut. The AT-cut is achieved after a single rotation of the quartz crystal about the X axis of $\theta = 35.3°$ as shown in Figure 5-2. The crystal cut required to achieve the performance of the subject specification is the stress compensated or SC-cut. The SC-cut requires two rotations from the principal axes alignment of $\theta = 33.9°$ and $\phi = 21.9°$. Figure 5-2, yielding what is known as a doubly rotated blank.

The θ and ϕ angles of the SC-cut must be determined within several arc seconds to achieve the required performance. To date yield of this x-ray, cut, grind, and polish process is relatively low, maybe 20 to 50% at best. However
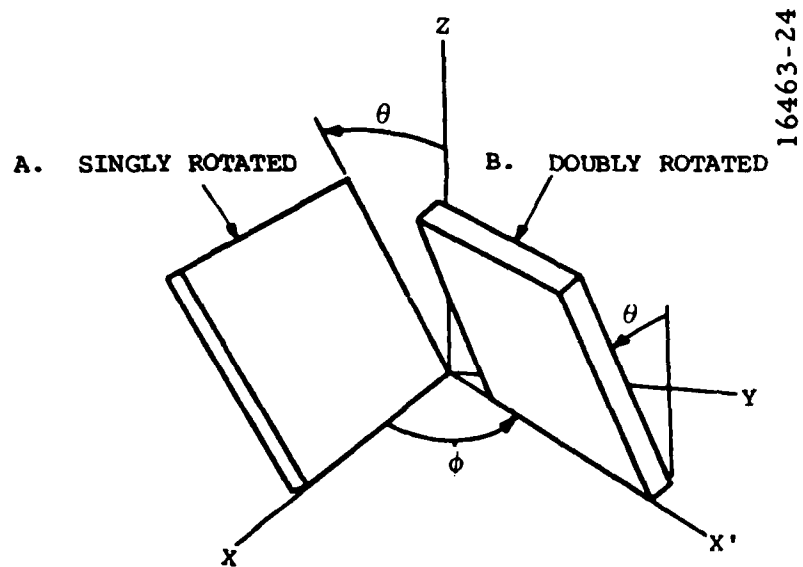
Figure 5-2. Rotated Crystal Blanks

this cutting process is bei g successfully mechanized. As a result good yield of high-quality quartz crystals should be available from the quartz crystals industry.

The subcontracted VCXO unit was designed and built to incorporate the state-of-the-art SC-cut crystal technology. Careful examination of the performance requirements for a Rb FSU concluded that low g-sensitivity and fast warm-up, both of which are essential for tactical applications, can only be met with the SC-cut VCXO.

Among the available SC-cut crystal technologies, the most advanced but well understood method of implementation was adapted. It is the 5 MHz, 3rd overtone SC-cut mounted on three electrodes with cold thermocompression bonds This configuration gives an excellent g-sensitivity with no inherent structural resonance rise below 2000 Hz.

Superior warm-up characteristics inherent to the SC-cut crystal to that of conventional AT-cut is well documented. It was determined however that, even with the SC-cut crystal oscillator, the traditional oven design would not meet the rapid warm-up requirement for a tactical FSU. It was therefore necessary to incorporate a separate oven of on-off type, in addition to the conventional double oven structure, that operates during the warm-up period.

The entire VCXO is packaged in a size significantly smaller than conventional VCXO's with no degradation in its stability performance. This significant reduction has been achieved through hybridization of electronic circuitry.

To date, two VCXO units have been received and tested. They represent a significant progress in the technology of crystal oscillators. Reported in this section are the performance test results of the VCXO in a static environment and under vibration.

5-4

5.2 VCXO CHARACTERIZATION

A summary of test data is shown in Table V-1 for the two VCXO units; also shown for comparison are the Litton specified design goals. Overall performance of the design is good, particularly in power consumption and warm-up characteristics. Some improvement is desireable in reduction of second harmonic distortion and frequency deviation with line voltage, load, and temperature variations. g-sensitivity of the first delivered unit is abnormally high due to an acceleration sensitive electronic component which was subsequently replaced; acceleration sensitivity of the second unit is considerably improved and close to the design goal value.

Test results of interest are highlighted in Figures 5-3 through 5-7. Shown in Figure 5-3 is the 10 MHz output harmonic spectrum as measured on and recorded from an HP 855A Spectrum Analyzer. As noted above the second harmonic content is larger than desired; however, higher harmonic content is acceptably low. The single side band phase noise spectrum of the VCXO is shown in Figure 5-4. Measurement was made with the Litton designed phase noise measurement system. It was analyzed and recorded with an HP 3582A Spectrum Analyzer; phase noise performance of the VCXO meets specification. The control voltage characteristic of the VCXO is shown in Figure 5-5. Design range is 2.5 volt to 12.5 volt. The nominal operating point is at 5 volts where the slope is 0.38 Hz/volt. Non-linearity of the control characteristic causes a change in the slope (a factor in the control loop forward gain) to 0.2 Hz/volt at the upper end of the range. Non-linearity and the associated change in loop gain has been purposely restricted to minimize performance variations between calibrations of the frequency standard.
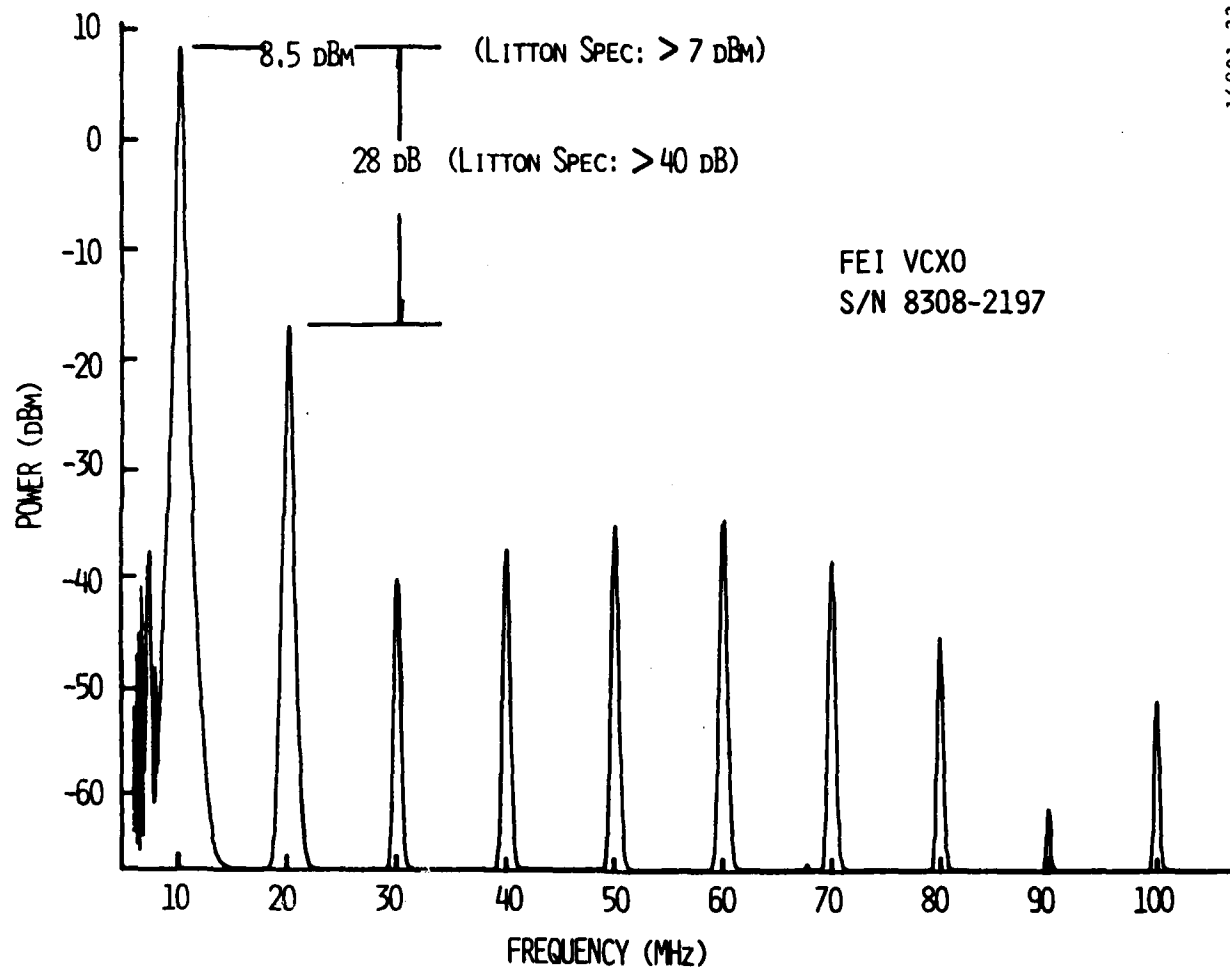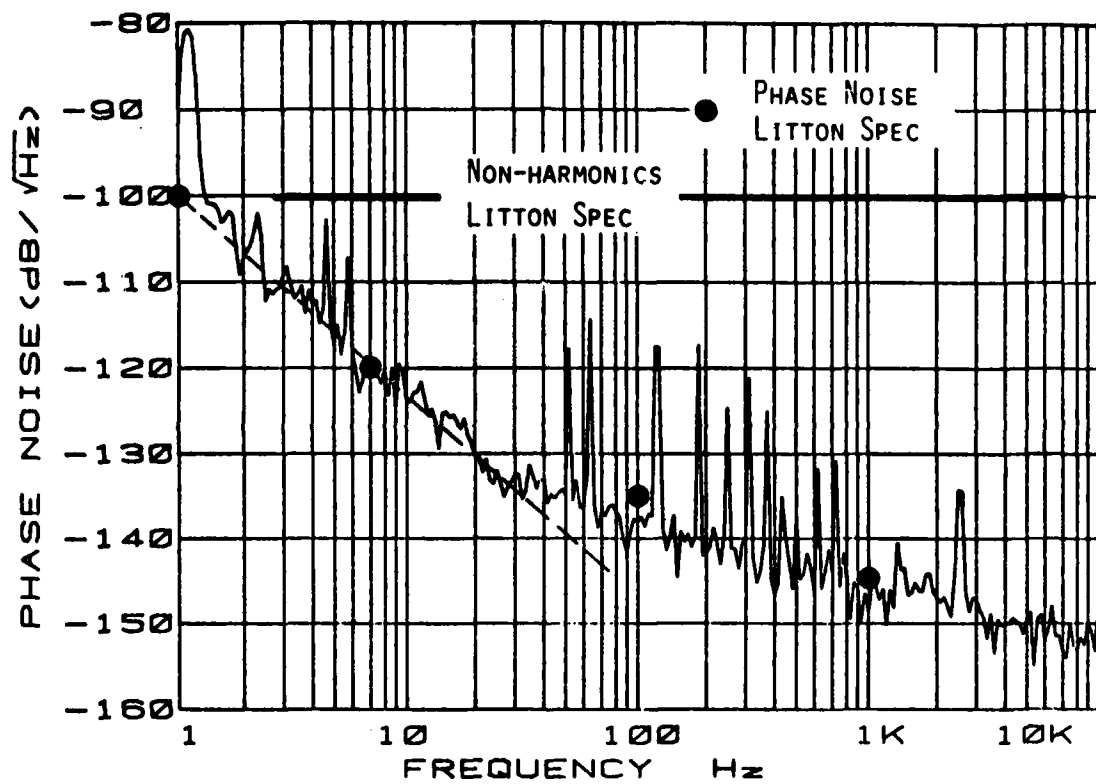
Figure 5-3.   VCXO Output Harmonic Content

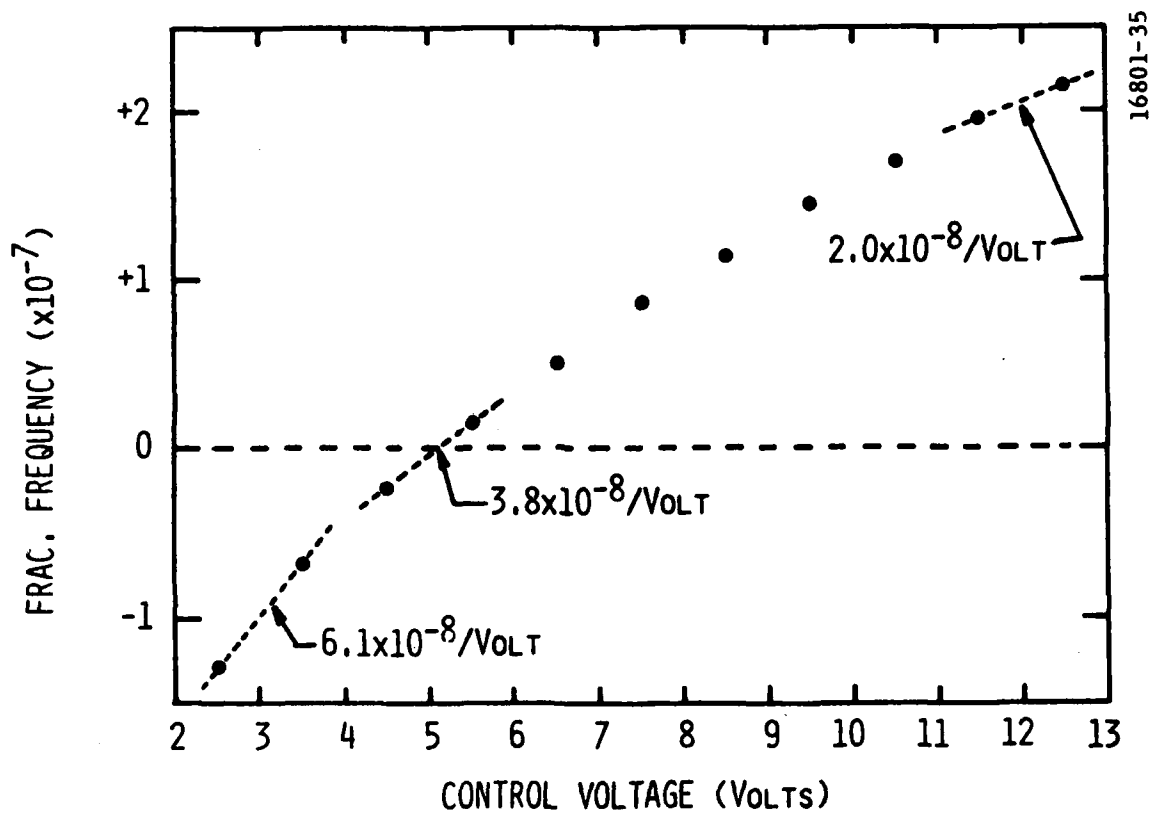Figure 5-4. Phase Noise of VCXO Output

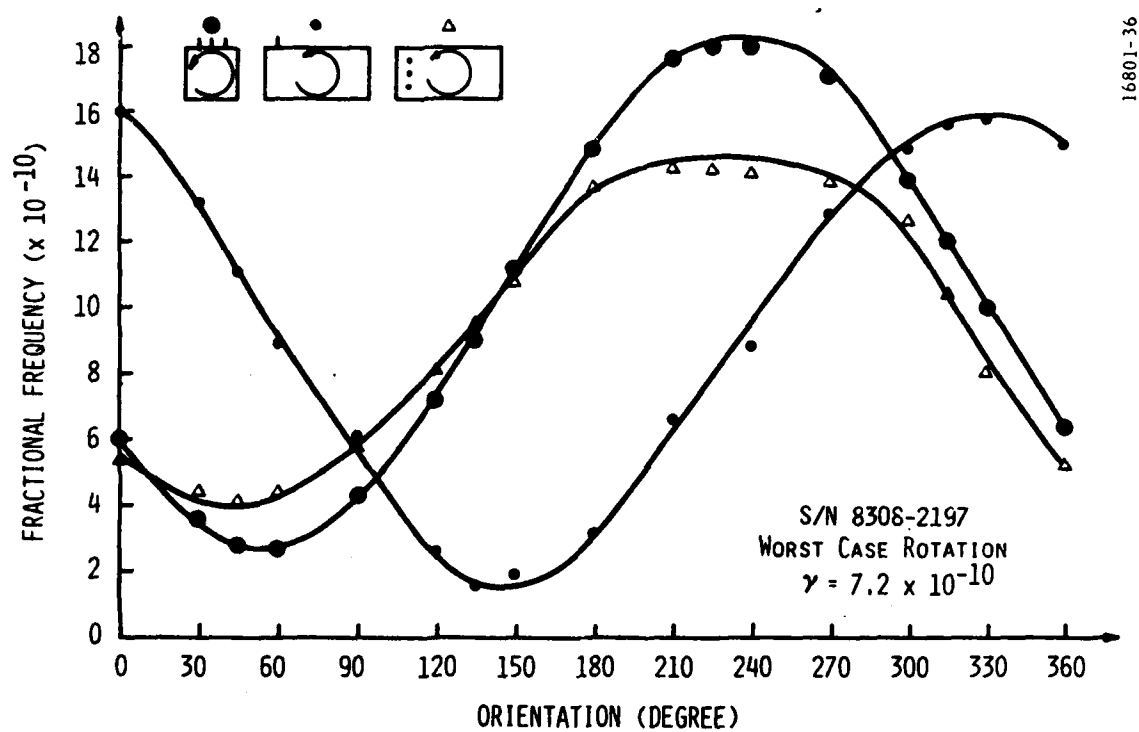Figure 5-5. VCXO Control Voltage Characteristics

Figure 5-6.   Static Acceleration Sensitivity - First VCXO Unit
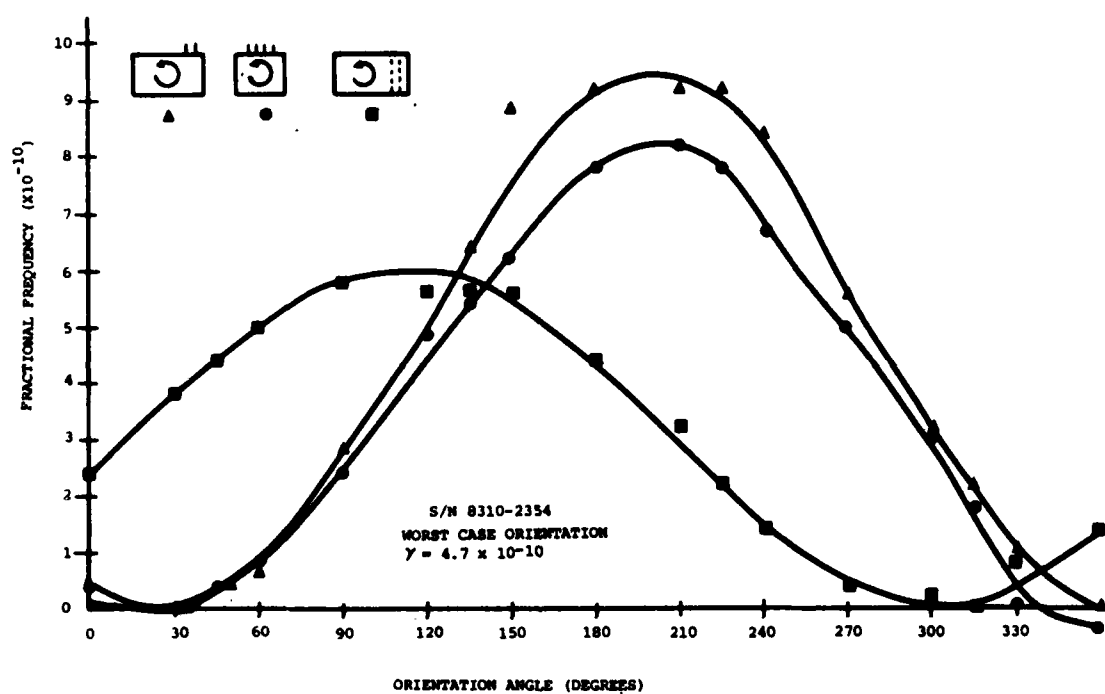
Figure 5-7.   Static Acceleration Sensitivity – Second VCXO Unit

TABLE V-1
VCXO TEST DATA

Test Item	1st Delivered Unit S/N 8308-2197	2nd Delivered Unit S/N 8310-2354	Litton Specified Design Goal
1. RF Output 10 MHz			
Output #1	0.58 vrms	0.58 vrms	0.5 vrms +30% -10%
Output #2	0.58 vrms	0.56 vrms	
2. Harmonic Distortion			
Output #1	-28 db second	-34 db second	-40 db
Output #2	-32 db second	-28 db second	
3. Nonharmonics			
Both outputs	below -100 db	below -100 db	< -100 db
4. Control Voltage			
10 MHz Nominal	4.95 v	5.35 v	
Range V = 12.5v	+1.89 Hz	+2.42 Hz	
V = 2.5v	-1.55 Hz	-1.45 Hz	
Total	3.44 Hz	3.87 Hz	4.0 Hz
5. Input Power 15v			
Warm-up peak	420 ma/6.3w	536 ma/8.0w	
Steady state -55C	152 ma/2.28w	109 ma/1.64w	
+25C	80 ma/1.2w	62 ma/0.93w	+25C 2w
+71C	39 ma/0.6w	33.7 ma/0.51w	
6. Transient Warmup Time to $\Delta f = 4 \times 10^{-8}$			
Room Temp	1.3 min	not	1.2 min
-55C amb	3.6 min	tested	3.5 min
7. Power Variation 15v ±5%	$\Delta f < 5 \times 10^{-11}$	$\Delta f < 2 \times 10^{-11}$	$< 1 \times 10^{-11}$
8. Load Variation No load to 50 Ω	$\Delta f < 2 \times 15^{10}$	$\Delta f < 1 \times 10^{-10}$	$< 1 \times 10^{-11}$
9. Temperature Variation			
-55C	$\Delta f = +0.25$ Hz	$\Delta f = +0.27$ Hz	± 0.1 Hz
+71C	$\Delta f = -0.52$ Hz	$\Delta f = -0.39$ Hz	
10. Acceleration Sensitivity	Worst case $\gamma = 7.2 \times 10^{-10}$	Worst case $\gamma = 4.7 \times 10^{-10}$	$\gamma = 3 \times 10^{-10}$
11. Physical			
Size	Spec value	Spec value	1.2 × 1.2 × 2.4 inch
Weight	4.7 oz	4.5 oz	0.5 pound ±10%

Static acceleration sensitivities of the two delivered units are shown in Figures 5-6 and 5-7. The fractional frequency deviation is measured as the VCXO unit is oriented to the discrete angular positions. The data points follow closely a sinusoidal variation with orientation angle. Improvement of the g-sensitivity of the second unit over that of the first is evident.

5.3 PERFORMANCE UNDER VIBRATION

Static acceleration sensitivities of the first VCXO unit as determined in Figure 5-8 show in the three orthogonal case axes:

$$\gamma_x = 7 \times 10^{-10}$$
$$\gamma_y = 5 \times 10^{-10}$$
$$\gamma_z = 3 \times 10^{-10}$$

Failure to meet the specification design goal of 3×10^{-10} for the first unit is attributed by the manufacturer to a g-sensitive electronic component, and is corrected in subsequent units.

Under vibration, the 10 MHz output of the VCXO is frequency modulated. During the vibration tests the vibration-induced side band level of the VCXO output was measured using the Litton designed phase noise measurement system. The output single sided interference spectrum was displayed on and recorded from an HP 3582A spectrum analyzer.

Results of the vibration test of the hard-mounted VCXO when subjected to a 5 g sinusoidal input in the three orthogonal case axes are shown in Figure 5-8. The two dashed lines for $\gamma = 3 \times 10^{-10}$ and 6×10^{-10} represent the side band levels predicted analytically by in Section 4. The actual test data, with minor deviations, is seen to correspond closely with predicted performance from the measured static acceleration sensitivities shown above. Noted exception is the systematic deviation of the measured data for z-axis shown in Figure 5-8
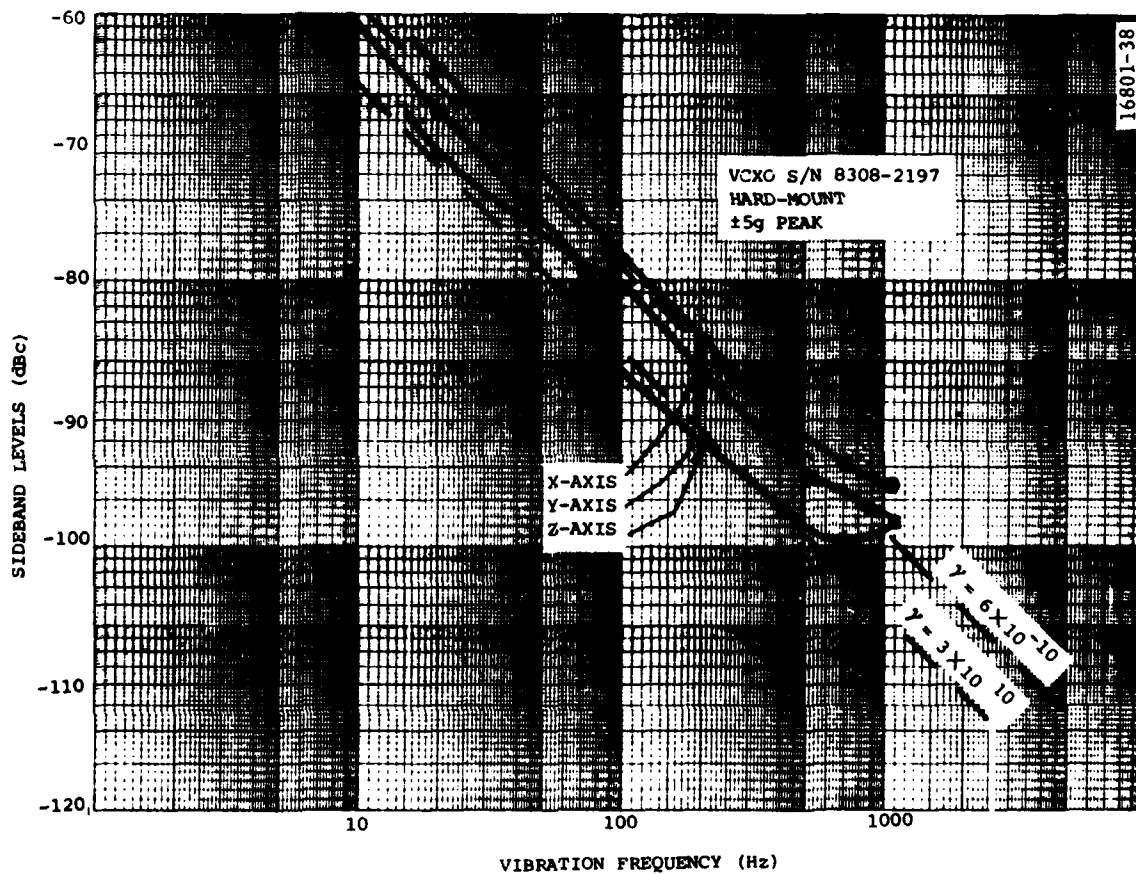
5-12

Figure 5-8. Vibration-Induced Sideband Level of Hard-Mounted VCXO

from the predicted values. Test data that were extended up to 3000 Hz of vibration frequency revealed that there existed moderate mechanical resonance rise internal to the VCXO unit at 2.5 KHz. The level of deviation is determined to be adequate for its application to the tactical Rb FSU's.

Following the hard-mount vibration tests, the VCXO was mounted with the set of four isolators and tested with a 5 g sinusoidal input. A small test accelerometer was attached to the VCXO to determine transmissibility of the isolator design.

Results of the vibration test for input along the y axis are shown in Figure 5-9. The transmissibility of the VCXO/isolator assembly is shown as the solid line curve. The resonance gain peaks at 55 Hz, a slightly higher frequency than was designed. The measured level of vibration-induced sideband is shown in the dotted line, and follows closely with the product of the transmissibility function and the static g-sensitivity, $\gamma \approx 5 \times 10^{-10}$, for y-axis.

5.4 DISCUSSIONS

The subcontracted SC-cut VCXO unit, as demonstrated in the previous sections, is compact in its size with exceptional functional performances. It offers excellent warm-up and respectable g-sensitivity. The test data indicate that its frequency performance under vibration environment follows closely with the analytical predictions. No structural resonance was observed below 1000 Hz. This VCXO unit, although it is intended for use in a tactical Rb FSU of Litton design, can be used as a stand-alone unit with better performance in many functional areas than that of a conventional AT-cut oscillators of double oven design.
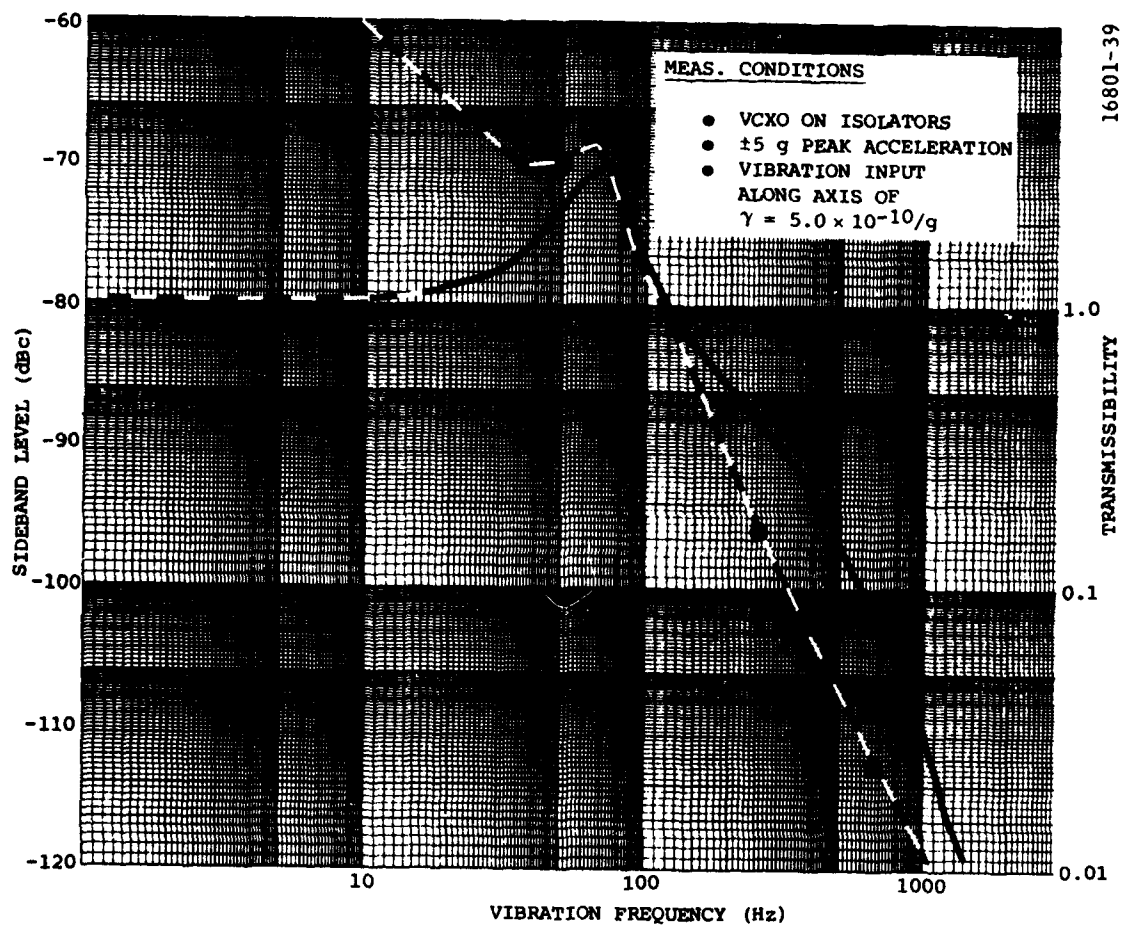
Figure 5-9. Vibration-Induced Sideband Level of Shock-Mounted
VCXO and Isolator Transmissibility

Noted excellence of the unit is its phase noise performance under vibra-
tion. Typical of a two-point-mount AT-cut oscillator, when subjected to vibra-
tion, is the serious degradation of phase noise, up to 30 db/√Hz, in addition
to the vibration-induced discrete sideband, above its static phase noise level.
This is believed due to microphonics of the electronic circuit components,
mounting structure, and g-sensitivity of the crystal. There appears to be no
such degradation in the SC-cut VCXO phase noise performance under vibration
other than the vibration-induced sideband. The level of sideband is within
±1 db from the analytically predicted values. Litton believes this is a
significant achievement in the art of crystal oscillator technology.

MISSION
of
Rome Air Development Center

RADC plans and executes research, development, test and selected acquisition programs in support of Command, Control Communications and Intelligence (C^3I) activities. Technical and engineering support within areas of technical competence is provided to ESD Program Offices (POs) and other ESD elements. The principal technical mission areas are communications, electromagnetic guidance and control, surveillance of ground and aerospace objects, intelligence data collection and handling, information system technology, ionospheric propagation, solid state sciences, microwave physics and electronic reliability, maintainability and compatibility.